2020

Evaluating the Performance and Impacts of Seawater Regeneration in an Anion Exchange Process

Daniel Whalen
University of Central Florida

EVALUATING THE PERFORMANCE AND IMPACTS OF SEAWATER REGENERATION IN AN ANION EXCHANGE PROCESS

by

DANIEL A. WHALEN
B.S.Env.E., Florida Gulf Coast University, 2014
M.S.Env.E., University of Central Florida, 2017

A dissertation submitted in partial fulfillment of the requirements
for the degree of Doctor of Philosophy
in the Department of Civil, Environmental, and Construction Engineering
in the College of Engineering and Computer Science
at the University of Central Florida
Orlando, Florida

Summer Term
2020

Major Professor: Steven J. Duranceau

ABSTRACT

This research investigated the use of seawater regeneration for anion exchange (AIX) processes. Seawater and salt-supplemented seawater regeneration of chloride-form anion resin were evaluated in regard to (1) operational performance efficiency of sulfate and natural organic matter removal, (2) competing exchange of bromide during regeneration, and (3) brominated disinfection by-product (DBP) formation due to bromide leakage. The first component involved bench-scale research that revealed that seawater-based regeneration led to bromide leakage that could be mitigated to an average of 1.82 mg/L using 1% salt-supplemented seawater, and 1.25 mg/L using 3% salt-supplemented seawater. Conceptual cost comparisons revealed that the use of seawater can reduce regeneration costs by up to $0.25/kgal compared to conventional 10% salt. The second segment of research demonstrated that bromide adsorption in the presence of chloride followed pseudo 2^{nd} order kinetics. Increasing the chloride-to-bromide ratio shifted intra-particle diffusion that revealed an exponential decay in bromide adsorption capacity. The equilibrium adsorption behavior could be described by both Freundlich and Langmuir isotherm models. The third segment of research evaluated the impacts of bromide leakage with respect to DBP formation. Results demonstrated that the 96-hr formation potential for total trihalomethanes (TTHMs) increased from 186 μg/L to 294 μg/L and haloacetic acids (HAA5) from 25.7 μg/L to 36.1 μg/L for a subsequent increase in bromide content from 0.22 mg/L to 2.13 mg/L, respectively, with a noticeable shift in chemical speciation from chlorinated to brominated forms. Coastal water utilities employing AIX might consider salt-supplemented seawater regeneration methods; however, further research is needed to confirm the long-term performance effects of this technique.

This dissertation is dedicated to my mother, Judith Richarz; and father, Ron Whalen. Without your love and support, this work would not have been possible.

ACKNOWLEDGMENTS

I would like to express my sincere appreciation and gratitude to Dr. Steven Duranceau for serving as my advisor and committee chair throughout this process. I would also like to thank Dr. Steven Duranceau for his profound influence on my academic and professional development; his time and effort have been essential to the success of this work and the knowledge I have accrued under his guidance. Thank you to Dr. Woo Hyoung Lee, Dr. Anwar Sadmani, and Dr. Melanie Beazley for serving on my committee and offering their time and counsel throughout this work. Additionally. I would like to thank the CECE staff for their support, especially our manager of facilities operations, Pete Alfieris; and our laboratory manager, Melissa Saint James.

This work would not have been possible without the help and support of the City of Sarasota Utilities Department, especially Bill Riebe, Verna Hall, Peter Perez, and Katherine Gusie for their assistance and guidance throughout this research. I would like to thank Mark Machacek from *Tonka Water, A U.S. Water Brand* for his advice and expertise related to ion exchange processes.

I would like to thank my fellow UCF colleagues in Dr. Duranceau's *Water Quality Engineering Research Group* who have all directly contributed to the research performed in this dissertation: Carlyn Higgins, Tulsi Shukla, Jessica Cormier, Courtney Powell, Paula Campesino, Devon Higgins, Zachary Protas, and Frances Martinez. I would like to give a special thank you to my girlfriend, Rafaela Frota; stepfather, Darrell Richarz; and stepmother, Paz Whalen, for their unwavering support and help throughout this research. I would also like to thank Marshall Bruce Mathers III for his input on lithium bromide equilibrium chemistry.

TABLE OF CONTENTS

LIST OF FIGURES

LIST OF TABLES

LIST OF EQUATIONS

LIST OF ABBREVIATIONS

%	Percent
α_j^i	Separation Factor
°C	Degrees Celsius
°F	Degrees Fahrenheit
AIX	Anion Exchange
b	Langmuir Isotherm Constant
BV	Bed Volumes
C	Concentration
C_{IPD}	Intra-Particle Diffusion Boundary Layer
$CaCO_3$	Calcium Carbonate
CBMR	Chloride to Bromide Molar Ratio
CITY	City of Sarasota Utilities Department
CIX	Cation Exchange
cm	Centimeter(s)
CSMR	Chloride to Sulfate Mass Ratio
DBPs	Disinfection By-Products
DOC	Dissolved Organic Carbon
EMCT	Equilibrium Multi-Component Theory
eq	Equivalence
eq/L	Equivalence per Liter
FIM	Freundlich Isotherm Model
ft	Feet

ft^2	Square Feet
ft^3	Cubic Feet
ft/s	Feet per Second
g	Gram(s)
g/L	Grams per Liter
g/mg-min	Grams per Milligram per Minute
gpd	Gallons per Day
gpm	Gallons per Minute
gpm/ft^2	Gallons per Minute per Square Foot
GS1	Groundwater Solution 1
GS2	Groundwater Solution 2
GS3	Groundwater Solution 3
GS4	Groundwater Solution 4
GSTs	Ground Storage Tanks
h_0	PSO Initial Adsorption Rate Constant
HAA5s	Haloacetic Acids
hrs	Hours
IPD	Intra-Particle Diffusion
I-Statistic	Industrial Statistic
IX	Ion Exchange
IXWTP	Ion Exchange Water Treatment Plant
K_j^i	Apparent Equilibrium Constant
K_f	Freundlich Isotherm Constant
k_{IPD}	Intra-Particle Diffusion Rate Constant

k1	PFO Rate Constant
k2	PSO Rate Constant
kgal	Kilogallon
kWh	Kilowatt-hour
L	Liter(s)
LCA	Life Cycle Assessment
L/g	Liters per Gram
LiBr	Lithium Bromide
LIM	Langmuir Isotherm Model
m	Mass
MCLs	Maximum Contaminant Levels
meq	Milliequivalence
meq/g	Milliequivalence per Gram
meq/L	Milliequivalence per Liter
meq/mmol	Milliequivalence per Millimole
mg	Milligram(s)
MG	Million Gallons
MGD	Million Gallons per Day
mg/g	Milligrams per Gram
mg/g-min	Milligrams per Gram per Minute
mg/L	Milligrams per Liter
MIEX	Magnetic Ion Exchange
min	Minute(s)
mL	Milliliter(s)

mL/min	Milliliters per Minute
mm	Millimeter(s)
mmol	Millimole(s)
mmol/mg	Millimoles per Milligram
mol	Mole(s)
mS/cm	Millisiemens per Centimeter
mV	Millivolt(s)
n	Freundlich Isotherm Constant
NaBr	Sodium Bromide
NaCl	Sodium Chloride
NOM	Natural Organic Matter
NPDWRs	National Primary Drinking Water Regulations
NSDWRs	National Secondary Drinking Water Regulations
NTU	Nephelometric Turbidity Units
O&M	Operations and Maintenance
ORP	Oxidation Reduction Potential
PCU	Platinum Cobalt Units
PFO	Pseudo 1^{st} Order
PSO	Pseudo 2^{nd} Order
q_e	Equilibrium Adsorption Capacity
q_{max}	Maximum Adsorption Capacity
q_t	Adsorption Capacity
q_T	Total Exchange Capacity
R^2	Coefficient of Determination

RO	Reverse Osmosis
ROWTP	Reverse Osmosis Water Treatment Plant
RS1	Regenerant Solution 1
RS2	Regenerant Solution 2
RS3	Regenerant Solution 3
RS4	Regenerant Solution 4
S6	Solution 6
SAC	Strong-Acid Cation
SBA	Strong-Base Anion
SBSW	Filtered Sarasota Bay Seawater
SDWA	Safe Drinking Water Act
SLCs	Saturation Loading Curves
SLR	Surface Loading Rate
SM	Standard Method
SMCLs	Secondary Maximum Contaminant Levels
SS1	Synthetic Solution 1
SS2	Synthetic Solution 2
SS3	Synthetic Solution 3
SS4	Synthetic Solution 4
SS5	Synthetic Solution 5
s.u,	Standard Units
TSS	Total Suspended Solids
TTHMs	Total Trihalomethanes
UCF	University of Central Florida

UCL	Upper Control Limits
µg	Microgram(s)
µg/L	Micrograms per Liter
µm	Micron(s)
µS/cm	Microsiemens per Centimeter
USEPA	United States Environmental Protection Agency
USP	United States Pharmacopeial Convention, Incorporated
USS	US Sieve Size
UV	Ultraviolet
UWL	Upper Warning Limits
V	Volume
WAC	Weak-Acid Cation
WBA	Weak-Base Anion
WTF	Water Treatment Facility
yr	Year

CHAPTER 1: INTRODUCTION

Safe Drinking Water Act

The Safe Drinking Water Act (SDWA) was originally passed by Congress in 1974 to protect public health by regulating the nation's public drinking water supply. This law focuses on those waters actually or potentially designed for drinking use, whether from above ground or underground sources. The Act authorized the United States' Environmental Protection Agency (USEPA) to establish minimum standards to protect tap water and required owners or operators of public water systems to comply with these primary (health-related) standards. The 1996 Amendments to the SDWA require that the USEPA consider a detailed risk and cost assessment, and best available peer-reviewed science, when developing numeric standards. State governments, which can be approved to implement these rules for the USEPA, also encourage attainment of secondary standards (nuisance-related).

The USEPA has established National Primary Drinking Water Regulations (NPDWRs), legally enforceable standards that apply to public water systems. These standards protect drinking water quality by limiting the levels of specific contaminants that can adversely affect public health and which are known or anticipated to occur in public water supplies, setting mandatory water quality standards for drinking water contaminants. These are enforceable standards called "maximum contaminant levels" (MCLs) that are established to protect the public against consumption of drinking water contaminants that present a risk to human health. An MCL is the maximum allowable amount of a contaminant in drinking water that is delivered to the consumer.

In addition, the USEPA has established National Secondary Drinking Water Regulations (NSDWRs) that set non-mandatory water quality standards for fifteen contaminants. They are established as guidelines to assist public water systems in managing their drinking water for aesthetic considerations, such as taste, color, and odor. These contaminants are not considered to present a risk to human health at the "secondary maximum contaminant levels" (SMCLs). Although the USEPA does not enforce SMCLs, they are enforced by the Florida Department of Environmental Protection per Chapter 62-560.430 (Florida Administrative Code 2011a).

Ion Exchange

Ion exchange (IX) is a process that removes aqueous ionic constituents by exchanging them with solid-phase ions of a similar charge. IX is typically employed in potable water applications to soften and demineralize water (Crittenden et al., 2005). Anion exchange (AIX) is a form of IX that is capable of removing negatively charged ionic constituents from water, such as sulfate, nitrate, phosphate, chloride, bromide, and natural organic matter (NOM); however, minimal research has been conducted to understand the impact of NOM, nitrate, and sulfate on AIX operating performance, in particular, with respect to alternative regeneration strategies (Ye et al., 2012). Additionally, limited research can be found on treating a sulfate-laden groundwater source with AIX for potable water production. For example, Runtti and colleagues (2018) discuss options for the removal of sulfate from mine drainage with no discussion of drinking water applications, other than the need for treatment in the drinking water of cattle (Digesti and Weeth, 1976).

Operational costs associated with IX are, in large part, due to the regeneration process. Regeneration of IX resin typically involves the use of a high strength brine solution, incurring the

cost of importing salt to the water utility. Alternative regeneration methods are explored in attempts to reduce regeneration costs and increase IX sustainability. Wilf et al. (1980) looked at seawater as an alternative regeneration method for a cation exchange (CIX) process. Coastal water utilities employing IX may benefit from seawater regeneration; however, further research is needed to identify performance efficiency and impacts of seawater regeneration. Alternative regeneration methods such as the use of seawater sources that are unlike the traditional methods that rely on highly processed, high-quality salty brine solutions, would be expected to also yield undesired ion leakage due to the incidental exchange of competing ions during the regeneration process, like bromide. The ionic composition of seawater impacts the equilibrium and kinetic processes taking place during AIX regeneration. Funasaki (1979) identified changes to equilibrium and kinetic reactions under variable salt conditions, which is typical of high concentrations of sodium- or chloride-form regenerant solutions. It appears then, that there is a need to further explicate the equilibrium and kinetic reactions of AIX seawater regeneration.

Increased bromide concentrations resulting from ion leakage caused by seawater regeneration have the potential to increase the formation of disinfection by-products (DBPs). It is known that bromide reacts with NOM and disinfectants to form brominated DBPs (Ackerson et al., 2020; Cooper et al., 1985; Liu et al., 2011; Richardson et al., 1999). It is also established that brominated DBPs carry higher health associated risks, correlating to higher cytotoxicity and genotoxicity than chlorinated DBPs (Kolb et al., 2017; Richardson et al., 1999; Sharma et al., 2014; Yang et al., 2014; Zhai & Zhang, 2011; Zhai et al., 2014). However, when compared to chlorinated DBPs, studies on brominated DBPs are still limited (Zhang & Yang, 2018).

Objectives

This dissertation reports on an investigation that evaluated the use of seawater, and salt-supplemented seawater, to regenerate an AIX process. Bench-scale column testing was used to investigate the performance and overall effectiveness of regenerating an AIX process with seawater-based solutions while targeting the removal of sulfate and organics from a sulfate-laden Florida groundwater. Batch jar testing was implemented to explore and better understand equilibrium and kinetic relationships between chloride and bromide in an AIX regeneration process. Experiments were conducted to assess changes in DBP formation and speciation to gain a better understanding of the impacts of bromide elution from seawater regeneration on DBP formation. The main objectives of the research presented in this work were as follows:

1. Investigate and compare the performance of AIX in removing sulfate and organics using seawater, and salt-supplemented seawater as regenerant solutions versus conventional salt regeneration.
2. Assess the impacts of bromide leakage resulting from seawater, and salt-supplemented seawater regenerant solutions.
3. Assess equilibrium, kinetics, and rate-controlling adsorption mechanisms of bromide in the presence of high chloride concentrations.
4. Assess and quantify the impacts of bromide elution from seawater regeneration to DBP formation and speciation.

City of Sarasota Utilities Department

In efforts to improve water quality, the University of Central Florida (UCF) implemented an investigation of the City of Sarasota's (CITY's) water treatment processes and distribution system (Project No. 16208213). The CITY is a publicly-owned water utility operating on Florida's west coast. The CITY's Utility Department oversees the production of safe drinking water from a combination of treatment processes that rely on a blend of reverse osmosis, ion exchange, and disinfected well water. The City's water treatment facility (WTF) is comprised of two major water treatment plants: a reverse osmosis water treatment plant (ROWTP), and an ion exchange water treatment plant (IXWTP). The facility, located at 1642 12th Street in Sarasota, Florida serves the residents of the City of Sarasota that live within the incorporated city limits. The two water sources relied on by the community's water system possess different water quality characteristics that require treatment using independent and separate processes. The Downtown brackish groundwater well field is treated at the 4.5 million gallon per day (MGD) capacity ROWTP, and the Verna groundwater well field is treated by aeration prior to a 5.2 MGD capacity IXWTP. Up to 2.3 MGD of Verna groundwater is by-passed and blended in a clearwell, where each of the process streams are combined and disinfected to provide a total WTF capacity of 12 MGD. Safe drinking water is then stored in nearby ground storage tanks (GSTs) and high-service pumps transport the water to the distribution system at appropriate rates and pressures. Table 1 and Table 2 display data illustrating the differences in water quality between the two groundwater sources. Figure 1 shows a schematic that depicts the overall process flow of the CITYs WTF. Currently benefiting from alternative regeneration, the CITY saves on salt import costs by utilizing filtered Sarasota Bay

seawater (SBSW) for regeneration purposes of their existing CIX process, and a permitted deep-well for disposal of WTF residuals, including ROWTP concentrate.

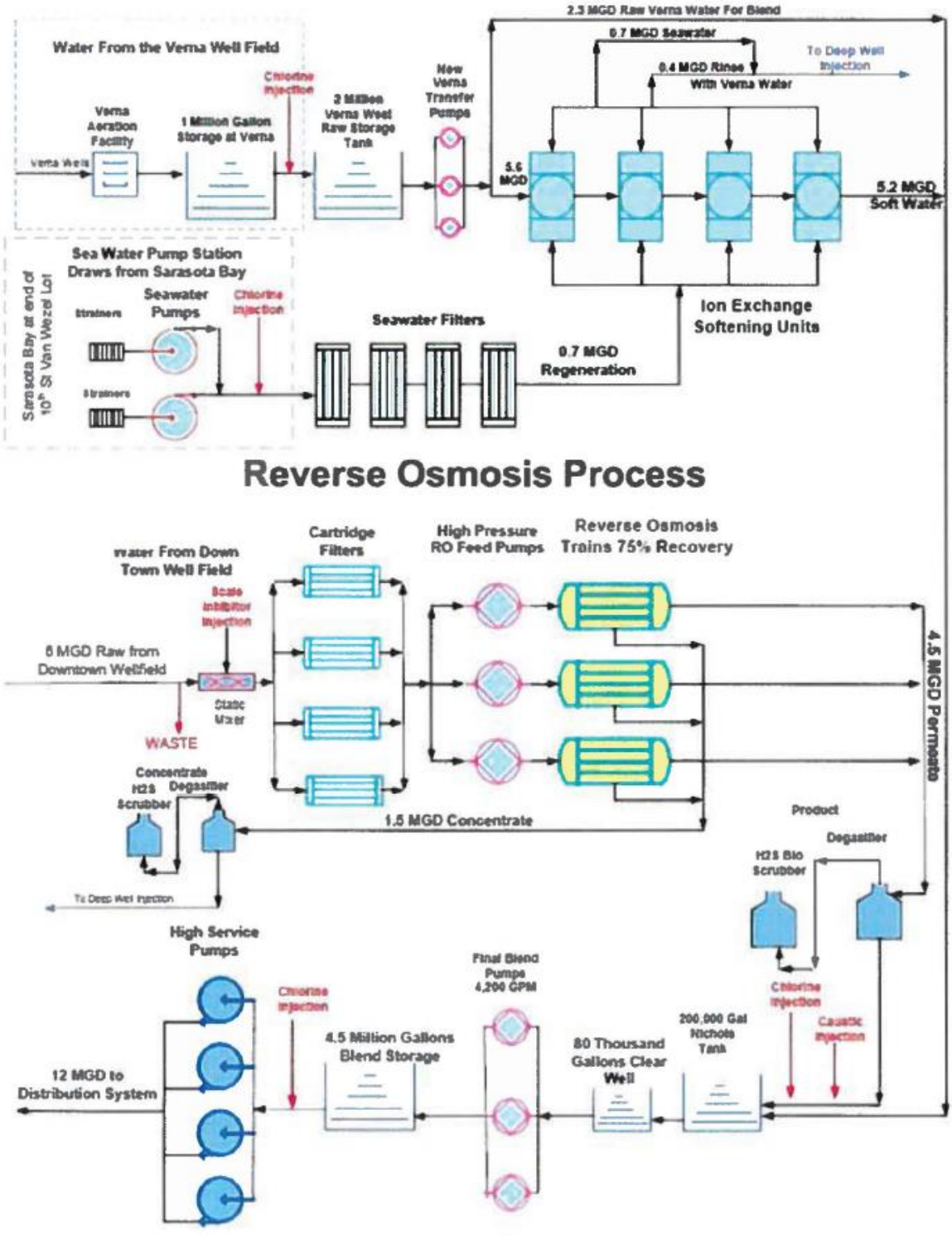

Figure 1: City of Sarasota WTF Schematic (Courtesy of City of Sarasota, FL)

Reverse Osmosis Process

Six MGD of raw groundwater is pumped from the Downtown brackish well field to the ROWTP. Historically, pretreatment consisted of adding scale inhibitor (antiscalent) and sulfuric acid prior to 1-micron cartridge filtration. However, sulfuric acid pretreatment was removed from service and permanently taken offline February 2012 (Tharamapalan, Boyd & Duranceau, 2013). The pre-treated water is then fed to a two-stage RO membrane process operating at seventy-five percent (%) recovery. Stage-1 consists of twenty-eight pressure vessels housing six Hydranautics CPA3 membrane elements per vessel and stage-2 consists of fourteen pressure vessels housing six Hydranautics ESPA2 membrane elements per vessel. The facility has a total of three existing membrane process trains, each with a 1.5 MGD production capacity. Following membrane treatment, the permeate water is degasified and pH adjusted with sodium hydroxide prior to blending with the treated CIX and by-pass water streams. The rejected concentrate water, approximately 1.5 MGD, is degasified and disposed of via deep well injection.

Table 1: Downtown Brackish Well Field Water Quality (Duranceau et al., 2014)

Parameter	Units	Average Value
pH	s.u.	7.13
Temperature	ºC	26.9
Conductivity	µS/cm	3,330
Turbidity	NTU	0.12
Alkalinity	mg/L as $CaCO_3$	136
TDS	mg/L	2,400
Sulfate	mg/L	858
Chloride	mg/L	588
Calcium	mg/L	279
Magnesium	mg/L	135
Sodium	mg/L	294
Potassium	mg/L	6.60
Strontium	mg/L	26.5
Silica	mg/L	21.9

Ion Exchange Process

The Verna groundwater well field provides up to 7.5 MGD of raw water for treatment by the IXWTP. The water is pretreated at the well field using tray aeration for hydrogen sulfide and carbon dioxide removal and pre-chlorination for biological control while gravity fed along a 20 mile pipeline prior to arrival at the treatment facility. The incoming pretreated water is bifurcated to allow for both CIX treatment and by-pass blending to occur. The CIX process uses a strong-acid cation (SAC) resin in the sodium form to soften 5.2 MGD. There are four softening units; three of which may be operated at full production, while the fourth is being regenerated by the innovative use of filtered, chlorinated and dechlorinated seawater that is pumped from a small pumping station on Sarasota Bay located 0.2 from the facility. The treated SBSW provides the needed sodium ions to complete the ion exchange regeneration component of the process.

Approximately 0.7 MGD of filtered SBSW is used for media regeneration, while approximately 0.4 MGD of raw well water is used for media rinse, both of which are disposed of after use.

Table 2: Verna Well Field Water Quality, Post Aeration

Parameter	Units	Average Value
pH	s.u.	7.64
Temperature	°C	29.1
Conductivity	µS/cm	1,090
Turbidity	NTU	0.18
Alkalinity	mg/L as $CaCO_3$	171
TDS	mg/L	830
Sulfate	mg/L	396
Chloride	mg/L	25.2
Bromide	mg/L	<0.2
Fluoride	mg/L	0.49
Calcium	mg/L	126
Magnesium	mg/L	60.2
Sodium	mg/L	13.5
Potassium	mg/L	2.46
Strontium	mg/L	21.8
Silica	mg/L	25.7

CHAPTER 2: LITERATURE REVIEW

In this chapter, literature relevant to IX processes for potable water production is presented. The literature reviewed herein provides a brief overview of IX, and is segmented into equilibrium and kinetic considerations, and operational performance. Ion exchange processes used in water treatment are reviewed, with specific emphasis on anion exchange for applications in removing sulfate from aqueous solutions. Alternative regeneration methods of IX are also examined and seawater regeneration is presented as an alternative process opportunity. A segment of this Chapter is also devoted to disinfection by-product concerns that water purveyors face, with specific focus on brominated DBP formation related to bromide originating from saline water sources.

Overview of Ion Exchange Processes

IX is a process used in water treatment to remove aqueous ionic constituents by exchanging them with solid-phase ions of a similar charge at the surface of an oppositely charged resin. The resin's charge comes from fixed functional groups located at the external and/or internal surface of the resin, known as exchange sites (Crittenden et al., 2005; Liberti & Helfferich, 1983; Wachinski, 2006). IX resin generally takes the shape of small, spherical beads (Figure 2), is commonly housed in a column or tank, and operated in a fixed or fluidized bed configuration.

Figure 2: Purolite A600E-9149 Anion Resin

At the initiation of the first operation cycle, the IX resin's exchange sites contain solid-phase, presaturant ions. As water passes through the resin bed, the presaturant ions are exchanged for aqueous ions in the water matrix. The IX treated water exiting the resin bed consists of an equivalent increase in the presaturant ion to that of the decreased exchanged aqueous ion. During continued operation, the available exchange sites on the resin begin to saturate with the targeted aqueous constituent(s) and the IX treated water increases in the targeted constituent(s) concentration; this is known as breakthrough. When the exchange sites of the IX resin become fully saturated with the targeted aqueous constituent(s), the resin bed is considered exhausted (Crittenden et al., 2005; Wachinski, 2006). Figure 3 displays a graphical representation identifying breakthrough and exhaustion of an IX system over time.

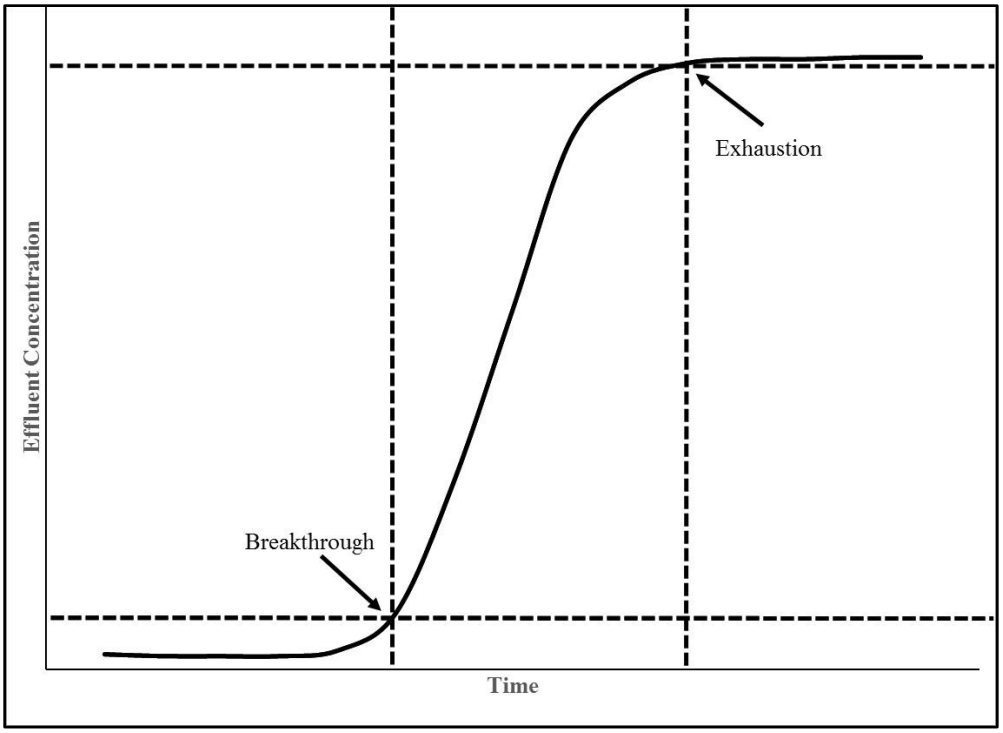

Figure 3: Ion Exchange Breakthrough/Exhaustion Curve

Once exhaustion is reached, the IX resin is replenished with the presaturant ion, in a process known as regeneration. Regeneration involves running a high concentration solution of the initial presaturant ion through the IX system, eluting the previously targeted constituent(s) off the exhausted IX resin and replacing it with the original presaturant ion. Common presaturant ions used in IX systems for water treatment include hydrogen, sodium, hydroxide, and chloride (Crittenden et al., 2005; Maul et al., 2014).

IX can be used in multiple applications, including water treatment, production of de-ionized water, industrial purposes, purification of organic and inorganic chemicals, analytical chemistry uses, ion mixture separation processes and treatment of mine drainage (Schubert & Nachod, 1956). Most IX applications in water treatment utilize synthetic organic resins that contain different charged

functional groups (Crittenden et al., 2005). There are four main types of IX resin, each consisting of a different organic functional group and exchanging ion. Table 3 presents different types of IX resin commonly used in water treatment applications.

Table 3: Ion Exchange Resin Characteristics, partially adapted from Crittenden et al., 2005

Resin Type	Acronym	Functional Group	Presaturant Ion(s)	Constituents Removed
Strong-Acid Cation	SAC	Sulfonate (RSO_3^-)	H^+ or Na^+	H^+: Monovalent, divalent, & polyvalent cations Na^+: Divalent cations
Weak-Acid Cation	WAC	Carboxylate ($RCOO^-$)	H^+	Divalent cations>monovalent cations until alkalinity is consumed
Strong-Base Anion	SBA	Quaternary Amine ($R(CH_3)_3N^+$)	OH^- or Cl^-	OH^-: Monovalent, divalent, & polyvalent anions Cl^-: Divalent & polyvalent anions
Weak-Base Anion	WBA	Tertiary Amine ($R(CH_3)_2N$)	OH^-	Divalent anions>monovalent anions until strong acid is consumed

Physical and chemical factors affect the affinity an IX resin has toward a particular ionic species in water, known as resin selectivity. Generally, ionic species with higher ionic radii, hydrated radii, molecular weight, atomic numbers, and valence are preferred (Crittenden et al., 2005; Tan & Kilduff, 2007). However, temperature, pressure, pH, ionic strength, and other physical/chemical properties can affect a resin's affinity for an ionic species (Wachinski, 2006).

Equilibrium and Kinetics

Understanding the chemical equilibrium and kinetic reactions taking place is important when determining which type of IX resin to use for a specific application. Generally, IX reactions can

be considered reversible, as equilibrium can be reached with reactants forming to create products during operation or products forming to create reactants during regeneration. A general stoichiometric equation for an IX resin can be seen in Equation (1) (Crittenden et al., 2005; Moody et al., 1968; Wachinski, 2006).

$$n[R^{\pm}]B^{\pm} + A^{n\pm} \leftrightarrow [nR^{\pm}]A^{n\pm} + nB^{\pm} \quad (1)$$

Where,
$R^{\pm}$ = charged functional group attached to IX resin
$B^{\pm}, A^{n\pm}$ = exchanging ions

Considering only one aqueous ionic species exchanging with the IX resin's solid-phase ions, an equilibrium expression can be written with respect to Equation (1) to develop an apparent equilibrium constant, $K_{B^{\pm}}^{A^{\pm}}$, identifying an IX resin's affinity for one ionic constituent over another using their concentrations (Crittenden et al., 2005; Moody et al., 1968). Shown in Equation (2), the present equilibrium notion illustrates solution ion A exchanging with an IX resin containing ionic species B.

$$K_{B^{\pm}}^{A^{\pm}} = \frac{C_B^n q_A}{q_B^n C_A} \quad (2)$$

Where,
$K_{B^{\pm}}^{A^{\pm}}$ = apparent equilibrium expression of exchanging ions
C_B^n = aqueous-phase concentration of presaturant ion, eq/L
q_A = resin-phase concentration of counter-ion, eq/L
q_B^n = resin-phase concentration of presaturant ion, eq/L
C_A = aqueous-phase concentration of counter-ion, eq/L

Apparent equilibrium constants, also known as a selectivity coefficients, have been used to characterize the behavior of AIX resins since their inception in the early 1950s. Gregor et al. (1954)

measured selectivity coefficients for AIX resins toward monovalent anions in different temperatures and concentrations. Since that time, selectivity coefficients have remained the key marker for comparing different IX resin functional groups and IX resin characteristics for their affinity to uptake certain ions over others. Soldatov et al. (2007) used selectivity coefficients, among other parameters, to distinguish between different strong-base AIX resins containing different functional groups on their ability to uptake chloride, nitrate, and sulfate. Similar work has been performed on the removal of iodide and bromide using chloride-form AIX resin under different temperatures for changes in the resin's equilibrium constants (Singare et al., 2009). For design purposes, equilibrium constants can be expressed in other ways, such as those suggested by Hu and coworkers (2016) that evaluated the resin selectivity of six strong-base anion resins based on their separation factor. Taking Equation (2) and replacing the concentration values with equivalent fractions yields a binary separation factor, α_B^A, that can be used to identify a resin's affinity for one aqueous-phase ion over another, displayed in Equation (3) (Crittenden et al., 2005).

$$\alpha_B^A = \frac{Y_A X_B}{X_A Y_B} \tag{3}$$

Where,
α_B^A = binary separation factor
Y_A = aqueous-phase equivalent fraction of presaturant ion
X_B= resin-phase equivalent fraction of counter-ion
X_A = resin-phase equivalent fraction of presaturant ion
Y_B = aqueous-phase equivalent fraction of counter-ion

In addition to identifying a resin's affinity for one ion over another, it is important to quantify the amount a resin can uptake of a certain ion. Accounting for resin volume, solution volume, and the

change in ion concentration, adsorption values can be experimentally calculated using Equation (4) to determine the adsorption capacity, q_t, at a given time.

$$q_t = \frac{(C_o - C_t)V}{m} \quad (4)$$

Where,
q_t = amount of ion adsorbed per gram of resin (mg/g_{res})
C_o = initial ion concentration (mg/L)
C_t = ion concentration at a given time (mg/L)
V = volume of solution (L)
m = mass of resin (g)

Applying an ion's concentration at equilibrium to Equation (**4**), yields the equilibrium adsorption capacity, q_e, displayed in Equation (5).

$$q_e = \frac{(C_o - C_e)V}{m} \quad (5)$$

Where,
q_e = amount of ion adsorbed per gram of resin at equilibrium (mg/g_{res})
C_e = equilibrium ion concentration (mg/L)

Calculating an ion's q_e over different initial concentrations allows for the development of adsorption isotherms, modeling the reaction and identifying the behavior of the adsorption process (Foo & Hameed, 2010). The Freundlich Isotherm Model (FIM) and the Langmuir Isotherm Model (LIM) have been widely used to fit equilibrium adsorption data, applying linearized forms of the models to obtain model parameters graphically (Kinniburgh, 1986). Proposed by Freundlich (1906), the FIM is an empirically derived model used to model gas-phase and solute adsorption, typically for heterogeneous adsorbents (Sparks, 2003). The linear-form FIM is presented in Equation (6).

$$log\ q_e = log\ K_f + \frac{1}{n} log\ C_e \quad (6)$$

Where,
K_f = Freundlich adsorption capacity constant
n = Freundlich adsorption intensity constant

The LIM was originally proposed by Langmuir (1918), and is used to describe adsorption between solution constituents and fixed sites on a surface. The linear-form LIM is given in Equation (7).

$$\frac{C_e}{q_e} = \frac{1}{bq_{max}} + \frac{C_e}{q_{max}} \quad (7)$$

Where,
q_{max} = maximum adsorbate concentration (mg/g)
b = Langmuir adsorption constant (L/mg)

Adsorption capacity, q_t, is used in IX studies for determining the kinetic reactions taking place. Adsorption kinetics describe the removal rates of ionic constituents over time. Rates of adsorption can be modeled through rate equations, or rate laws, by comparing different kinetic rate equations to the change in reactant concentrations over time. For ion exchange processes, kinetics have shown high correlation to pseudo 1st order (PFO) and pseudo 2nd order (PSO) rate laws and have been widely used when describing the rate of adsorption in liquid-solid interactions (Moussout et al., 2018). Ding et al. (2012) demonstrated that bromide removal through magnetic ion exchange (MIEX) can be well described by PSO kinetics. Rengaraj et al. (2003) found that the removal of chromium using CIX resin followed PFO kinetics and Chubar et al. (2005) modeled the adsorption of fluoride, chloride, bromide and bromate in IX using PSO kinetics.

The PFO rate equation, originally proposed by Lagergren & Sven (1898), is displayed as a differential equation in Equation (8).

$$\frac{dq_t}{dt} = k_1(q_e - q_t) \tag{8}$$

Where,
k_1 = pseudo 1st order rate constant (min^{-1})

Integrating Equation (8) with boundary conditions of t = 0, qt = 0, t = t, and qe = qt yields the integrated PFO rate equation in its liner form, displayed in Equation (9). A full integration of the PFO rate equation can be found in Appendix A.

$$\ln(q_e - q_t) = lnq_e - k_1 t \tag{9}$$

The PSO rate equation, presented by Ho & McKay (1998), is shown as a differential equation in Equation (10).

$$\frac{dq_t}{dt} = k_2(q_e - q_t)^2 \tag{10}$$

Where,
K_2 = pseudo 2nd order rate constant (g/mg-min)

Integrating Equation (10) with boundary conditions of t = 0, qt = 0, t = t, and qe = qt yields the integrated PSO rate equation in its liner form, shown in Equation (11). A full integration of the PSO rate equation can be found in Appendix A.

$$\frac{t}{q_t} = \frac{1}{k_2 q_e^2} + \frac{1}{q_e} t \tag{11}$$

Assessing the reaction rates of IX resins toward particular ions in synthetic solutions has been extensively studied (Alyüz & Veli, 2009; Chen at al., 2002; Gando-Ferreira et al., 2011; Hsu & Singer, 2010; Nawaz & Sengupta, 2017). Additionally, IX kinetics of complex water matrices have been evaluated: surface water (Walker & Boyer, 2011), seawater (Jung & Kim, 2016), groundwater (Piazzoli & Antonelli, 2018), and wastewater (Muhammad et al., 2019). The majority of IX kinetic studies focus on the forward reaction approaching equilibrium as solid-phase, presaturant, ions are exchanged with aqueous-phase ions in solution; Equation (**1**) proceeding from left to right. Less research is available on the kinetics of the reverse reaction approaching equilibrium during the regeneration process; Equation (1) proceeding from right to left. Lokhande & Singare (1998) studied the forward and reverse reaction rates of IX resin when removing radioactive iodide ions with inactive iodide exchanging ions, but the kinetic impacts of alternative regenerant solutions were not evaluated. The ionic concentration and composition of regenerant solutions impact the equilibrium and kinetic processes taking place. Funasaki (1979) identified changes to equilibrium and kinetic reactions under variable salt conditions, which is typical of sodium- or chloride-form regenerant solutions. There is a need to explicate the equilibrium and kinetic reactions during IX regeneration to optimize the IX process and determine if alternative regenerant solutions containing high ionic strengths and competing ions, like seawater, can be considered.

In addition to understanding the rate of a reaction, it is necessary to identify the rate determining step(s). The adsorption process generally consists of three steps, external mass transfer across a boundary layer (film diffusion), internal diffusion to sorption sites (internal/intra-particle diffusion) and sorption/exchange on the surface of the adsorbent (Ding et al., 2012; Largitte &

Pasquier, 2016; Liberti & Helfferich, 1983). High correlation to the PSO model displayed in Equation (10) infers that chemical adsorption (chemisorption) is the rate limiting step when compared with diffusion-based mass transfer mechanisms (Chubar et al., 2005; Muhammad et al., 2019;). It is possible that the adsorption process may be controlled by more than one step and the limitations of the proposed PSO model, representing adsorption as a one-step binding process, cannot elucidate the diffusion-based mass transfer mechanisms that may be present (Acelas et al., 2015; Fierro et al., 2008). Testing parameters such as agitation speed, temperature, and resin particle diameter can also influence certain rate mechanisms, making it difficult to accurately interpret rate data (Liberti & Helfferich, 1983). Additionally, the equivalence concentration ratio of solution ions to resin exchange sites impacts the ability to model diffusion.

The intra-particle diffusion (IPD) model proposed by Weber & Morris (1963) can be used to interpret kinetic data from a diffusion-based mechanistic stand-point.

$$q_t = k_{IPD} t^{1/2} + C_{IPD} \tag{12}$$

Where,
k_{IPD} = intra-particle diffusion rate constant (mg/(g-min$^{1/2}$))
C_{IPD} = boundary layer thickness constant (mg/g)

Presented in Equation (12), the IPD model can be applied to analyze adsorption kinetics. If a plot of q_t *versus* $t^{1/2}$ yields a straight line, then the sorption process is controlled by intra-particle diffusion (Ding et al., 2012; Dixit et al., 2018; Wu et al., 2009). Moreover, intra-particle diffusion is the only rate-controlling step if the plot passes through the origin (Ding et al., 2012; Wu et al.,

2009). If the data reveals multi-linear plots, then two or more steps affect the adsorption process (Fierro et al., 2008; Wu et al., 2009).

Operational Performance

When implementing IX for treatment purposes, engineering properties of system performance should be monitored during operations. How the IX system is designed and how it performs is largely dictated by the water quality of the raw water being treated and the level of treatment desired (Michener & Lundberg, 1956). In addition to breakthrough and exhaustion, other values should be monitored for use in assessing IX performance. Several parameters of interest are described in this section for their relevance toward IX system performance and operation.

Exchange Capacity

Defined as the total quantity of exchange groups per unit volume of resin, exchange capacity is used to calculate the amount of aqueous-phase ions that can be exchanged onto resin of a certain volume (Crittenden et al., 2005; Wachinski, 2006; Michener & Lundberg, 1956). Equations (13) through (16) illustrates the use of exchange capacity to calculate the amount of a given source water that can be softened using a SAC resin operated to exhaustion.

Given:

SAC Resin Exchange Capacity ($\frac{meq}{g,resin}$):	2
SAC Resin Volume (g):	830
Calcium in source water (mg/L):	126
Magnesium in source water (mg/L):	60.2

$$\text{Calcium Equivalence: } \left(\frac{126mg\ Ca^{2+}}{L}\right)\left(\frac{mmol}{40.08mg}\right)\left(\frac{2meq}{mmol}\right) = 6.29 \text{ meq/L} \quad (13)$$

$$\text{Magnesium Equivalence: } \left(\frac{60.2mg\ Mg^{2+}}{L}\right)\left(\frac{mmol}{24.31mg}\right)\left(\frac{2meq}{mmol}\right) = 4.95 \text{ meq/L} \quad (14)$$

$$\text{Resin Exchange Capacity: } \left(\frac{2meq}{g,resin}\right)(830g,resin) = 1{,}660 \text{ meq} \quad (15)$$

$$\text{Volume of Treated Water: } (1{,}660\ meq)\left(\frac{L}{(6.29+4.95)meq}\right) = 148 \text{ L} \quad (16)$$

Specific Throughput

Specific throughput pertains to the volume of water treated per mass of resin used for a pre-determined level of treatment. Helpful in engineering calculations, specific throughout aids in determining the amount of resin necessary for a desired treatment objective. In addition to previously discussed differences in IX resins, they also differ in density, diameter, and moisture retention (Crittenden et al., 2005). Equation (17) demonstrates the use of specific throughput to determine the amount of resin necessary for treatment of a given source water.

Given:

Specific Throughput ($\frac{L,water}{g,resin}$):	0.25
Desired Treatment Volume (MG/Cycle):	0.5
IX Resin Bulk Density (dry) ($\frac{g,resin}{L,resin}$):	700
IX Resin Moisture Retention (%):	45

$$\text{Resin Required: } \left(\frac{0.5MG}{cycle}\right)\left(\frac{3.78541x10^{6}L}{MG}\right)\left(\frac{g,resin}{0.25L,water}\right)\left(\frac{L,resin}{700g,resin}\right)(1.45)\left(\frac{ft^3}{28.3168L}\right) = 554 \text{ ft}^3 \quad (17)$$

Leakage

Leakage of an aqueous ionic species occurs from incomplete regeneration or the exchange of competing ions during regeneration of an IX process, whereby the unremoved/exchanged ions remaining on the resin can leak into the effluent stream during successive operational runs. Leakage in an IX process occurs more frequently when alternative regeneration solutions are used that contain additional ionic species and varying concentrations of the original presaturant ion. For example, during the process of treating and recycling a used brine solution for regeneration of an anion exchange process for perchlorate and nitrate removal, Lehman et al. (2008) monitored leakage after each run as the continually-recycled brine solution's perchlorate concentration increased. Using the equilibrium multi-component theory (EMCT) program developed by the University of Houston, Lehman et al. (2008)'s study predicted an increase in perchlorate leakage as perchlorate concentration in the brine solution increased. Alternative regeneration solutions like seawater can also yield unwanted leakage due to the high composition of additional ionic species.

Potable Water Applications of Ion Exchange

Ion exchange is a water treatment process commonly used for water softening or demineralization, but it is also used to remove other substances from aqueous solutions in processes such as dealkalization and deionization. Cation exchange is an IX process used in water treatment to remove positively charged ions from water sources. A common applied use of CIX in potable water treatment includes the removal of dissolved calcium and magnesium ions that contribute to hardness in water (Wachinski, 2006). Although Ross (1927) attributes the IX phenomena to Aristotle, Thompson (1850) and Way (1850) were the first to recognize the exchange properties

of water flowing through soils. However, the technology would not be applied to water treatment until the early 1900's when Gans (1905) discovered that water could be softened using zeolite materials. In the mid 1900's, a sulphonated polystyrene cation exchange resin was invented by D'alelio (1942) and forms the basis of today's SAC resin for hardness removal.

Anion exchange is an IX process used in water treatment, targeting negatively charged ionic species in water. Invented 5 years after modern sulfonated polystyrene CIX, a polystyrene anion exchange resin was developed in 1947 by McBurney (1952) in the United States, incorporating the amine functional group that is seen in today's treatment applications of AIX

Calcium and Magnesium

Florida groundwater contains elevated calcium and magnesium concentrations, generally ranging between 120 and 180 mg/L as calcium carbonate and deemed "hard" water (USDOI & USGS, 2016). A fair amount of research has been documented related to enhancing and refining the use of cation exchange for the removal of calcium and magnesium ions from water sources (Domaine et al., 1943; Kearney & Rearick, 2003; Kumar & Jain, 2013; Millar et al., 2014). Recent literature on cation exchange has shifted focus to understanding the interactions that take place between divalent cations, such as calcium and magnesium, and organic matter (Adusei-Gyamfi et al., 2019). Organic matter appears to have negligible effects on the exchange of divalent cations in water when equivalence concentrations of the targeted cation species are much greater than that of the organic matter (Indarawis & Boyer, 2012). Studies of removing cations and organic matter are becoming more relevant as IX processes can incorporate combined IX, comprising both CIX resin and AIX resin in the same system for the simultaneous removal of hardness and organics.

Sulfate and Organics

Because proportions of NOM contain carboxylic acid groups, the organic molecules can carry a negative charge in water, allowing them to be removed by AIX (Comstock & Boyer, 2014). AIX has been shown to be a competitive treatment process in terms of operation and cost for the removal of NOM from drinking water sources (Hongve et al., 1999). Understanding the composition of NOM has been studied to further identify which types of organic matter carry negative charges and are optimal for removal through AIX. Recently, Levchuck et al. (2018) reviewed the increased interest of NOM in the scientific community, evaluating water treatment methods for removal and identifying the different acids, neutrals and bases of NOM. Approximately 60 to 90% of NOM, found in potable water sources carry a negative charge, allowing them to be removed by AIX (Bolto et al., 2004). Bolto et al. (2004) also displayed the evaluation of 19 different SBA resins for their ability to reduce NOM.

In addition to NOM removal, AIX can be used to remove targeted inorganic ionic species in water, such as sulfate, nitrate, perchlorate, phosphate, hexavalent chromium, fluoride, chloride, bromide and others. Potable water sources for drinking water and wastewater treatment contain a spectrum of different anionic species that can compete for space on an AIX resin, limiting a resins ability to remove a specific constituent. Vaaramaa & Lehto (2003) studied the removals of cations and anions using CIX and AIX resins, respectively, from a ground water source, demonstrating competition between ionic species for exchange space on the resin. Removing specific inorganic ionic species requires synthesizing of the AIX resin to be selective toward a particular ion to reduce competition of other aqueous ionic species that may be found in the water matrix. Chubar (2011) developed methods for synthesizing AIX resin to target arsenate while lowering the resins affinity

for competing anionic contaminants that were also present in the water stream. Similar processes have been studied for the selective removal of fluoride (Emaraa et al., 2017), phosphate (Chubar et al., 2005), nitrate (Samatya et al., 2006), hexavalent chromium (Korak et al., 2017; Piazzoli & Antonelli, 2018), and bromide (Boyer & Singer, 2006; Hsu & Singer, 2010; Walker & Boyer, 2011); however, further research is needed to understand the impact of affecting factors in water, such as sulfate (Ye et al., 2012).

Sulfate has been studied for its affects as a competing anion during the targeted removal of NOM. It has been shown that NOM removal decreases when sulfate concentrations increase, demonstrating that sulfate is a competing anion to NOM during AIX processes (Wang et al., 2012; Phetrak et al., 2012; Ates & Incetan, 2013). Polyacrylic AIX resins with close spacing functional groups, such as trimethylamine, have been shown to favor hydrophilic substances such as sulfate (Hu et al., 2016). Sulfate has also been studied for its role in corrosion. Chloride-form anion exchange resin tends to increase the chloride-to-sulfate mass ratio (CSMR) due to release of chloride and uptake of sulfate, and thus has the potential to increase the corrosivity of treated water towards lead. Research has shown that an increase in the CSMR can increase lead corrosion in water distribution systems (Edwards and Triantafyllidou 2007). Ishii & Boyer (2011) used the CSMR to monitor corrosion and found that AIX processes increased the CSMR in the distribution system, increasing corrosion potential. Willison & Boyer (2012) also found that higher concentrations of sulfate and chloride significantly increased the release of lead in the distribution system. It appears that a limited amount of research has been performed to understand the kinetics and equilibrium of sulfate removal as it pertains to AIX when treating a potable water source. A good portion of the research that has been reported has been dedicated to the understanding of the

selectivity and kinetic behavior of AIX when removing nitrate with solutions spiked with competing anions (Samatya et al., 2006); kinetic, equilibrium, and thermodynamics of bromide have also been investigated using AIX on known concentrations of bromide diluted with distilled water (Ding et al., 2012). Tan et al. (2018) recently studied the equilibrium and kinetics of selenate and sulfate removal through AIX with single and binary anion solutions. Nonetheless, a fundamental understanding of the factors that occur during regeneration of anion exchange resins targeting the removal of sulfate from groundwater remains lacking.

Alternative Regeneration Methods

Regeneration involves the replacement of the original presaturant ion onto the IX resin and eluting the previously targeted ion off the exhausted resin. This is accomplished by running a high concentration solution of the original presaturant ion across the resin. As displayed in Table 3, typical presaturant ions for IX processes in water treatment are sodium, hydrogen, chloride, and hydroxide. Chloride-form resin can pose challenges to the regeneration process, whereby a high ionic strength sodium chloride solution (i.e., brine) is used to regenerate the resin, resulting in IX waste disposal limitations and chloride ion release to finished water (Hu & Boyer, 2017).

Alternative brine methods have been investigated. Brine solutions can be reused for multiple regenerations in certain instances, saving on costs and reducing brine waste. The ability of the brine solution to regenerate an IX process decreases after each regeneration use as it begins to decrease in the presaturant ion and increase in the previously targeted ion. Medina et al. (2018) studied the efficiencies of regenerating a magnetic ion exchange (MIEX) system for dissolved organic carbon (DOC) removal in the chloride form using a fresh brine solution, reused brine

solution, and a treated reused brine solution for brine management options. Studies have also been accomplished with regards to regenerating IX resin through multiple stages of different strength brine solutions (Korak et al., 2017). In addition to reuse and multiple stage regeneration, Maul et al. (2014) compared the use of sodium chloride, potassium chloride, sodium bicarbonate, and potassium bicarbonate for their regeneration efficiencies and their overall impact in terms of a life cycle assessment (LCA).

Based on the foregoing discussion, it appears that there has been minimal research on utilizing alternative brine streams for regeneration. In coupled hybrid IX-RO applications, RO waste brines have been successfully used as regenerant streams for the IX pretreatment process (Venkatesan & Wankat, 2011; Zhu et al., 2011). Though alternative brine streams are rarely applied, IX processes are regularly found in conjunction with brine related water matrices, such as seawater. Newer research has demonstrated the removal of contaminants from seawater using IX: magnesium (Tang et al., 2018), carbon dioxide (Willauer et al., 2010), boron (Alharati et al., 2017; Darwish et al., 2015; Jung & Kim, 2016), lithium (Arroyo et al., 2019; Chen et al., 2017), and strontium (Koshy & Pathak, 2020). Documentation regarding the application of seawater as an alternative regenerant stream for IX is scarce. Wilf et al. (1980) experimented with seawater taken from the red sea to regenerate a CIX system for calcium removal, resulting in a feasible implementation of the process. Muraviev et al. (1997) also experimented with seawater as a regenerant solution for a CIX system removing copper from acidic mine waters. The performance and impacts of seawater regeneration for AIX processes, notably potable water production applications, remains unclear. Coastal water utilities employing IX might benefit from seawater regeneration; however, further research is needed to identify performance efficiency and secondary impacts that may arise.

Brominated Disinfection By-Products in Potable Water Production

Chemical disinfectants and oxidants are used in water treatment to control microbial growth and to kill/inactivate pathogens and viruses. Many public water systems add a disinfectant to the water; the CITY adds chlorine for primary and secondary disinfection purposes. In Florida, the monitoring of disinfectant residuals is regulated by the Florida Department of Environmental Protection per Chapter 62-550.514 of the Florida Administrative Code (2011) that mandates that a residual be maintained throughout the distribution system at no less than 0.2 mg/L. It is well known that chemical disinfectants and oxidants used in water treatment form DBPs when in contact with NOM and other types of inorganic material (Crittenden et al., 2005; Lange & Kawczynski, 1978; Rook, 1974). It is known that bromide reacts with NOM and disinfectants to form brominated DBPs (Ackerson et al., 2020; Cooper et al., 1985; Liu et al., 2011; Richardson et al., 1999). It is also established that brominated DBPs carry higher health associated risks, correlating to higher cytotoxicity and genotoxicity than chlorinated DBPs (Kolb et al., 2017; Richardson et al., 1999; Sharma et al., 2014; Yang et al., 2014; Zhai & Zhang, 2011; Zhai et al., 2014). However, when compared to chlorinated DBPs, studies on brominated DBPs are less prevalent (Zhang & Yang, 2018).

Although over 600 DBPs have been identified in drinking water, only a few by-products are regulated under the SDWA (Hrudey, 2009). Among them are total trihalomethanes (TTHMs), regulated as the cumulative total of four specific by-products at 80 μg/L, and haloacetic acids (HAA5s), regulated as the cumulative total of five specific by-products at 60 μg/L. Table 4 displays the regulated by-products for each class and their molecular composition.

Table 4: Regulated Disinfection By-Products

Class	By-Product	Compound
TTHMs	Trichloromethane (chloroform)	$CHCl_3$
	Bromodichloromethane	$CHCl_2Br$
	Dibromochloromethane	$CHClBr_2$
	Tribromomethane (bromoform)	$CHBr_3$
HAA5s	Monochloroacetic Acid	$C_2H_3O_2Cl$
	Dichloroacetic Acid	$C_2H_2O_2Cl_2$
	Trichloroacetic Acid	$C_2HO_2Cl_3$
	Monobromoacetic Acid	$C_2H_2O_2Br$
	Dibromoacetic Acid	$C_2H_2O_2Br_2$
Bromate	Bromate	BrO_3^-
Chlorite	Chlorite	ClO_2^-

As presented in Table 4, six regulated DBPs contain bromide, making it an important parameter in DBP formation (Richardson et al., 1999; Heeb et al., 2014). Ding et al. (2012) demonstrated the adsorption ability of MIEX resin to remove bromide from raw water to reduce brominated DBPs. Similarly, Soyluoglu et al. (2020) recently investigated the use of bromide-selective IX resins for the removal of bromide to reduce DBPs. Not only does bromide contribute to increased DBPs, it also shifts the type of DBP species that are formed; decreasing chlorinated DBP species as brominated DBP species increase (Dyck et al., 2015; Kolb et al., 2017; Richardson et al., 1999).

Seawater contains bromide, thus leading to potential increased amounts of bromide in treated water. Szczuka et al. (2017) and Liu et al. (2018) identified brominated DBP formation from a saline water source due to elevated levels of bromide. Ged & Boyer (2014) also investigated the correlation between seawater intrusion and increased brominated DBPs. Additional research is needed to investigate the impacts of bromide leakage from AIX seawater regeneration on brominated DBP formation when a disinfectant is added.

CHAPTER 3: MATERIALS AND METHODS

Bench-Scale Column Testing

The performance and impacts of regenerating an AIX process with seawater while targeting the removal of sulfate from groundwater was investigated at the bench-scale using small-scale columns. Varied salt concentrations were added to Sarasota Bay seawater and used as regenerant solutions to assess the effects of increased chloride concentrations on the regeneration process when compared to the manufacturer-recommended 10 % (by volume) salt method. The objectives during column testing were as follows:

1. Investigate the performance of AIX to remove sulfate and NOM during regeneration activities using seawater, and salt-supplemented seawater, conditions.
2. Assess the secondary impacts of regenerating an AIX process with seawater, and salt-supplemented seawater solutions.

Bench-Scale Equipment

An AIX bench-scale column unit was constructed to evaluate the performance and impacts of seawater regeneration. The bench unit was operated using a parallel four-column design using *DWK Life Sciences*™ (1501 North 10th Street Millville, New Jersey) *Kontes*™ *FlexColumn*™ chromatography columns, constructed of 15 mm diameter borosilicate glass with luer-lock polypropylene inlet and outlet fittings containing a 20 μm polyethylene bed support disc for media retention, were employed for column testing experiments. Inlet and outlet fittings were equipped with *Cole-Parmer*™ (625 East Bunker Court Vernon Hills, Illinois) polypropylene stopcock

tubing adaptors for flow-rate adjustment. Additional media support was provided by a 5 cm layer of 3 mm diameter glass beads, housed above the 20 μm polyethylene bed support disc. A *Cole Palmer™ Masterflex®* peristaltic pump, attached with an extended four-roller adaptable pump head, and four *Click'n'go™* adjustable occlusion minicartridges, provided flow to each column in parallel. *Masterflex L/S® Precision* pump tubing was connected to *Thermo Scientific™* (168 Third Avenue Waltham, Massachusetts) *Nalgene® 180 Clear Plastic PVC* tubing and used to transport feed solutions from a 20 L cylindrical *Nalgene®* storage tank through the peristaltic pump and into each column. Figure 4a displays a picture of the column arrangement and Figure 4b exhibits the solution storage, tubing, and pumping configuration used throughout column testing. A desiccator was used to properly dry the anion resin prior to column loading.

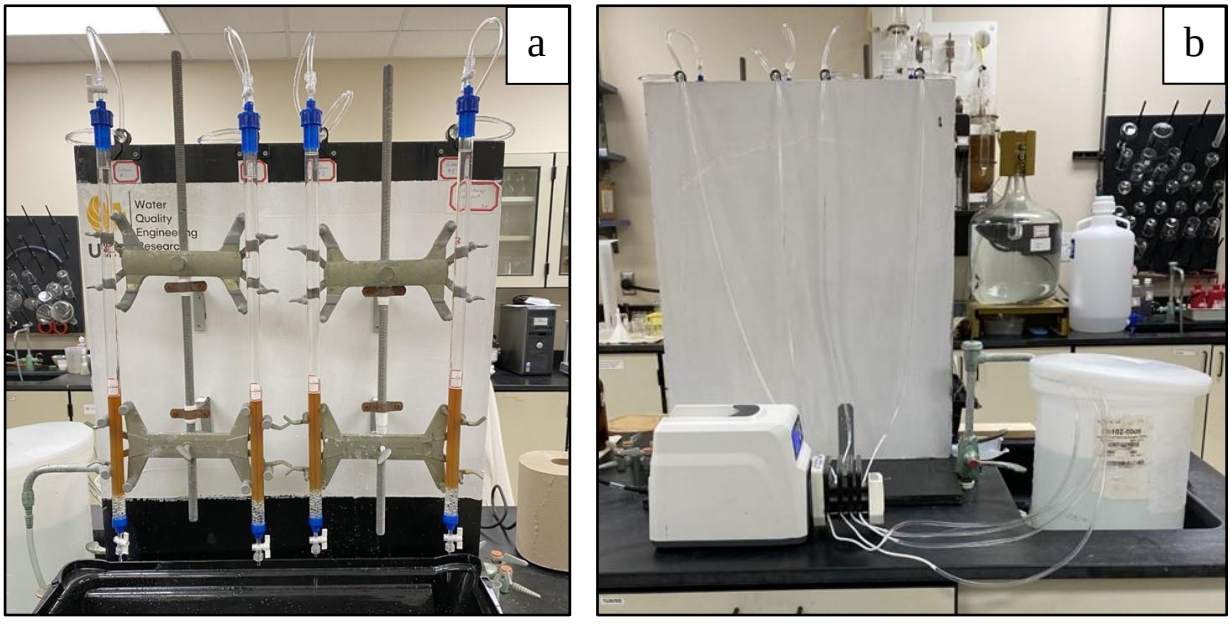

Figure 4: Bench-Scale AIX Column Unit (4a); Peristaltic Feed Pump (4b)

Water Quality and Reagents

Table 5 presents a listing of values for a number of parameters that describe the quality of the Verna groundwater and Sarasota Bay. Significant differences are noted between the two different waters, except listed pH and temperature components.

Table 5: Average Experimental Water Quality

Parameter	Units	Aerated Verna Groundwater	Sarasota Bay Seawater
pH	s.u.	7.83	7.83
Temperature	°C	25.3	25.3
Conductivity	μS/cm	992	47,400
Turbidity	NTU	0.613	2.24
ORP	mV	+174	+100
Alkalinity	mg/L as $CaCO_3$	113	103
DOC	mg/L	1.77	< 0.25
UV-254	cm^{-1}	0.047	0.029
TDS	mg/L	821	33,600
TSS	mg/L	1.88	64
Sulfate	mg/L	597	3,520
Chloride	mg/L	27.3	18,600
Bromide	mg/L	< 0.2	81.3
Fluoride	mg/L	< 0.5	< 0.1
Calcium	mg/L	126	344
Magnesium	mg/L	60.2	1,150
Sodium	mg/L	13.5	9,710
Potassium	mg/L	2.46	4,100
Strontium	mg/L	21.8	5.89
Silica	mg/L	25.7	< 0.005

The CITY's aerated Verna groundwater was used as the feed solution during column operations. Bulk samples of Verna groundwater were collected in 15-gallon plastic drums from the CITY's WTF and transported to UCF, where they were stored at 4°C prior to use. Sulfate concentrations of the Verna feed water ranged from 583 mg/L to 626 mg/L, equating to an equivalent strength of

approximately 12.1 meq/L to 13.0 meq/L. In addition to removing sulfate, AIX resin has the affinity to exchange with negatively charged organics, reducing sulfate removal efficiency. DOC of the Verna groundwater averaged 1.77 mg/L, with an average UV-254 reading of 0.047cm^{-1}. Bulk Verna groundwater samples also contained an average of 1.88 mg/L of total suspended solids (TSS), possessing the potential to interfere with the AIX resin bed.

The SBSW was utilized during the regeneration process. Bulk samples of SBSW were collected in 15 gallon plastic drums, from the CITY's WTF and transported to UCF, where they were stored at 4°C prior to use. Samples were warmed to room temperature, around 25.3°C, before use as a regenerant solution. Conductivity values of SBSW ranged between 44.3 mS/cm and 49.5 mS/cm, with an average total dissolved solids (TDS) concentration of 33,600 mg/L. Chloride concentrations in SBSW averaged 18,600 mg/L, making it an attractive option for regeneration purposes; however, SBSW also contained 3,520 mg/L of sulfate and 81.3 mg/L of bromide, both carrying the potential to act as competing anions to chloride. Additionally the filtered SBSW also contained approximately 64 mg/L of TSS, possessing the potential to interfere with the AIX resin bed.

In order to investigate the performance and impacts of SBSW regeneration, four different regenerant solutions were prepared and tested. Figure 5 outlines the composition of each regenerant solution. Solutions were prepared in 1 L volumetric flasks as shown in Figure 6 using SBSW, distilled water, and sodium chloride (NaCl). *Pinch-a-Penny*® (PO Box 6025 Clearwater, Florida) *Salinity Fine Grain Pool Salt* was used for NaCl addition, consisting of >99% sodium chloride purity and certified United States Pharmacopeial Convention (USP) Grade salt.

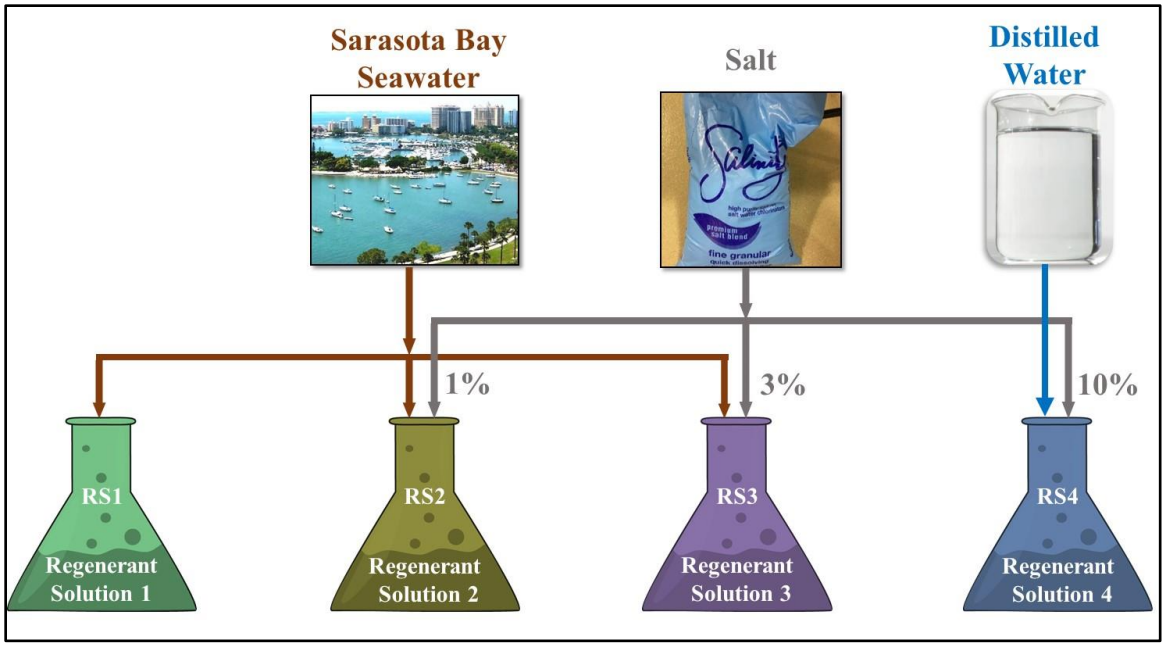

Figure 5: Regenerant Solution Compositions

Figure 6: Regenerant Solutions

Regenerant solution 1 (RS1) consisted of SBSW. Regenerant solution 2 (RS2) consisted of SBSW with the addition of 1% (by volume) NaCl, approximately 10 g/L. Regenerant solution 3 (RS3) consisted of SBSW with the addition of 3% (by volume) NaCl, approximately 30 g/L. Regenerant solution 4 (RS4) modeled conventional salt regeneration, containing 10% (by volume) NaCl; approximately 100 g/L in distilled water. Solutions were then transferred to 500 mL Erlenmeyer flasks prior to use. Table 6 presents the average pH and conductivity of each regenerant solution.

Table 6: Regenerant Solution Water Quality

Regenerant Solution	pH (s.u.)	Conductivity (µS/cm)
RS1	7.83	47,400
RS2	7.83	62,200
RS3	7.73	83,300
RS4	7.01	125,000

Thermax (Pune, India) Tulsion® A-32 (A-32) anion resin (Figure 7) was chosen for column testing operations because of its attractive resin characteristics for the application of removing sulfate and delineating the performance and impacts of seawater regeneration. The A-32 resin is a SBA Type-2 resin in the chloride form, comprised of a polystyrene copolymer matrix structure with quaternary ammonium functional groups and wields a theoretical exchange capacity of 1.3 eq/L, capable of handling the high sulfate loading from Verna groundwater. Table 7 outlines the resin characteristics of the A-32 anion resin.

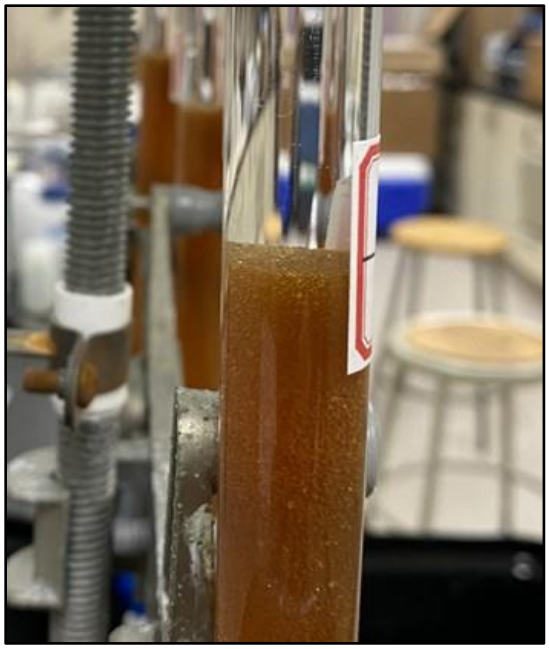

Figure 7: *Thermax Tulsion*® A-32 Anion Resin Contained in the Laboratory Column Set-up

Table 7: *Thermax Tulsion*® A-32 Anion Resin Characteristics

Resin Characteristic	**Thermax Tulsion® A-32**
Type	Strong Base Type 2
Matrix Structure	Polystyrene Copolymer
Functional Group	Quaternary Ammonium
Physical Form	Moist Spherical Beads
Ionic Form	Chloride
Screen Size USS (wet)	16 to 50
Particle Size (mm)	0.3 to 1.2
Total Exchange Capacity (eq/L)	1.3
Swelling (%)	12
Moisture Content (%)	44 to 50
Backwash Settled Density (g/L)	690 to 720
Maximum Operating Temperature	60°C (140°F)
pH Range	0 to 14
Solubility	Insoluble in all common solvents

Bench-Scale Experimental Procedures

A total of four operational runs (R1 through R4) and three regeneration cycles (Reg1 through Reg3) were carried out over the course of column testing to elucidate the performance and impacts of seawater-based regeneration when compared to manufacturer-recommended, 10 % (by volume) salt, regeneration methods. Each run consisted of four columns (Column 1 through Column 4) operating in parallel, treating Verna groundwater in a co-current flow configuration. Each regeneration cycle consisted of Column 1 through Column 4 undergoing regeneration in a counter-current flow configuration, each column receiving a different regenerant solution.

R1 consisted of a preliminary operational run, intended to exhaust the resin bed and exchange initial solid-phase ions with aqueous ions in the Verna groundwater. Operational runs were performed three times (R2 through R4), with a regeneration cycle between each run (Reg1 through Reg3). Column 1 was consistently regenerated using RS1, Column 2 was consistently regenerated using RS2, Column 3 was consistently regenerated using RS3, and Column 4 was consistently regenerated using RS4. Figure 8 denotes the order of operational runs and regeneration cycles.

Figure 8: Column Testing Experimental Order

Prior to the start of operations, each column was loaded with 11 g of dry anion resin to a resin bed depth of approximately 16.7 cm. Virgin anion resin was first dried in a desiccator for a minimum of 24 hours and weighed using an analytical balance to an accuracy of one hundredth of a gram. Dried anion resin was then mixed with distilled water and added in the form of resin “slurries” to

each of the four columns. After column loading, a 5-minute backwash cycle was performed on each column to evenly distribute the virgin resin bed. The backwash cycle was performed at a flowrate of 20 mL/min, in a counter-current flow configuration, using distilled water. Verna groundwater was poured into a 20 L *Nalgene*™ cylindrical tank and allowed to warm to room temperature, approximately 25.3°C, prior to column operations. Tubing was primed with Verna groundwater and adjusted to a targeted flowrate of 20 mL/min, equating to a surface loading rate (SLR) of 2.8 gpm/ft^2. A list of bench-scale operating parameters can be found in Table 8.

Table 8: Bench-Scale Column Operating Parameters

Parameter	Value
Flowrate (mL/min)	20
Column Diameter (mm)	15
Total Bed Height Per Column (mm)	167
Bed Volume Per Column (mL)	29.5
Surface Loading Rate (mm^3/min-mm^2)	113
Volumetric Loading Rate (mm^3/min-mm^3)	0.70
Empty Bed Contact Time Per Column (min)	1.47

During R1 through R4, columns were operated in parallel over a 5-hour period to obtain sufficient exhaustion of the resin beds. A sample of Verna groundwater was collected at the initiation of each operational run whereas effluent samples were collected from each column at time intervals specified in Table 9.

Table 9: Column Sample Frequency

Sample No.	Time (hrs)	Bed Volumes (BV)
1	0	0
2	1.0	40.8
3	2.0	81.5
4	2.5	102
5	3.0	122
6	3.5	143
7	4.5	183
8	5.0	204

During Reg1 through Reg3, columns were regenerated individually at a flowrate of 40 mL/min in a counter-current flow configuration until effluent conductivity values matched regenerant solution values, approximately 18-20 minutes. Conductivity values were measured every 2 minutes using a *Hach*® (PO Box 389 Loveland, Colorado) *HQ 40d* field probe. A rinse cycle, consisting of distilled water, was performed on each column after regeneration to remove saturated ions from the resin bed. Rinse cycles were executed at a flowrate of 40 mL/min in a counter-current flow configuration until effluent conductivity values dropped below 100 μS/cm, approximately 6-8 minutes.

Bench-Scale Sample Preparation and Data Analysis

Samples were collected in 125 mL polyethylene bottles and filtered using a 0.45 micron *MilliporeSigma*™ (400 Summit Drive Burlington, Massachusetts) mixed cellulose ester membrane. Dilutions, where appropriate, were made using high purity *Fisher Scientific NERL* water. Anion analysis was performed using a *Dionex ICS-1100* ion chromatograph, depicted in Figure 9. DOC samples were measured using a *Teledyne Tekmar Total Organic Carbon Fusion*

UV/Persulfate Analyzer, pictured in Figure 10. Additional organic measurements were taken with a *Hach® DR 5000™ UV-Vis* spectrophotometer, displayed in Figure 11. Samples were executed in accordance with *Standard Methods for the Examination of Water and Wastewater* (Baird et al., 2017) during instrument analysis. Appendix B provides a list of the methods, required equipment, and method detection levels of each pertinent water quality parameter.

Figure 9: Dionex ICS-1100 Ion Chromatograph

Figure 10: Teledyne Tekmar Total Organic Carbon Fusion UV/Persulfate Analyzer

Figure 11: Hach® DR 5000™ UV-Vis Spectrophotometer

Instrument data was analyzed using *Microsoft*® (1 Microsoft Way Redmond, Washington) *Excel* to build breakthrough/exhaustion curves and constituent graphs depicting removal/elution rates of constituents. Instrument data was used to calculate breakthrough/exhaustion times, exchange capacity, specific throughput, ion leakage, and other operational parameters to assess changes in column performance from different seawater-based regeneration methods.

Jar Testing

Batch jar testing was carried out to explore the equilibrium and kinetic relationship between chloride and bromide in an AIX regeneration process. Synthetic solutions using distilled water, spiked with bromide and varying salt concentrations, and SBSW, were added with AIX resin for the determination of equilibrium values, kinetic rates, and rate-controlling mechanisms. The objectives of jar testing experiments were as follows:

1. Identify equilibrium, kinetics, and rate-controlling steps of bromide in an AIX process.
2. Assess changes to equilibrium, kinetics, and rate-controlling steps of bromide in the presence of high chloride concentrations.
3. Determine the amount of bromide exchanged onto AIX resin at equilibrium from a seawater matrix, and at what rate compared to water matrices containing lower concentrations of chloride.

Jar Test Equipment

A *Phipps & Bird™ PB-900* programmable jar tester (Figure 12a) capable of mixing six jars in parallel was used to explicate the equilibrium and kinetics of bromide adsorption in the presence of chloride. Six *Phipps & Bird™ B-KER2* square, acrylic, 2 L jar testing jars (Figure 12) were used, containing 1 L solutions. A constant mixing speed of 100 rpm was maintained during experiments. Ding et al. (2012) identified 100 rpm as an optimum stirring speed at a solution volume of 1L. Each testing jar was equipped with a sample port, located at the 500 ml mark, and was used to obtain samples during analysis. A 20 L *Nalgene™* cylindrical tank, housed on top of a magnetic

stirring plate, was used to consistently mix solutions prior to jar testing. The magnetic stirring plate was set to a stable mixing speed as solutions were added and allowed to mix.

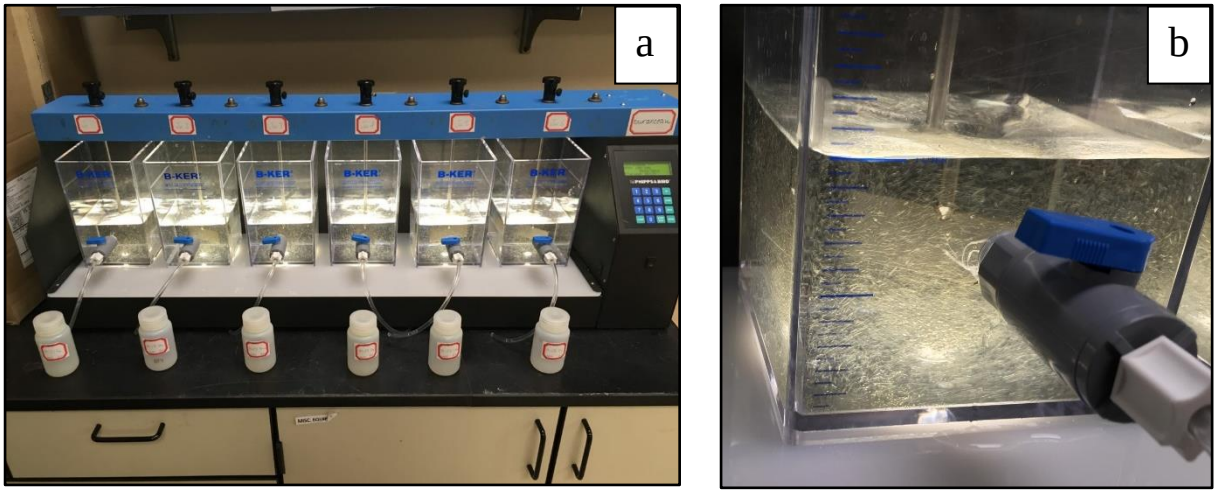

Figure 12: *Phipps & Bird™ PB-900* Jar Tester (12a); *Phipps & Bird™ B-KER2* Square, Acrylic, 2 L Jar (12b)

Water Quality and Reagents

Solutions of varying salt strengths, spiked with bromide, were synthesized with distilled water and used throughout jar testing experiments. Figure 13 outlines the different solution compositions. *Salinity Fine Grain Pool Salt* was used for NaCl addition, consisting of >99% sodium chloride purity and certified USP Grade salt. *Alfa Aesar™*, 99.9% (metals basis) purity, lithium bromide (LiBr) anhydrous was used to achieve desired bromide concentrations. NaCl and LiBr were weighed using an analytical balance and mixed with distilled water in 2 L volumetric flasks. The SBSW was also utilized during jar testing experiments. Bulk samples were collected in 15 gallon plastic drums, from the CITY's WTF and transported to UCF, where they were stored at 4°C prior

to use. Samples were warmed to room temperature, around 25.3°C, before use. A full list of the average SBSW quality can be found in Table 5.

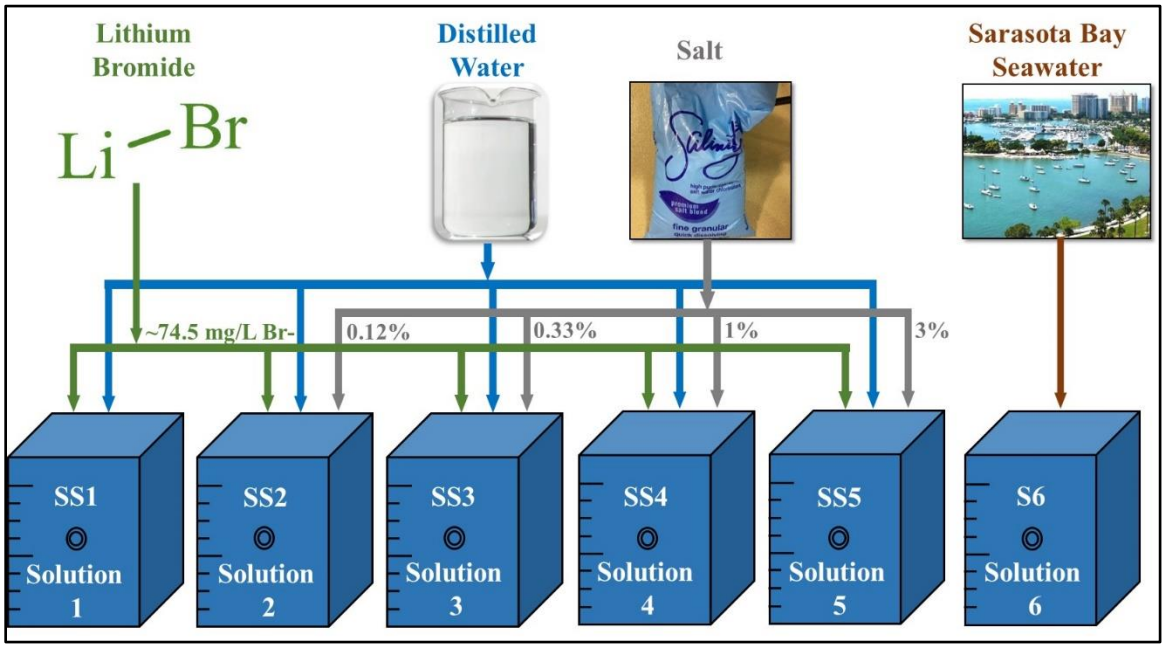

Figure 13: Synthetic Solution Compositions

Synthetic solution 1 (SS1) consisted of distilled water, spiked with lithium bromide anhydrous to a bromide concentration of approximately 71.5 mg/L. Synthetic solution 2 (SS2) consisted of distilled water, 72.3 mg/L bromide, and 0.12% (by volume) of NaCl. Synthetic solution 3 (SS3) consisted of distilled water, 71.0 mg/L bromide, and 0.33% (by volume) of NaCl. Synthetic solution 4 (SS4) consisted of distilled water, 77.3 mg/L bromide, and 1% (by volume) of NaCl. Synthetic solution 5 (SS5) consisted of distilled water, 80.1 mg/L bromide, and 3% (by volume) of NaCl. Solution 6 (S6) consisted of SBSW. Solutions were synthesized and tested at room temperature, approximately 25.3°C. Table 10 presents the water quality of each solution used during jar testing experiments.

Table 10: Solution Water Quality

Solution	pH (s.u.)	Conductivity (μS/cm)	Chloride (mg/L)	Bromide (mg/L)	Cl-/Br- Ratio (mg/l)	rCl-/Br- Ratio (M)
SS1	5.72	999	0	71.5	0	0
SS2	5.75	2,350	702	72.3	9.71	21.9
SS3	5.62	5,620	1,840	71.0	25.9	58.4
SS4	5.78	15,400	5,410	77.3	70.0	158
SS5	5.98	47,400	17,800	80.1	222	496
S6	7.79	50,500	18,900	77.2	245	553

Thermax Tulsion® A-32 anion resin (Figure 7) was retained for use during jar testing experiments because of its useful implementation in potable water applications for removing negatively charged ionic constituents. *Thermax Tulsion® A-32* is a SBA Type-2 resin in the chloride form, comprised of a polystyrene copolymer matrix structure with quaternary ammonium functional groups. *Thermax Tulsion® A-32* wields a theoretical exchange capacity of 1.3 eq/L. Table 7 outlines the resin characteristics of *Thermax Tulsion® A-32* anion resin.

Jar Test Experimental Procedures

A total of 18 experiments (Exp1 through Exp18) were carried out during jar testing procedures. Five synthetic solutions (SS1-SS5) and SBSW (S6) were evaluated, in triplicate, for AIX bromide equilibrium and kinetics. Each experiment consisted of six (consistently mixed) jars operating in parallel until AIX equilibrium was achieved, approximately two hours. Samples were collected at periodic time intervals and analyzed for changes in bromide concentration. Figure 14 outlines the order of experiments.

.

SS1	SS2	SS3	SS4	SS5	S6
• Exp1 • Exp2 • Exp3	• Exp4 • Exp5 • Exp6	• Exp7 • Exp8 • Exp9	• Exp10 • Exp11 • Exp12	• Exp13 • Exp14 • Exp15	• Exp16 • Exp17 • Exp18

Figure 14: Jar Testing Experimental Order

Experiments were performed in triplicate for each tested solution. Prior to the start of Exp1 through Exp3, 20 L of SS1 was synthesized in a *Nalgene*™ cylindrical tank and mixed using a magnetic stirring plate set to a stable mixing speed. A sample of SS1 was collected and used as the starting sample for Exp1 through Exp3. Exp1 began by filling each of the six jars with 1 L of SS1 and set to a mixing speed of 100 rpm. 5 g of dried *Thermax Tulsion® A-32* anion resin was then added simultaneously to each jar and mixed for two hours. Samples were collected from Jar's one through six at 5 min, 10 min, 20 min, 40 min, 60 min, and 120 min respectively. Exp2 and Exp3 were carried out in the same fashion. The procedure for Exp1 through Exp3 was then repeated for each solution, resulting in triplicate samples of each time interval.

Jar Test Sample Preparation and Data Analysis

Samples were collected in 125 mL polyethylene bottles and filtered using a 0.45 micron *MilliporeSigma*™ mixed cellulose ester membrane. Dilutions, where appropriate, were made using high purity *Fisher Scientific NERL* water. Anion analysis was performed using a *Dionex ICS-1100* ion chromatograph, depicted in Figure 9. Samples were executed in accordance with the *Standard Methods for the Examination of Water and Wastewater* (Baird et al., 2017) during

instrument analysis. Appendix B provides a list of the methods, equipment, and method detection levels of each pertinent water quality parameter.

Instrument data was analyzed using *Microsoft® Excel* to evaluate changes in bromide concentration over time. Adsorption rates were graphed and fitted to various rate equations. Adsorption values and rate constants were derived from best fit rate equations. Equilibrium constants, selectivity coefficients, and separation factors were developed from instrument data to demonstrate bromides affinity for AIX resin in the presence of varying chloride concentrations.

Disinfection By-Product Formation Chemistry

Experiments were conducted with the CITY's aerated Verna groundwater, spiked with various bromide concentrations, to assess changes in DBP formation and speciation. Bromide concentrations observed in the effluent samples of column testing experiments were applied in attempts to correlate the impacts of bromide elution from seawater-based regeneration to DBP formation. Free chlorine was used as a disinfectant, simulating post treatment operations of potable water production. Samples were incubated for up to 4 days and analyzed for TTHM formation potential, 4-day HAA5 concentration, and chlorine residual. The objectives of DBP formation experiments were as follows:

1. Assess changes to TTHM formation when bromide concentration is varied.
2. Illuminate shifts in DBP speciation when bromide concentration is varied.
3. Correlate brominated DBP formation impacts to seawater-based regeneration methods.

Equipment for DBP Experiments

Bench-scale equipment was used to investigate the changes in DBP formation from various bromide concentrations. A 3 L glass beaker situated on a magnetic stirring plate, set to a constant stirring speed, was used to mix different groundwater solutions. A 2 L volumetric flask was used to dose aqueous sodium bromide (NaBr) into Verna groundwater. 60 ml glass amber bottles were used for TTHM and chlorine samples, 125 ml plastic bottles were used for solution samples, and 40 ml glass amber vials were used for HAA5 samples. Figure 15 displays a picture of bench-scale dosing experiments.

Figure 15: Bench-Scale Dosing Experiments

Water Quality and Reagents for DBP Experiments

The CITY's aerated Verna groundwater was used during DBP formation experiments. Bulk samples of Verna groundwater were collected in 15-gallon plastic drums, from the CITY's WTF and transported to UCF, where they were stored at 4°C prior to use. The Verna groundwater contained an average of 1.77 mg /L of DOC and an average UV-254 reading of 0.047 cm^{-1}.

Additional data regarding the average Verna groundwater quality was presented previously in Table 5. Bromide concentrations were achieved by dosing Verna groundwater with known volumes of *SPEX CertiPrep™, 1000 μg/mL, Bromide Standard for Ion Chromatography* solution, in the form of NaBr. Chlorine addition was accomplished by adding known volumes of a sodium hypochlorite stock solution. Quenching agents were used to prevent further TTHM and HAA5 formation in samples during hold times between sample collection and analysis. 10 g of sodium sulfite anhydrous was dissolved in 100 mL of distilled water and used to quench TTHM samples. 5 g of ammonium chloride anhydrous was dissolved in 100 mL of distilled water and used to quench HAA5 samples.

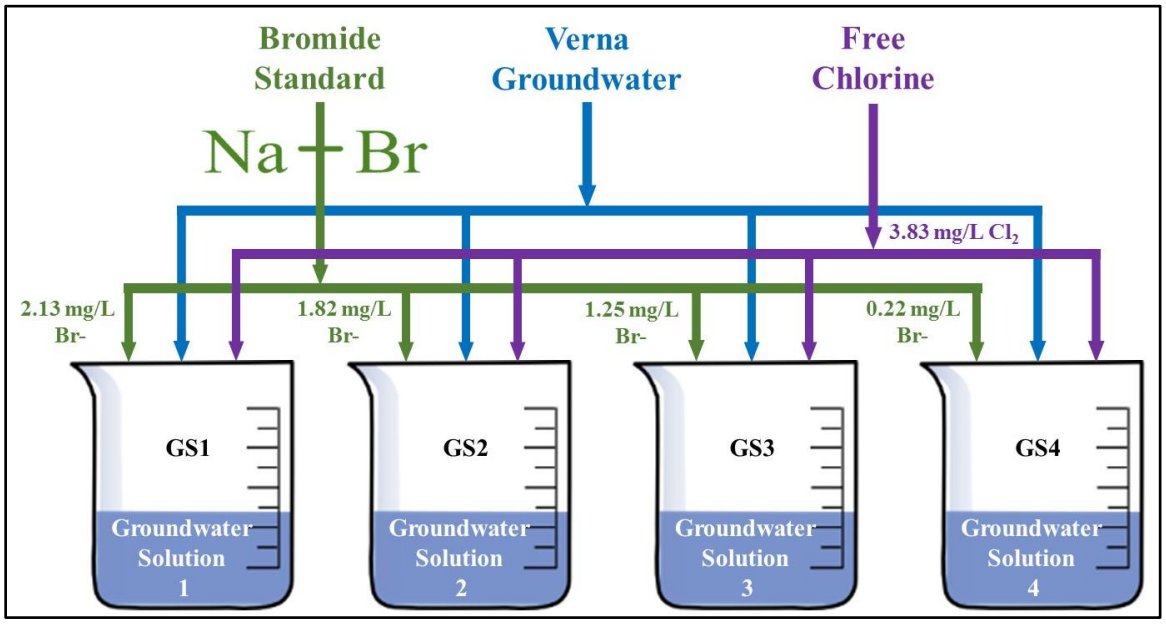

Figure 16: Groundwater Solution Compositions

Each groundwater solution was spiked with a different concentration of bromide, outlined in Figure 16. Bromide concentrations were chosen from the average bromide elution concentration

observed during column testing of each column. Column testing identified that NaCl addition to SBSW decreased bromide exchange during regeneration, subsequently reducing bromide elution. Groundwater solution 1 (GS1) contained aerated Verna groundwater and 2.13 mg/L bromide, correlating to the average bromide elution concentration observed in samples from Column 1. Groundwater solution 2 (GS2) contained aerated Verna groundwater and 1.82 mg/L bromide, corresponding to the average bromide elution concentration observed in samples from Column 2. Groundwater solution 3 (GS3) contained aerated Verna groundwater and 1.25 mg/L bromide, correlating to the average bromide elution concentration observed in samples from Column 3. Groundwater solution 4 (GS4) contained aerated Verna groundwater and 0.22 mg/L, corresponding to the minimum detection level of bromide (0.20 mg/L) for samples observed in Column 4. Bromide was not detected in Column 4 samples; the minimum detection value of approximately 0.20 mg/L was added to GS4 to simulate the highest amount of bromide elution that might have been present. Each groundwater solution was dosed with 3.83 mg/L of chlorine at the start of experiments.

Experimental Procedures for DBP Evaluation

Chlorine demand of the aerated Verna groundwater was first determined to establish a chlorine dosage that would provide a residual concentration of 0.2-1.0 mg /L after four days of incubation at 30°C. This range was chosen to simulate distribution system residuals of potable water utilities. Chlorine doses of 2 mg/L, 3 mg/L, and 4 mg/L were added to three different glass beakers containing 2 L of aerated Verna groundwater. Each solution was mixed, via a magnetic stirring plate, for 30 seconds after chlorine addition and poured into 60 mL glass vials. Chlorine concentrations were measured at the start of the experiment and consecutively at 8 hours, 24 hours,

48 hours, and 96 hours after chlorine addition. Interpolation of the collected chlorine measurements resulted in an optimal chlorine dose of 3.83 mg/L.

A total of 12 formation potential experiments (FPE1 through FPE12) were performed. Four groundwater solutions (GS1-GS4) were evaluated, in triplicate, to determine 96-hr TTHM formation potential, 96-hr HAA5 concentrations, and DBP speciation. Figure 17 outlines the order of experiments.

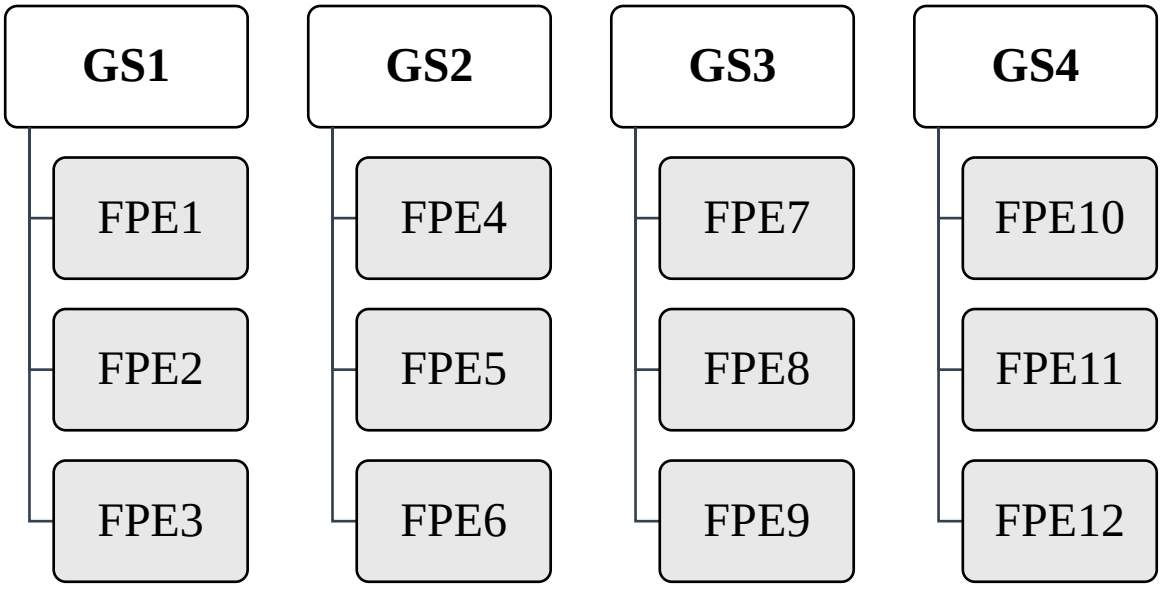

Figure 17: Formation Potential Experimental Order

Groundwater solutions were synthesized in a 2 L volumetric flask and added to a 3 L glass beaker. The glass beaker was situated on top of a magnetic stirring plate, set at a constant mixing speed. A chlorine dose of 3.83 mg/L was added and allowed to mix for 30 seconds. The disinfected groundwater solution was then used to fill 60 mL glass amber bottles, 40 mL glass amber vials, and 125 mL plastic bottles. 60 mL glass amber bottles were incubated at 30°C for up to four days

and were used to measure TTHM concentration and free chlorine. 40 mL glass amber vials were incubated at 30°C for four days and transported to *Advanced Environmental Laboratories, Inc.* for HAA5 analysis. 125 mL plastic bottles were used to measure bromide concentration and general water quality parameters. Quenched samples were stored at 4°C until analysis. A picture of the sample containers used in FPE1 through FPE12 are shown in Figure 18 and a picture of samples incubating at 30°C are displayed in Figure 19.

Figure 18: DBP Formation Experiment Sample Vials

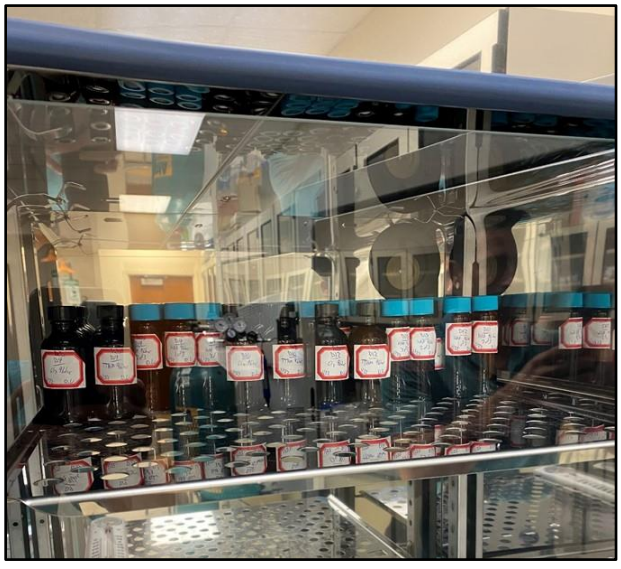

Figure 19: Samples Incubating at 30°C

Sample Preparation and DBP Data Analysis

Free chlorine samples were diluted, when appropriate, to below 2 mg/L and measured using a *Hach® DR 2700* spectrophotometer (Figure 20). TTHM samples were quenched and prepared in accordance with Standard Method (SM): 5710 of the *Standard Methods for the Examination of Water and Wastewater* (Baird et al., 2017). TTHM samples were then analyzed using a *Perkin Elmer®* gas chromatograph (Figure 21). HAA5 samples were quenched and stored at 4°C. HAA5 samples were then transported to *Advanced Environmental Laboratories, Inc.* and analyzed according to USEPA method 552.2. Appendix B provides a list of the methods, equipment, and method detection levels of each pertinent water quality parameter.

Figure 20: Hach® DR 2700 Spectrophotometer

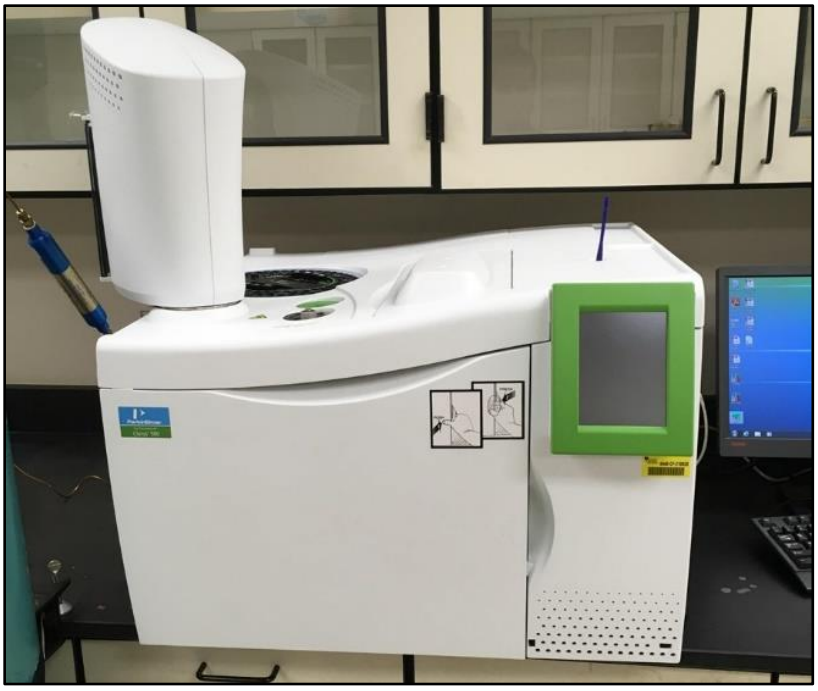

Figure 21: Perkin Elmer® Gas Chromatograph

Instrument data was analyzed using Microsoft® Excel software to create chlorine decay curves, TTHM formation potential curves, and HAA5 analysis. TTHM and HAA5 speciation compositions were evaluated to determine shifts in DBP formation types. Concentrations were compared and correlated to bromide concentrations observed in column samples after seawater-based regeneration methods were used.

CHAPTER 4: RESULTS

Bench-Scale Column Testing

Bench-scale columns were fabricated and operated to investigate the relative performance and secondary impacts of using alternative seawater-based regeneration methods for an AIX process designed to remove sulfate and NOM. Sarasota Bay seawater, and synthesized salt solutions as regenerant streams were compared to conventional regeneration methods. This investigation relied on the use of four bench-scale columns, housed with SBA resin, operating in parallel under different regeneration conditions. Sulfate saturation loading curves (SLCs) for each column are graphed and displayed. Sulfate breakthrough, exhaustion, exchange capacity, and specific throughput are calculated and compared to delineate changes in AIX performance. Natural organic matter uptake is analyzed by observing changes in DOC and UV-254 measurements. Impacts of seawater regeneration is assessed through the determination of ion leakage, comparing AIX feed water quality to treated water quality. Summarized performance values and individual SLCs, including chloride release, DOC uptake, and bromide elution are provided in Appendix C.

Each column was regenerated individually with a different solution until effluent conductivity values exiting the column matched the conductivity of the regenerant, approximately 18 to 20 minutes. Column's 1 through 4 were regenerated with solutions RS1 through RS4 (Figure 5). Regeneration curves for each column are presented in Figure 22.

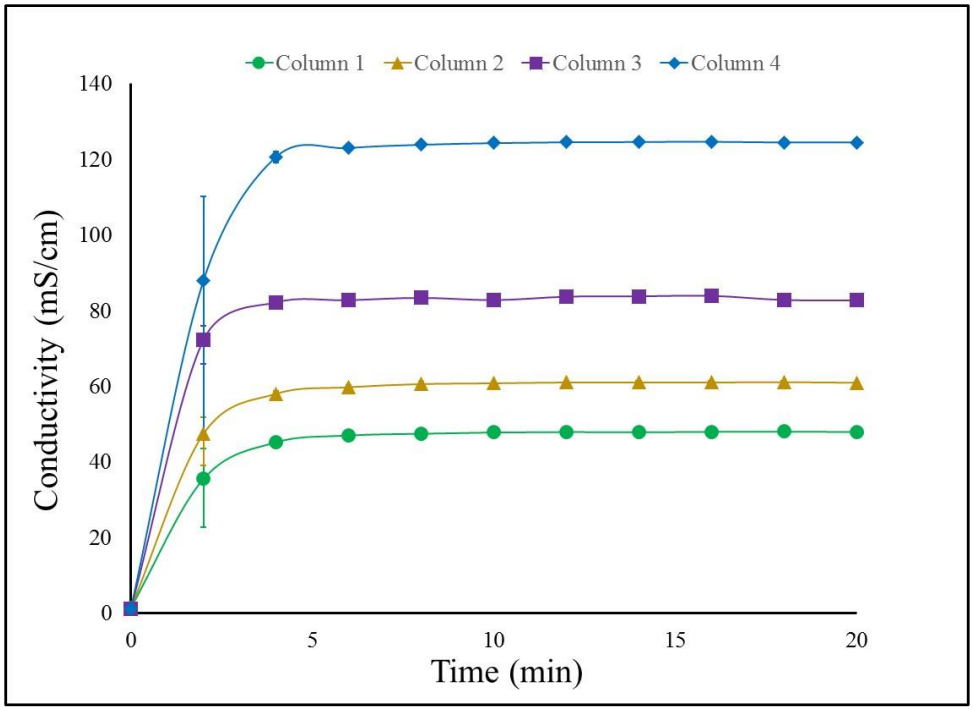

Figure 22: Regeneration Curves

Once regenerated, the four columns were operated in parallel until sulfate exhaustion was reached. Sulfate SLCs of each column are presented in Figure 23. It appears from Figure 23 that Column 1, regenerated with SBSW, began to saturate first. Column's 2 and 3, regenerated with 1% and 3% salt enhancements of SBSW, followed suit and saturated at comparable rates. Column 4, regenerated with 10% salt in distilled water, operated the longest before sulfate saturation. Column's 2 through 4 seemed to experience sulfate breakthrough around similar bed volumes; however, Column 1 reached breakthrough considerably quicker than the other three columns. The SLCs suggest that increasing the chloride concentration of the regenerant solution increases the amount of treated water capable of being produced before sulfate saturation occurs.

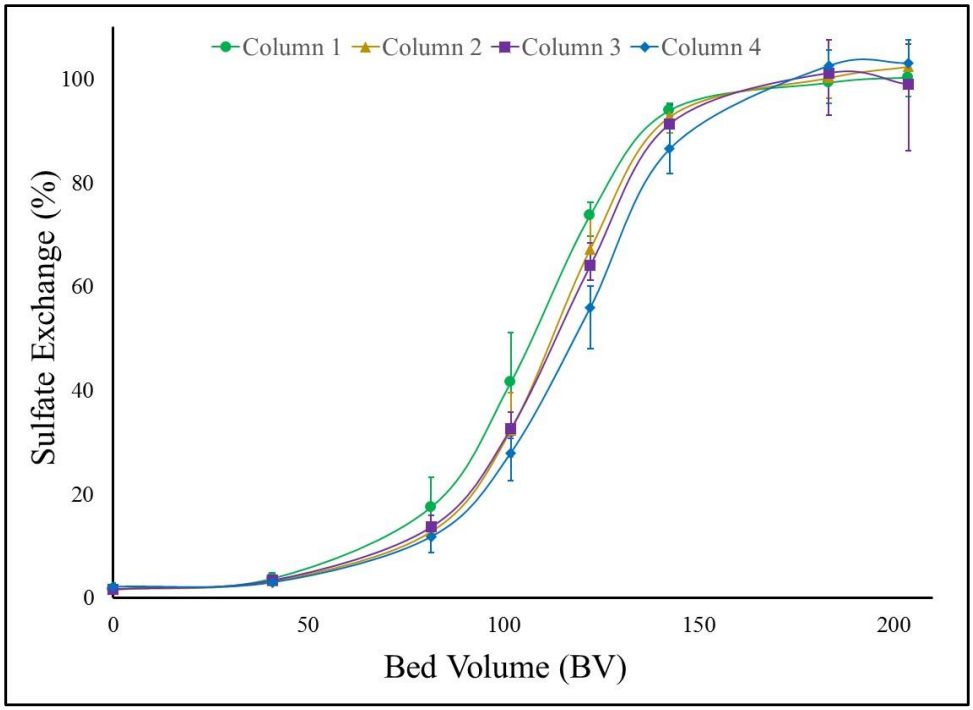

Figure 23: Sulfate Saturation Loading Curves

Breakthrough and Exhaustion

Breakthrough occurs when effluent concentrations of the targeted ionic constituent exceed a predetermined level of treatment. For this work, a sulfate value exceeding 10% of the feed water sulfate concentration, approximately 60 mg/L, was determined as the breakthrough point. Exhaustion occurs when effluent concentrations match feed water concentrations. To account for slight variations in sulfate, a value exceeding 90% of the feed water sulfate concentration, approximately 540 mg/L, was chosen as the exhaustion point. Breakthrough values were calculated through exponential interpolation and exhaustion values were calculated through logarithmic interpolation. Table 11 presents the average breakthrough and exhaustion values for each column.

Table 11: Average Sulfate Breakthrough and Exhaustion Values

Parameter	Column			
	1	2	3	4
Breakthrough (BV) (10% of feed)	67.5	74.4	72.4	76.6
Exhaustion (BV) (90% of feed)	138	141	147	151

Breakthrough was first reached in Column 1, at 67.5 BV. Breakthrough is then reached at 72.4 BV in Column 3, followed two bed volumes later by Column 2. Column 4 had the longest time to breakthrough, at 76.6 BV. Time to exhaustion was reached sequentially in Column's 1 through 4, ranging from 138 BV to 151 BV respectively. Breakthrough and exhaustion data concur with the observations made from column SLCs.

Exchange Capacity

Exchange capacity is defined as the total quantity of exchange groups per unit volume of resin (Crittenden et al., 2005; Wachinski, 2006; Michener & Lundberg, 1956). Exchange capacity allows for a commensurate comparison of resin performance, capable of comparing runs that differ in feed sulfate concentrations. During this study, equivalent feed concentrations of sulfate ranged from 12 to 13 meq/L. Applying the operational parameters outlined in Table 8 and using exhaustion values given in Table 11, exchange capacity of sulfate was calculated for each column. Table 12 displays the average sulfate exchange capacity for each column.

Table 12: Average Sulfate Exchange Capacity

Parameter	Column			
	1	2	3	4
Exchange Capacity ($eq/L_{res,wet}$)	1.74	1.77	1.85	1.90

Column 4, Conventional 10% salt regeneration, experienced a resin exchange capacity of 1.90 eq/L. A performance loss of 2.63% was observed in Column 3 when compared to Column 4, yielding an exchange capacity of 1.85 eq/L. Performance decreased by 6.84% in Column 2 when compared to Column 4, resulting in 1.77 eq/L exchange capacity. Performance decreased by 8.42% in Column 1 when compared to Column 4, resulting in 1.74 eq/L exchange capacity. Results indicate that salt enhancement to SBSW improves resin performance. Comparing Column's 1 through 3 to Column 4, we see that alternative seawater regeneration methods decrease the AIX resin's capacity to uptake sulfate in succeeding operations.

Specific Throughput

Specific throughput pertains to the volume of water treated per mass of resin used for a pre-determined level of treatment. Applying the operational parameters outlined in Table 8 and using exhaustion values given in Table 11, specific throughput was calculated for each column. Table 13 displays the average specific throughput for each column.

Table 13: Average Specific Throughput

Parameter	Column			
	1	2	3	4
Specific Throughput ($L/g_{res,dry}$)	0.371	0.378	0.395	0.405

Specific throughput values increased from Column 1 through Column 4. With an increase of 1% salt to SBSW (Column 2), specific throughput increased by 7 mL/$g_{res,dry}$. Increasing salt addition by 3% to SBSW (Column 3), specific throughput increased by 24 mL/$g_{res,dry}$. Specific throughput increased by 34 mL/$g_{res,dry}$ when regenerating with a 10% salt solution (Column 4) compared to SBSW (Column 1).

Natural Organic Matter Removal

In addition to removing selective anions like sulfate, additional anionic constituents have the potential to compete for exchange groups on the resin. Because proportions of NOM contain carboxylic acid groups, the organic molecules can carry a negative charge in water, allowing them to be removed by anion exchange (Comstock & Boyer, 2014). Natural organic matter removal was monitored throughout column testing by measuring DOC and UV-254. The Verna groundwater used during column experiments contained an average DOC value of 1.77 mg/L and a UV-254 reading of 0.047 cm^{-1}. Figure 24 presents the average DOC removed and average UV-254 decrease in each column.

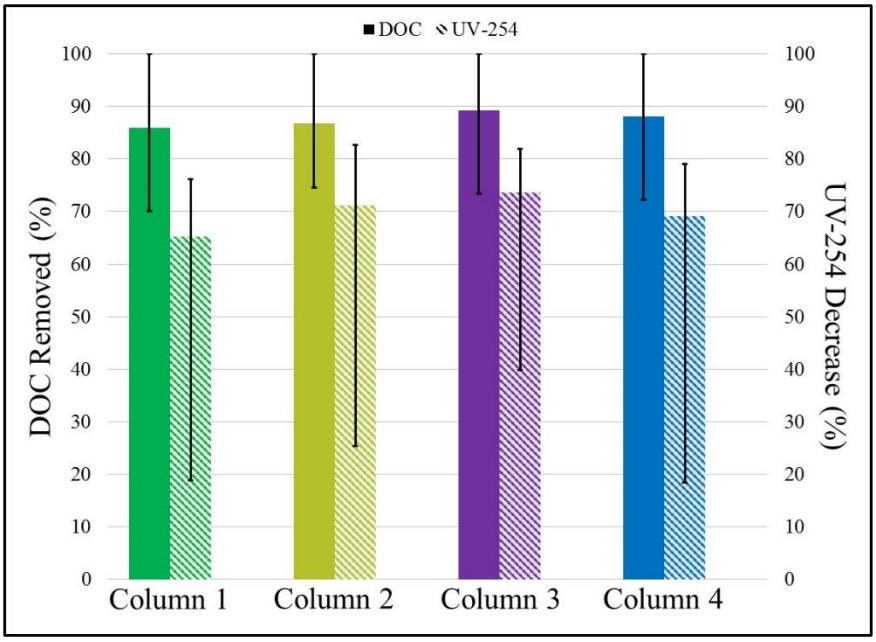

Figure 24: DOC and UV-254 Values

DOC removal among the four columns was consistent, between 85.8% and 89.2%. Similar observations were noted in UV-254 measurements, averaging 65.2% to 73.6% reduction. There was a slight observed improvement in DOC removal from Column 1 through Column 3. The same trend was also noticed for a decrease in UV-254 measurements. Column 4 experienced a slight decrease in organic removal capabilities compared to Column 3, but outperformed Column's 1 and 2. Appendix C displays each Column's average organic removal rates during operational runs to exhaustion.

Suspected Fouling/Clumping

During column operations, small clumps of an unknown material formed in each of the four columns (Figure 25). This clumping/fouling of the anion resin may have resulted in performance loss due to channeling or resin poisoning (resin inactivation). Clumping was observed to form at

the top of the resin bed during column operation (Figure 25a). During counter-current regeneration, the clumped resin material began to descend through the resin bed (Figure 25b) and settled at the bottom of the resin bed (Figure 25c). Clumping/fouling of the anion resin was observed in each of the four columns during each operational experiment. Analysis was not performed on the unknown material in this work. The complex water matrix of the Verna groundwater that is a natural water supply contains a mixture of organics and other constituents, including microbiologicals, that may contribute to the irreversible fouling observed during column experiments. Because these systems are natural systems, it is possible that a microbiologically mediated solids formation was a contributing factor, taking into account the fact that the regenerant had been disinfected, filtered and scavenged to remove the disinfectant prior to use. This phenomena was not fully vetted in this research, but clumping did not appear to impact the operating performance experienced. The Verna groundwater contained an average of 1.88 mg/L TSS, an average turbidity value of 0.613 NTU, and an average ORP value of +174 mV.

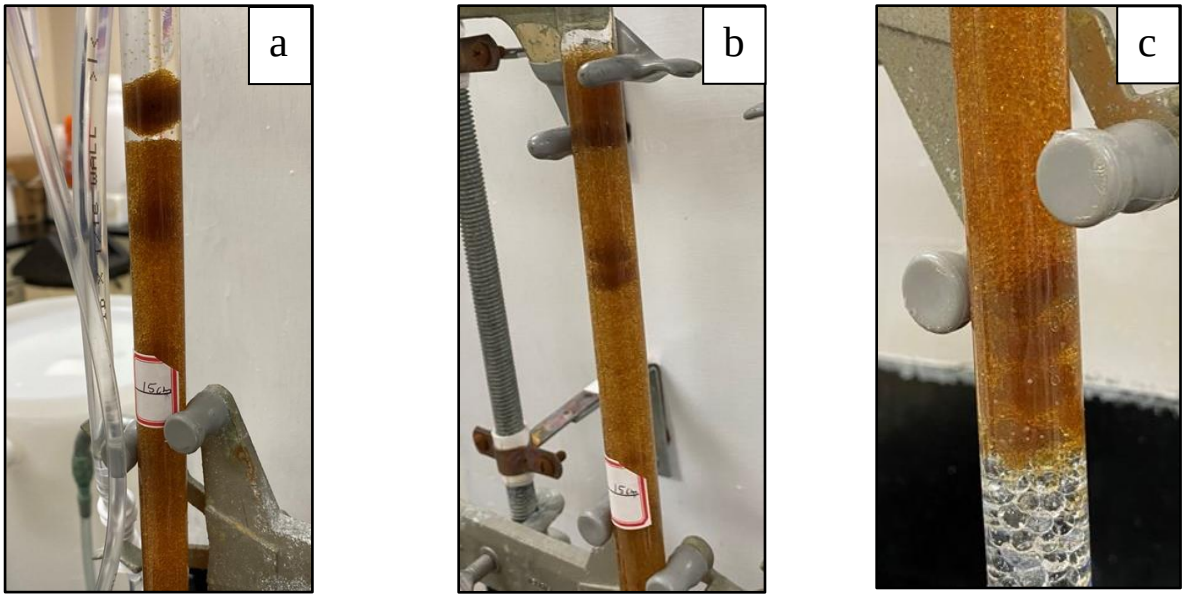

Figure 25: Resin Clumping/Fouling Formed at Top of Resin Bed (25a); Descending Through Resin Bed (25b); Settled at Bottom of Resin Bed (25c)

Bromide Exchange from Sarasota Bay Seawater

In addition to investigating performance conditions, the study assessed potential impacts that the use of SBSW as a regenerant may impart to treated water quality. This included a composition analysis of the treated column effluent, comparing the results to the Verna feed water matrix. Because SBSW contains an array of additional constituents, including microbiologicals, there is potential for interference in the ion competition with chloride during the regeneration process. Bromide contains a larger molecular weight, ionic radius, and atomic number than chloride, although both share the same valence state. Generally, ionic species with higher ionic radii, hydrated radii, molecular weight, atomic numbers, and valence are preferred (Crittenden et al., 2005; Tan & Kilduff, 2007). The SBSW contains approximately 81 mg/L of bromide, representing a strong competing anion for exchange sites on a chloride-form AIX resin.

Bromide concentrations were detected in the treated effluent of the columns regenerated with SBSW (Columns 1 through 3). Bromide concentrations were not detected in Column 4. Bromide was also not detected in the Verna feed water based on a method detection limit of 0.2 mg/L. The observed bromide concentrations were presumed to be from the SBSW supply, exchanging onto the AIX resin during the regeneration process and subsequently eluting during succeeding column runs. Figure 26 displays the bromide elution curves of Columns 1 through 3. Appendix C displays individual bromide elution curves for Columns 1 through 3.

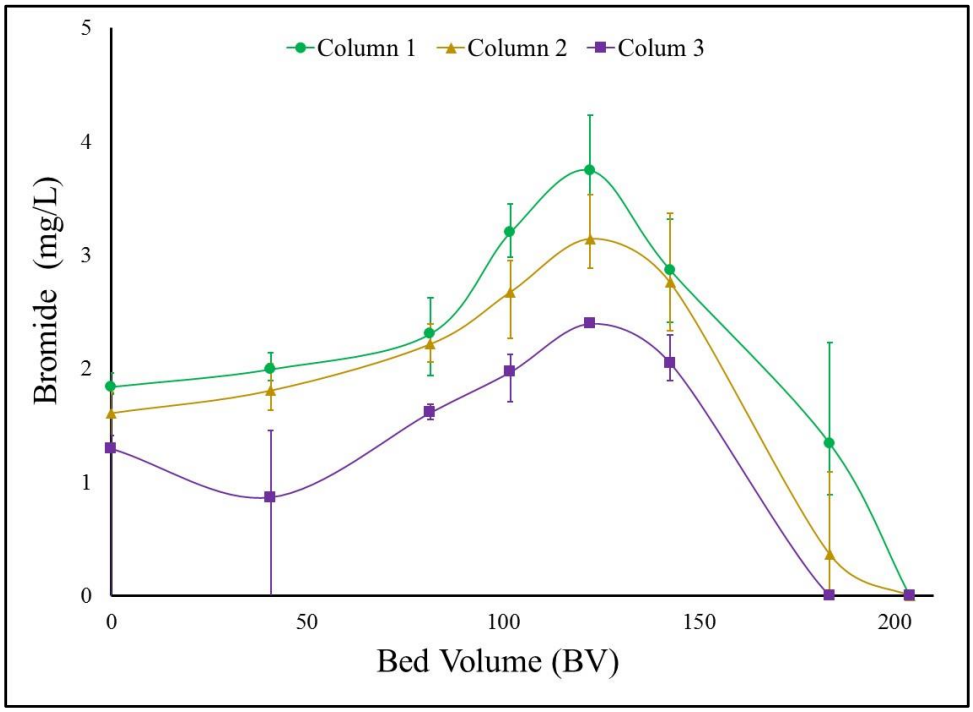

Figure 26: Bromide Elution Curves

The bromide elution curves in Figure 26 demonstrate a correlation between bromide elution and salt concentration. Column 1 experiences the highest amount of bromide elution, yielding an average of 2.13 mg/L. With the addition of 1% salt to SBSW, bromide elution decreased in Column

2 to an average of 1.82 mg/L. Continuing with the addition of 3% salt, bromide elution in Column 3 decreased to an average of 1.25 mg /L. Bromide elution was not detected in Column 4, utilizing a 10% strength salt solution in distilled water for regeneration. Average bromide elution concentrations are presented in Table 14.

Table 14: Average Column Bromide Elution Concentrations

Parameter	**Column**			
	1	**2**	**3**	**4**
Bromide Elution (mg/L)	2.13	1.82	1.25	<0.20

Increasing the salt content of SBSW increases the ratio of chloride ions to bromide ions in the water matrix. As the ratio of chloride ions to bromide ions increases, the resin's selectivity toward chloride increases, decreasing bromide exchange and subsequent bromide elution. The separation factor of the AIX resin at the chloride to bromide molar ratio (CBMR) found in SBSW appears to allow for bromide exchange. As the CBMR increases, the AIX resin's affinity toward bromide decreases, presenting a direct relationship between the two. Previous research has utilized chloride to bromide ratios for use in identifying movements and origins of salinity in groundwater and potable water (Alcalá & Custodio, 2005; Davis et al., 1998). It appears that chloride to bromide ratios can also be used in chloride-form AIX processes to predict resin selectivity of bromide. Table 15 presents the chloride to bromide molar and concentration ratios in the regenerant solutions used during column testing.

Table 15: Chloride to Bromide Concentration and Molar Ratios

Parameter	Regenerant Solution			
	RS1	RS2	RS3	RS4
rCl^-/Br^- (M) (CBMR)	516	684	1021	-
Cl^-/Br^- (mg/L)	229	303	453	-

Jar Testing

The purpose of this section was to explore the equilibrium and kinetic relationship between bromide and chloride in an AIX regeneration process. Chloride-form AIX resin is typically regenerated using a salt solution containing high concentrations of chloride. Alternative regenerant solutions, such as seawater, contain appreciable amounts of bromide that have the potential to compete with chloride for resin exchange sites during regeneration. Jar testing experiments were carried out to examine changes to equilibrium values, kinetic rates, and rate-controlling steps of bromide adsorption in the presence of high chloride concentrations.

Kinetic studies were performed using four synthetic solutions (SS1-SS4) to evaluate changes in kinetic rates. SS1 was used as a baseline for bromide adsorption, containing no added chloride. SS2 through SS4 represented bromide adsorption at increasing CBMR solutions. Figure 27 presents the bromide adsorption curves for the four tested solutions. It appears from Figure 27 that the rate of adsorption increases slightly from SS1 through SS4 respectively. The adsorption capacity of bromide, q_{Br-}, noticeably decreases as the CBMR increases from SS1 through SS4. Equilibrium was reached after 120 minutes.

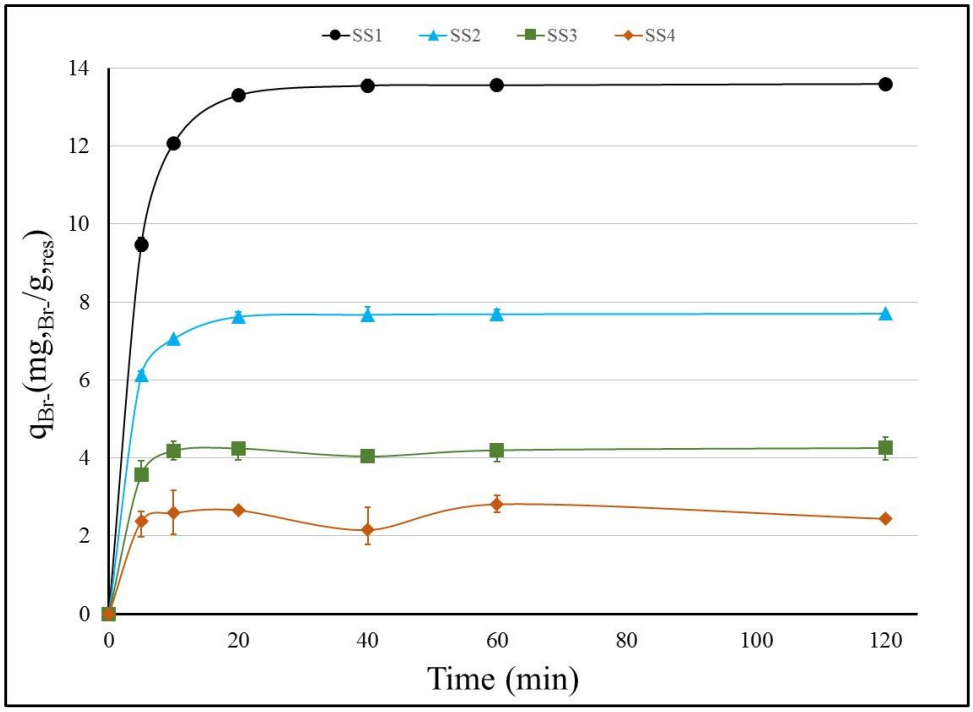

Figure 27: Bromide Adsorption Kinetics

Equilibrium experiments were carried out with six solutions (SS1-S6) to identify equilibrium adsorption values, % exchange values, and separation factors. SS5 and S6 were comprised of CBMRs that required high sample dilution factors, >180, for instrument analysis. Anion analysis of kinetic values were considered inaccurate at sample dilution factors greater than 180. As such, SS5 and S6 samples were only analyzed for final equilibrium adsorption values. Figure 28 presents the equilibrium isotherm of bromide in terms of increasing CBMR solutions. There is a clear trend denoting an exponential decay of bromide equilibrium adsorption capacity, $q_{e,}$ as the CBMR increases. Representing the CITY's seawater, S6, has a similar CBMR as SS5, but is observed at a much lower q_e. This is likely due to the array of additional ions found in SBSW that are capable

of competing for resin exchange sites; it is also possible that microbiological interferences may have been present that impacted diffusional mass transfer as this phenomenon was noted at longer exposure times of the resin and the water supplies tested. Efforts to understand this phenomenon was not further investigated as the clumping did not have an impact on column operation.

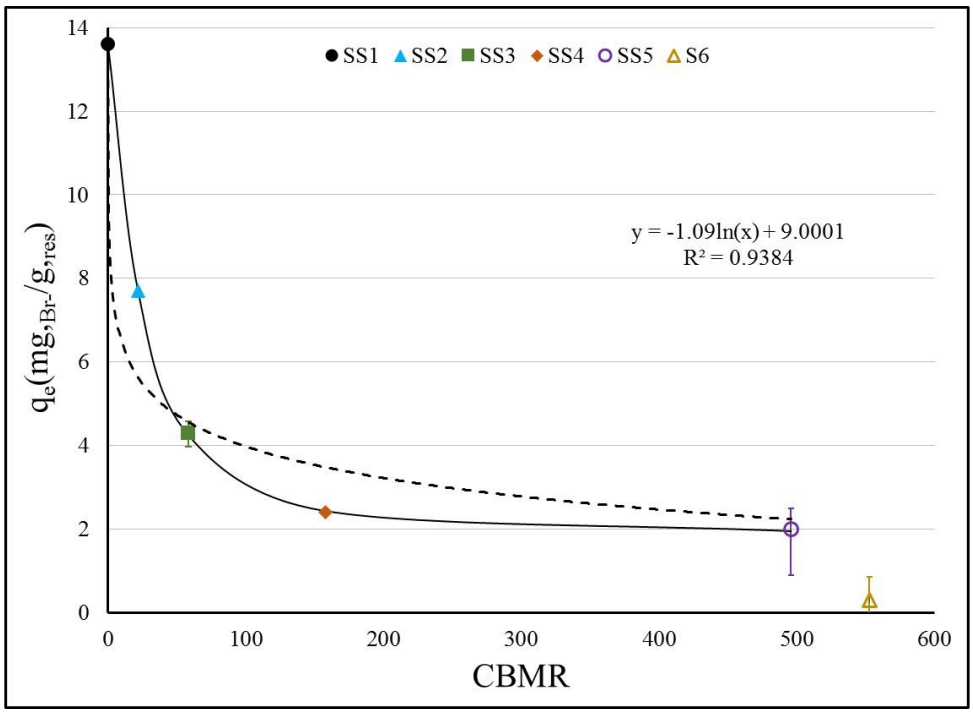

Figure 28: Bromide Equilibrium Isotherm

Table 16 displays the equilibrium adsorption capacity, percent of bromide exchanged at equilibrium, and associated resin separation factors for bromide with respect to chloride. As noticed in Figure 28, equilibrium capacity decreases as the CBMR of solution increases. Percent exchange of bromide with no chloride was found to be 95.1%, sequentially decreasing from SS1 to S6. Percent exchange of bromide in S6, comprised of SBSW, was observed to be 2.19%. During bench-scale column testing, bromide elution from SBSW in Column 1 was around 2.62%.

Observed bromide exchange from SBSW during bench-scale column testing and equilibrium jar testing were comparable.

Equilibrium adsorption capacity values obtained from synthetic solutions appeared to follow a logarithmic decay as the CBMR of solution increased. Equation (18) displays the experimentally derived logarithmic decay function of q_e in relation to CBMRs, yielding an R^2 of 0.938. Using Equation (18), equilibrium adsorption capacity of bromide can be approximated for solutions containing different CBMRs, such as brackish groundwater and seawater commonly used in potable water production; however, this function does not account for the additional ions found in natural water matrices. Additional competing ions have the potential to decrease bromide adsorption; demonstrated by S6 in Figure 28.

$$q_e = -1.09 \ln(CBMR) + 9.0001 \tag{18}$$

AIX resin separation factors were also calculated from each solution's experimental q_e values. In the case of monovalent to monovalent IX, the apparent equilibrium constant is equal to the separation factor, α, (Crittenden et al., 2005). Substituting α into Equation (2), for the exchange of chloride for bromide, yields Equation (19).

$$\alpha_{Cl^-}^{Br^-} = \frac{C_{Cl^-} q_{Br^-}}{q_{Cl^-} C_{Br^-}} \tag{19}$$

Where,
$\alpha_{\boldsymbol{Cl^-}}^{\boldsymbol{Br^-}}$ = separation factor for bromide with respect to chloride

In the binary exchange of chloride for bromide, our total exchange capacity, q_T, is equal to the resin phase chloride concentration plus the resin phase bromide concentration, Equation (20).

$$q_T = q_{Cl^-} + q_{Br^-} \quad (20)$$

Where,
q_T = total exchange capacity of resin, eq/L

Rearranging and substituting Equation (20) into Equation (19), outputs Equation (21).

$$q_{Br^-} = \frac{C_{Br^-}(q_T)}{C_{Br^-} + C_{Cl^-}(\frac{1}{\alpha_{Cl^-}^{Br^-}})} \quad (21)$$

In the case of multicomponent exchange, q_T is equal to the summation of the resin phase ion concentrations. Configuring Equation (21) to account for multicomponent ion exchange, produces Equation (22).

$$q_{Br^-} = \frac{C_{Br^-}(q_T)}{\sum_{i=1}^{n} C_{j^-}(\frac{1}{\alpha_{j^-}^{i^-}})} \quad (22)$$

Where,
C_{j^-} = concentration of anion j, eq/L
$\alpha_{j^-}^{i^-}$ = separation factor for anion i with respect to anion j

Binary exchange calculations utilized Equation (21) for SS1, modeling bromide exchange for chloride with no other anions present. Multicomponent exchange calculations harnessed Equation (22) for SS2 through SS5, assuming bromide exchange for chloride in the presence of varying chloride concentrations. Multicomponent exchange calculations for S6 used Equation (22), assuming bromide exchange for chloride in the presence of chloride and sulfate. Other ions in S6 were considered negligible. SS1 resulted in a separation factor of 1.18. Increasing the CBMR in

solutions SS2 through SS5 indicated that the resins affinity for bromide increases even though the overall adsorbed amount has decreased. The same trend is observed in S6, denoting a high separation factor for bromide adsorption when competing with high concentrations of chloride and sulfate.

Table 16: Equilibrium Bromide Values

Parameter	Solution					
	SS1	SS2	SS3	SS4	SS5	S6
q_e ($mg_{,Br-}/g_{,res}$)	13.6	7.70	4.26	2.44	1.96	0.338
Br^- Exchange (% @ Equilibrium)	95.1	53.3	30.0	15.8	12.1	2.19
$\boldsymbol{\alpha_{Cl^-}^{Br^-}}$	1.18*	0.623**	0.908**	1.30**	4.52**	73.7***

* = Calculated using Equation (19)
** = Calculated using Equation (22) ($\alpha_{Br^-}^{Br^-}$= 1)
*** = Calculated using Equation (22) ($\alpha_{Br^-}^{Br^-}$= 1 & $\alpha_{Br^-}^{SO_4^{2-}}$ = 7.70)

Disinfection By-Product Formation Chemistry

The intent of this portion of work was to evaluate the impacts of bromide elution from AIX seawater regeneration on the formation of DBPs. Bromide concentrations detected during bench-scale column studies, outlined in Table 14, were applied to the aerated Verna groundwater and dosed with chlorine to assess TTHMs and HAA5s. GS1 simulated bromide elution from seawater regeneration using SBSW. GS2 and GS3 modeled bromide elution from seawater regeneration supplemented with salt. GS4 represented bromide elution pertaining to AIX regeneration using a 10% strength salt solution. Although bromide elution was undetected after using a 10% strength salt regenerant solution, 0.22 mg/L was added to GS4 to simulate minimum detection levels. Free

chlorine decay curves were produced, meeting a targeted 96-hr residual concentration range of 0.2 mg/L to 1 mg/L. 96-hr TTHM formation potential curves were developed and 96-hr HAA5 concentrations were analyzed. Changes in regulated DBP species were evaluated and presented in the form of composition graphs. Individual groundwater solution TTHM formation potentials, 96-hr HAA5 concentrations, and DBP composition graphs are available in Appendix D.

Figure 29 presents the average free chlorine decay curves for each groundwater solution (GS1-GS4). Initial chlorine demand over the first 8hrs were consistent between solutions. From 8-hrs and on, GS4 appeared to maintain a higher chlorine residual through 96-hrs. This was to be expected as GS4 contained the least amount of added bromide, approximately 0.22 mg/L. The four solutions managed a 96-hr chlorine residual between 0.2 mg/L to 1 mg/L, shown in Table 17.

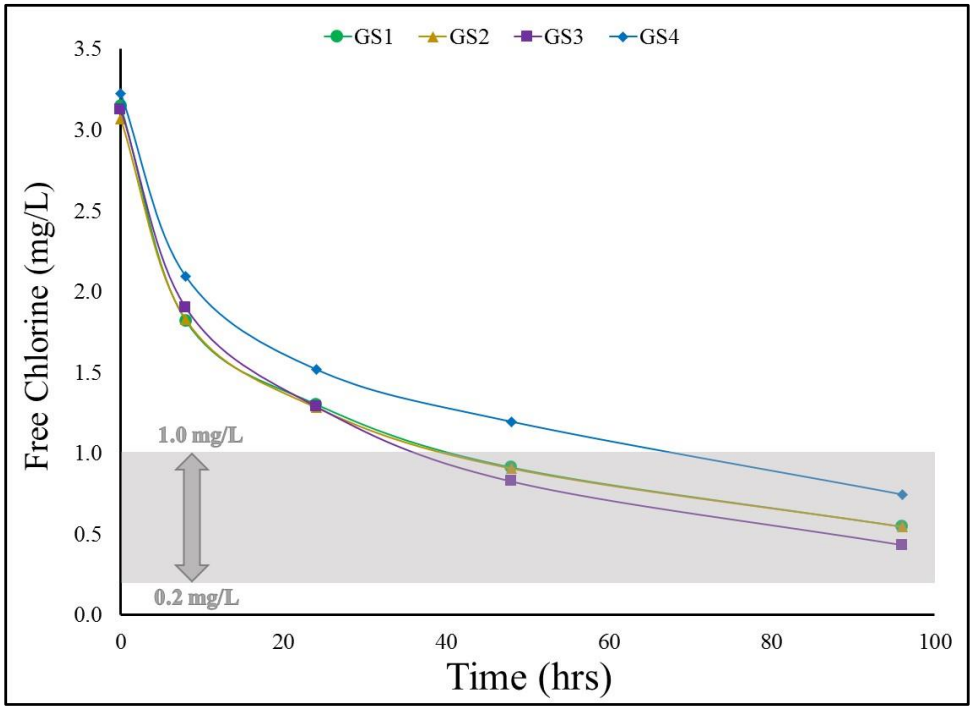

Figure 29: Free Chlorine Decay Curves

Table 17: Average 96-hr Free Chlorine Residuals

Free Chlorine Residual	Solution			
	GS1	GS2	GS3	GS4
96-hr (mg/L)	0.55	0.55	0.43	0.75

TTHM formation potentials of each groundwater solution are graphed in Figure 30 and 96-hr TTHM formation concentrations are detailed in Table 18. GS4 experienced the lowest TTHM formation through 96-hrs, at 186 μg/L. With increased bromide concentrations of 1.82 mg/L and 1.25 mg/L in GS2 and GS3 respectively, TTHM formation increased to an average of 260 μg/L. GS1, containing an added bromide concentration of 2.13 mg/L, resulted in the highest 96-hr TTHM formation of 294 μg/L. Figure 30 demonstrates a trend of increased TTHM formation potential as bromide concentration increases.

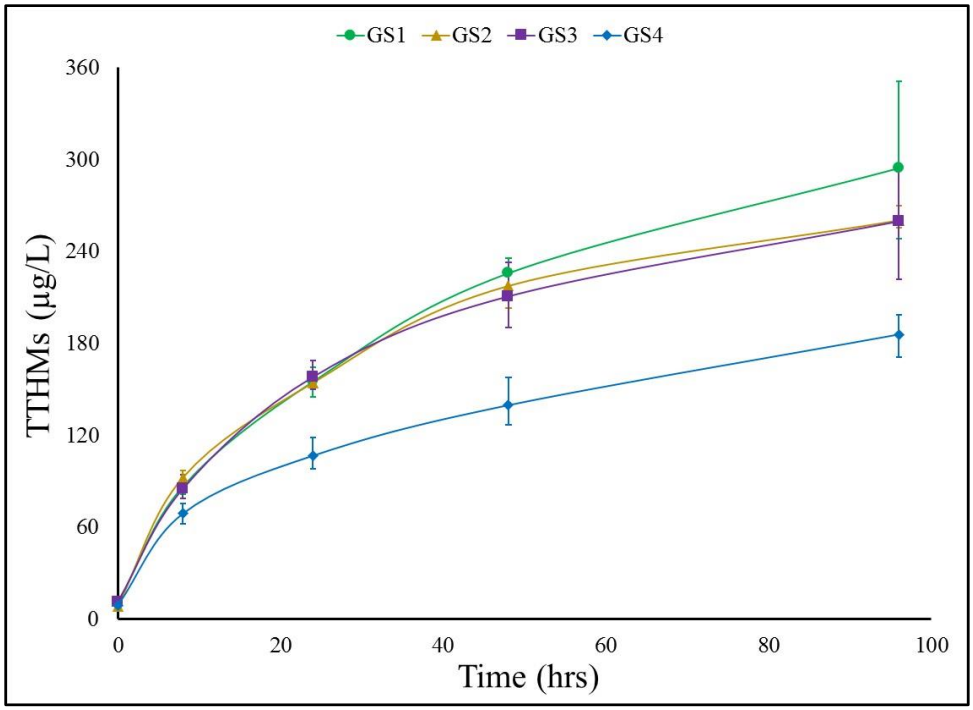

Figure 30: TTHM Formation Potential Curves

Table 18: Average 96-hr TTHM Formation Potential

TTHM Formation Potential	Solution			
	GS1	GS2	GS3	GS4
96-hr (µg/L)	294	260	260	186

The 96-hr TTHM compositions are graphed in Figure 31 and the percent composition of regulated TTHMs for each solution is presented in Table 19. Bromoform was found to be the dominant species formed in GS1, followed by dibromochloromethane. Bromodichloromethane and chloroform were found at lower concentrations in GS1. The same trend was observed in GS2 and GS3. Comparable amounts of the four TTHMs were detected in GS4. The data suggests that

speciation shifts from bromoform to more chlorinated DBP species as initial bromide concentrations decreased.

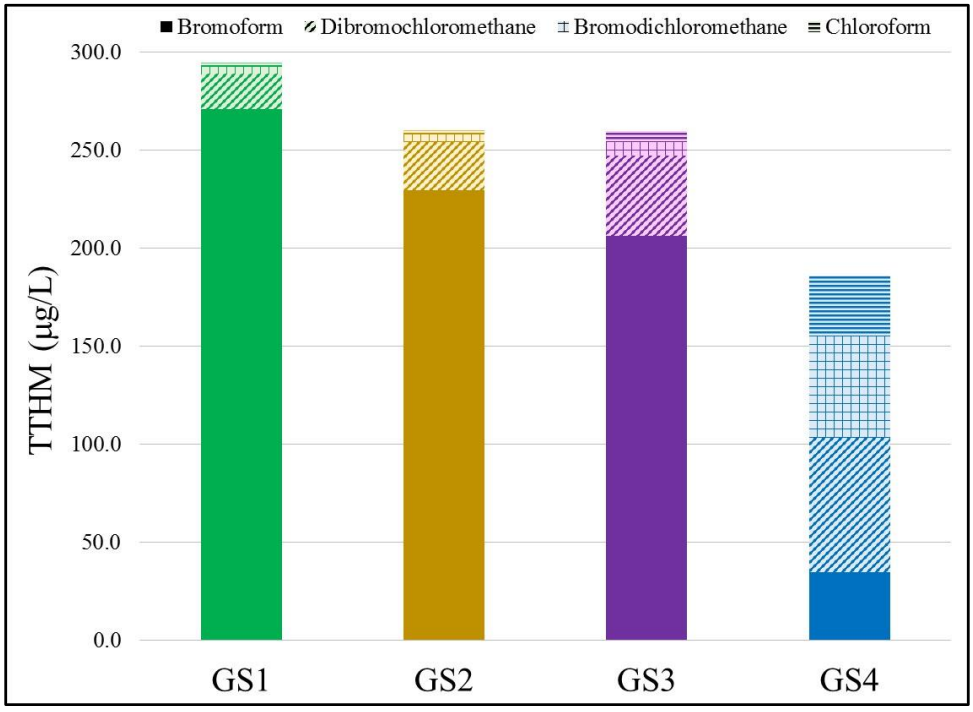

Figure 31: 96-hr TTHM Composition Graph

Table 19: Average 96-hr TTHM Composition

96-hr TTHM Composition	Solution			
	GS1	GS2	GS3	GS4
Bromoform (%)	92.0	88.1	79.4	18.6
Dibromochloromethane (%)	6.25	9.51	15.9	36.9
Bromodichloromethane (%)	1.09	1.54	2.65	27.8
Chloroform (%)	0.68	0.82	2.09	16.7

The 96-hr HAA5 concentration and composition of the four solutions were analyzed. GS1 resulted in a 96-hr HAA5 concentration of 36.1 μg/L, followed by GS2 at 34.6 μg/L. GS3 contained a 96-hr HAA5 concentration of 32.9 μg/L and GS4 yielded the lowest HAA5 concentration of 25.7 μg/L. A similar compositional trend appeared in HAA5 speciation. Dibromoacetic acid was the dominant species formed, shifting to less brominated HAA5 species as initial bromide concentrations decreased.

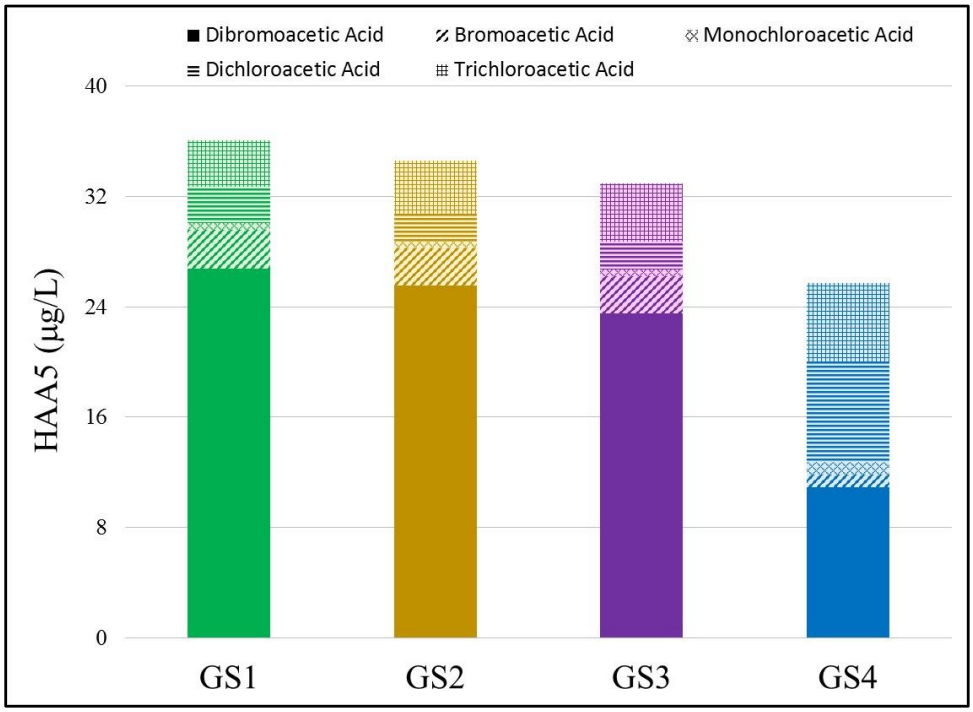

Figure 32: 96-hr HAA5 Composition Graph

Table 20: Average 96-hr HAA5 Composition

96-hr HAA5 Composition	Solution			
	GS1	GS2	GS3	GS4
Dibromoacetic Acid (%)	74.1	73.8	71.4	42.4
Monobromoacetic Acid (%)	7.88	7.83	8.20	3.61
Monochloroacetic Acid (%)	1.39	1.45	1.52	3.48
Dichloroacetic Acid (%)	7.25	5.68	6.13	28.4
Trichloroacetic Acid (%)	9.41	11.3	12.8	22.1

CHAPTER 5: DISCUSSION

Conceptual Regeneration Cost Comparison

Bench-scale column testing revealed different operational performance capabilities of the four regenerant solutions. Performance numbers of the four tested solutions (RS1-RS4) were used to delineate conceptual full-scale capital costs as well as the operations and maintenance (O&M) costs associated with the regeneration process. A flow diagram of seawater regeneration using SBSW (RS1) is provided in Figure 33. A flow diagram of salt-supplemented seawater regeneration (RS2 and RS3) is displayed in Figure 34. A flow diagram of conventional salt regeneration is shown in Figure 35.

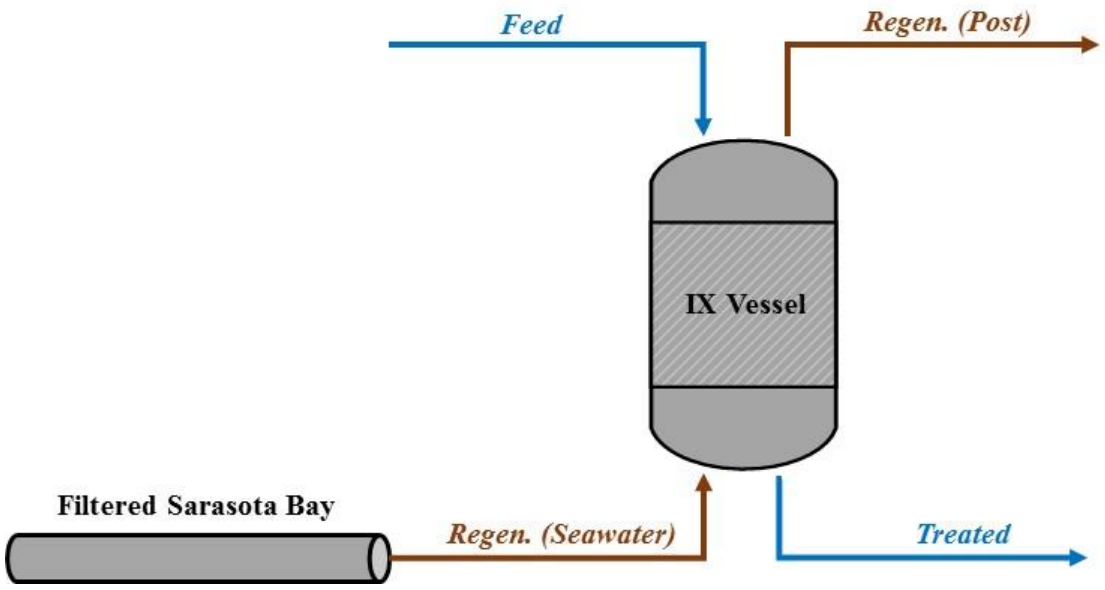

Figure 33: Seawater Regeneration Flow Diagram

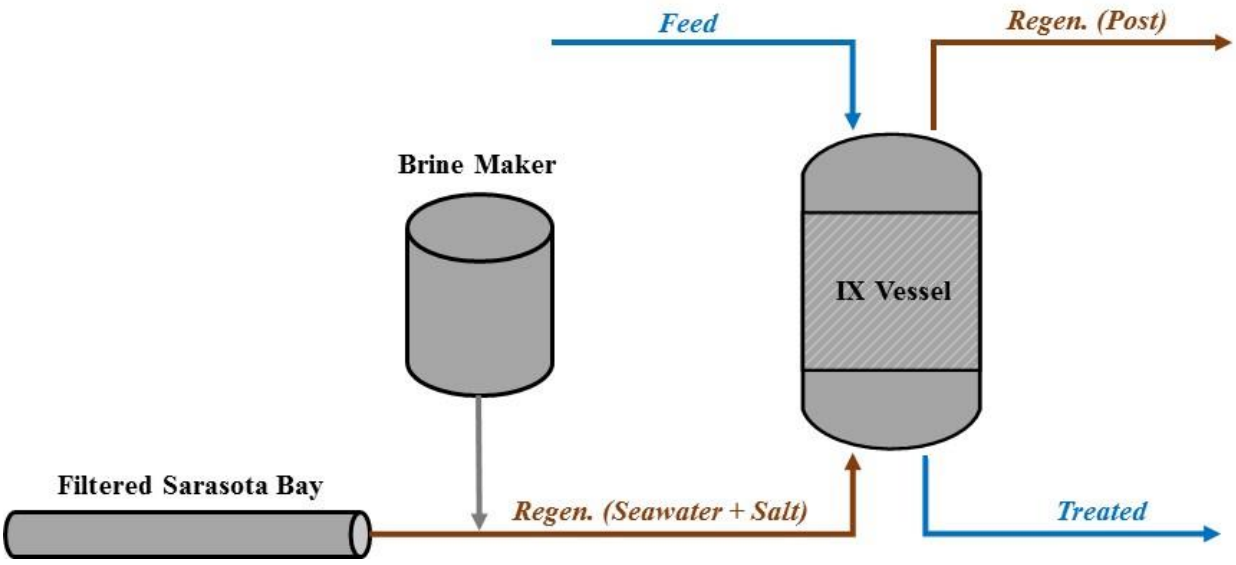

Figure 34: Salt-Supplemented Seawater Regeneration Flow Diagram

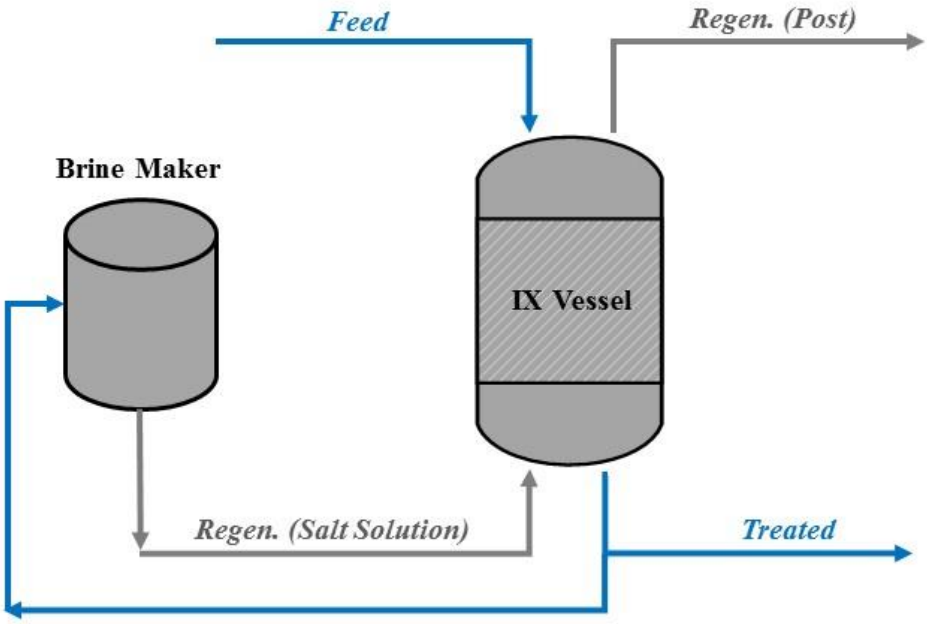

Figure 35: Salt Solution Regeneration Flow Diagram

A 0.455 MGD AIX process with a flowrate of 316 gpm for sulfate removal was used to approximate regeneration cost projections. The conceptual IX bed dimensions were designed to meet a surface loading rate that matched bench-scale column studies, approximately 2.8 gpm/ft^2. For cost projection purposes, the IX process was assumed to operate continuously, with no resin loss or performance decline. A constant sulfate concentration of 500 mg/L in the CITY's Verna groundwater was simulated as the feed solution, assuming negligible impacts from other water quality constituents. A list of the conceptual full-scale operating parameters applied for regeneration cost estimations are detailed in Table 21.

Table 21: Conceptual Full-Scale IX Operating Parameters

Operating Parameter	Value
Capacity (MGD)	0.455
Flowrate (gpm)	316
Media Height (ft)	6.20
Media Diameter (ft)	12.0
Media Volume (ft^3)	701
Surface Loading Rate (gpm/ft^2)	2.80
Volumetric Loading Rate (gpm/ft^3)	0.453

Observed exchange capacity values of the A-32 anion resin from each regenerant solution was applied to derive throughput values, operation time, and regeneration cycles needed per year. Operating the conceptual full-scale system under the stated assumptions, RS1 would require approximately 189 regenerations annually. Supplementing salt to SBSW, RS2 and RS3 would require 186 and 178 annual regenerations respectively. Conventional IX regeneration modeled with RS4 yielded the best performance, only requiring 173 regenerations annually. A list of the performance values for each regenerant solution is listed in Table 22.

Table 22: Regenerant Solution Performance

Performance	Regenerant Solution			
	RS1	RS2	RS3	RS4
Exchange Capacity (eq/L_{resin})	1.74	1.77	1.85	1.90
Throughput (MGD/cycle)	0.877	0.893	0.933	0.958
Operation (hrs/cycle)	46.3	47.1	49.2	50.5
Regenerations per Year	189	186	178	173

Capital Costs

The capital costs for each regeneration method are provided in Table 23: broken down into direct and indirect capital costs. Costs associated with the IX operational process, including feed water pumping, IX vessels, resin media, storage tanks, power supplies, piping, additional infrastructure, and appurtenances have been excluded. Costs associated with the installation of an onsite seawater storage tank was also excluded. Direct capital costs associated with seawater regeneration include the installation of a seawater pipeline and sand filtration. The seawater pipeline is estimated at 1.2 miles in length with an inside diameter of 4 inches. Installation costs of the seawater pipeline were estimated using values obtained from BCC Research (2016) and sand filtration costs were scaled from cost projections done by Yonge (2016). Direct capital costs affiliated with salt supplementation/mixing involved the installation of an onsite brine maker, capable of housing 36 tons of salt. Brine maker costs were derived from sales information pertaining to *Plas-Tanks Industries, Inc.* (39 Standen Drive Hamilton, Ohio) brine maker model, *Bryneer*™, and acts as both a storage tank and brine mixing vessel. Indirect capital costs were related to construction, insurance, bonding, and contingencies. Seawater regeneration resulted in a total capital cost of

$282,000. Salt additions to seawater totaled $402,000. The least expensive capital cost was conventional salt regeneration, at $120,000.

Table 23: Conceptual Regeneration Capital Costs

Regeneration Capital Costs	Regenerant Solution ($1000)			
	RS1	**RS2**	**RS3**	**RS4**
Direct Regeneration Capital Costs				
Seawater Pipeline (4" @ 1.2 miles)	176	176	176	n/a
Piping Materials				
Installation				
Excavation				
Backfill				
Media Filtration	36.1	36.1	36.1	n/a
Pressure Filters				
Underdrains & Distributors				
Instrumentation & Controls				
Media (Gravel/Sand)				
Additional Materials & Appurtenances				
Bulk Salt Storage/Brine Maker (36 ton)	n/a	90.0	90.0	90.0
Shell Construction				
Downflow Brine Maker				
Water Inlet Distributor				
Brine Collector				
Salt Inlet/Air Venting System				
Clean-Out Underdrain				
Instrumentation & Controls				
Additional Materials & Appurtenances				
Total Direct Capital Costs	212	302	302	90.0
Indirect Regeneration Capital Costs				
Construction (20%)	42.4	60.4	60.4	18.0
Permitting				
Overhead				
Profit				
Insurance & Bonding (3%)	6.36	9.06	90.6	2.70
Contingencies (10%)	21.2	30.2	30.2	9.00
Total Indirect Capital Costs	70.0	99.7	99.7	29.7
Total Estimated Capital Costs	282	402	402	120
$/gpd Capital Installed	0.62	0.88	0.88	0.26

Operations and Maintenance Costs

The conceptual annual O&M costs for each regeneration method are provided in Table 25. O&M costs of seawater regeneration pertained to pumping costs, and were calculated using the assumed values listed in Table 24. Head loss through the seawater pipeline was calculated using the Darcy-Weisbach equation, shown in Equation (23), using a friction factor, f, of 0.015. O&M costs of salt addition involved salt import and freight costs, obtained from general industry market values. Energy costs were gathered from the CITY's current power rates, approximately $0.057/kWh. Additional O&M costs involved administration and supplies, overhead, and miscellaneous costs.

$$h_L = f\frac{L}{D} * \frac{v^2}{2g} \tag{23}$$

Where,
h_L = head loss (ft)
f = friction factor
L = length of pipe (ft)
D = pipe diameter (ft)
v = velocity (ft/s)
g = gravity, 32.2 (ft/s^2)

Table 24: Conceptual Regeneration Cost Assumptions

Assumptions	Value
Energy Cost ($/kWh)	0.057
Salt & Freight Cost ($/ton)	110
Seawater Pipeline Head Loss (ft)	288
Seawater Elevation Difference (ft)	16.0
IX Vessel Head Difference (ft)	12.0
Pump Efficiency (%)	0.75
Motor Efficiency (%)	0.75
Regeneration Time (hr)	1.00

Seawater regeneration had the lowest annual O&M costs, requiring no salt addition. Salt supplementation of 1% and 3% salt resulted in increased annual O&M costs. Conventional salt solution regeneration generated the highest annual O&M costs, resulting in over $50,000 per year in salt import costs alone.

Table 25: Conceptual Annual O&M Regeneration Costs

Annual O&M Regeneration Costs	Regenerant Solution ($)			
	RS1	**RS2**	**RS3**	**RS4**
Pumping	361	355	340	18.9
Pipe Head Loss				
Elevation Head Loss				
IX Vessel Head Difference				
Chemicals	n/a	5,430	15,600	50,500
Salt				
Freight				
Administration & Supplies	5,000	5,290	5,800	7,530
Overhead (15%)	804	1,660	3,260	8,710
Miscellaneous	1,000	1,000	1,000	1,000
Total Annual Operating Cost	7,170	13,700	26,000	67,800
$/gpd O&M	0.02	0.03	0.06	0.15

Total Regeneration Process Costs

Total regeneration process costs are presented in Table 26, and were calculated by combining amortized capital costs and O&M costs. Capital costs were amortized at an annual interest rate of 4.5% over an IX operational design life of 10 years. The cheapest option was seawater regeneration, at a cost of $42,200 per year and resulted in a total process cost of $0.25/kgal. Supplementing SBSW with 1% salt yielded a cost of $63,700 per year, equating to $0.38/kgal. Increasing the salt addition to 3% increased costs to $76,000 per year, netting $0.46/kgal. The most expensive option was conventional salt regeneration, requiring $82,700 per year and equaling

$0.50/kgal. Over a design life of 10 years, conventional regeneration using 10% salt was found to be approximately twice as expensive compared to seawater regeneration.

Table 26: Total Regeneration Process Costs

Regeneration Process Costs	Regenerant Solution			
	RS1	**RS2**	**RS3**	**RS4**
Amortized Annual Capital Cost ($)	35,100	50,000	50,000	14,900
Annual O&M Cost ($)	7,170	13,700	26,000	67,800
Total Annual Process Cost ($)	42,200	63,700	76,000	82,700
10yr Total Process Cost ($/kgal)	0.25	0.38	0.46	0.50

Modeling Kinetics and Equilibrium

Kinetic studies were performed using four synthetic solutions (SS1-SS4) to classify kinetic rates, identify changes to rate constants, and to describe the adsorption process in terms of rate-controlling steps for bromide adsorption at different CBMR conditions. PFO and PSO models were used to fit kinetic data of bromide adsorption and were plotted linearly for adsorption rates. Rate constants were examined and described in terms of changes in different CBMR solutions. The IPD model was applied to kinetic data to determine rate-controlling steps, elucidating intra-particle and film diffusion mechanisms.

Equilibrium isotherm models were applied to bromide adsorption data in an unconventional manner to describe the changes in bromide equilibrium adsorption. Instead of increasing the bromide concentration and observing changes to equilibrium values, bromide concentrations were held constant and chloride concentrations were increased to observe changes in bromide equilibrium. SS1 was used as a baseline for bromide adsorption, containing approximately 71.5

mg/L bromide with no chloride. SS2 through SS4 represented bromide adsorption at increasing CBMR solutions of 21.9, 58.4, and 158 respectively. SS5 modeled CBMR ratios found in seawater, 496, and was used during equilibrium isotherm modeling.

Kinetics

The linearized form of the PFO model, presented in Equation (9), was used to investigate rate kinetics of bromide. If the reaction is described by PFO kinetics, a linear plot of $ln(q_e-q_t)$ *against t* will yield a straight line. The linear PFO plots of kinetic data against time did not result in a straight line, indicating that bromide adsorption does not follow PFO kinetics. Table 27 displays the results of PFO linear plots. Coefficient of determination (R^2) values of SS1 were found to be 0.889, decreasing to 0.860 in SS2, and then significantly decreasing in SS3 and SS4 as CBMRs increased.

Table 27: PFO Model Values

Synthetic Solution	**CBMR**	**$q_{e\ (exp)}$ ($mg\ g^{-1}$)**	**k_1 (min^{-1})**	**R^2**
SS1	0	13.6	0.099	0.889
SS2	21.9	7.70	0.100	0.860
SS3	58.4	4.26	0.051	0.285
SS4	158	2.44	<0.001	<0.100

In addition to the PFO model, the linearized form of the PSO model, Equation (11), was applied to kinetic data to determine reaction rates. The PSO initial adsorption rate constant, h_0, was also calculated; squaring the equilibrium adsorption capacity value, q_e, and multiplying by the PSO rate constant, k_2. A plot of t/q_{Br-} *against t* has been analyzed for the different CBMR solutions and is exhibited in Figure 36. Individual PSO plots are available in Appendix E.

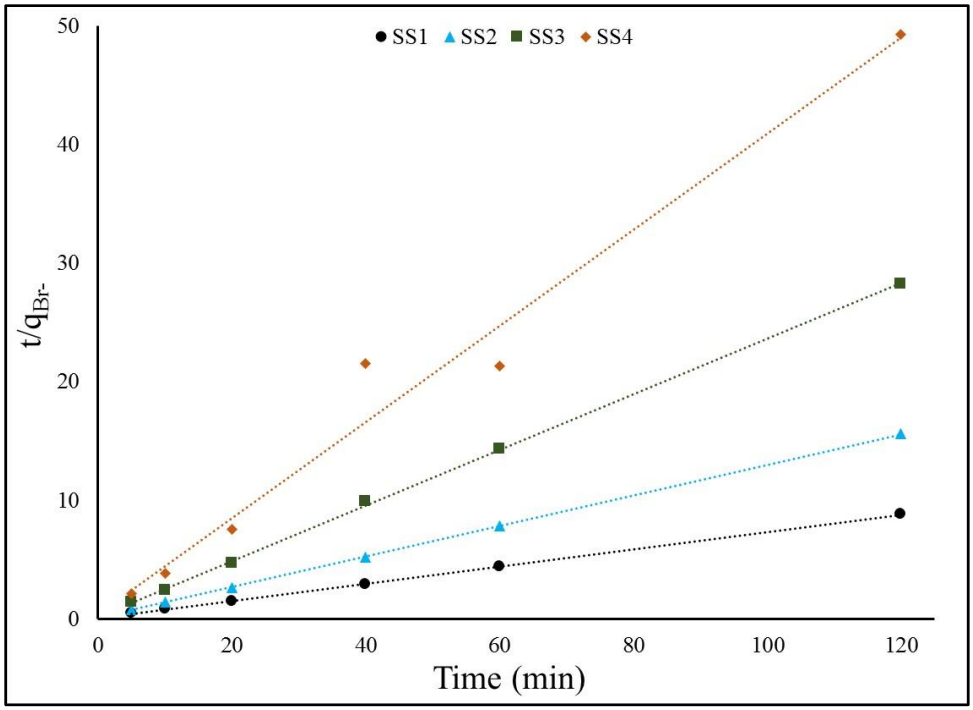

Figure 36: PSO Linear Plots

Figure 36 suggests that PSO kinetics accurately describe bromide adsorption, yielding straight line plots of t/q_{Br-} *against t* and indicating that bromide adsorption is controlled by chemisorption. Fitted PSO model kinetic parameters are detailed in Table 28, identifying rate constants of each plotted solution. R^2 values of SS1 through SS3 were 0.999, with SS4 producing 0.976. It is clearly shown that as the CBMR of each solution increases, so does the PSO rate constant, k_2. SS1 contained a k2 value of 0.057, increasing to 0.159 in SS2, further to 0.275 in SS3, and more so to 0.429 in SS4. This is demonstrated in Figure 36, exhibiting increased slopes from SS1 to SS4.

Table 28: PSO Model Values

Synthetic Solution	CBMR	$q_{e\ (exp)}$ (mg g^{-1})	k_2 (g mg^{-1} min^{-1})	h_o (g mg^{-1} min^{-1})	R^2
SS1	0	13.6	0.057	10.5	0.999
SS2	21.9	7.70	0.159	9.43	0.999
SS3	58.4	4.26	0.275	4.98	0.999
SS4	158	2.44	0.429	2.55	0.976

Inversely correlated to k_2 values, the initial adsorption rate, h_o, decreased as the CBMR of each solution increased. As the CBMR of the solution increased, the driving force of the bromide concentration diminished, thus resulting in a lower h_0. To demonstrate this relationship, k_2 and h_0 have been plotted in Figure 37.

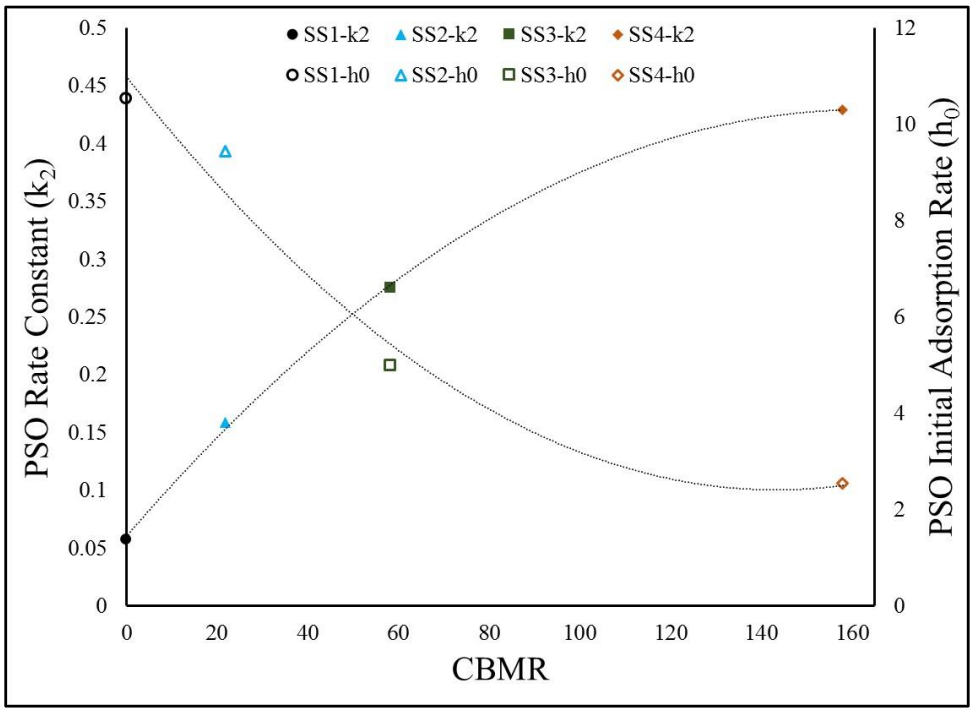

Figure 37: PSO Rate Constant and Initial Adsorption Rate Constant Plots

Although the PSO model indicates that reaction kinetics are controlled by chemisorption, there may indeed be more than one rate controlling step. In order to elucidate the driving mechanisms of bromide adsorption kinetics, the linearized form of the IPD model (Equation (12)) was employed to kinetic data to better understand diffusion based mechanisms. If a linear plot of q_t *against* $t^{1/2}$ yields a straight line, adsorption kinetics are said to be controlled by intra-particle diffusion. Figure 38 displays the linear plots of the IPD model, revealing two lines that do not pass through the origin. This indicates that there is more than one step controlling the adsorption rate. The first line occurs from 5min to 20min of adsorption and is denoted by IPD 1. The second line occurs from 40min to 120min of adsorption and is identified as IPD 2. Individual IPD plots are available in Appendix E.

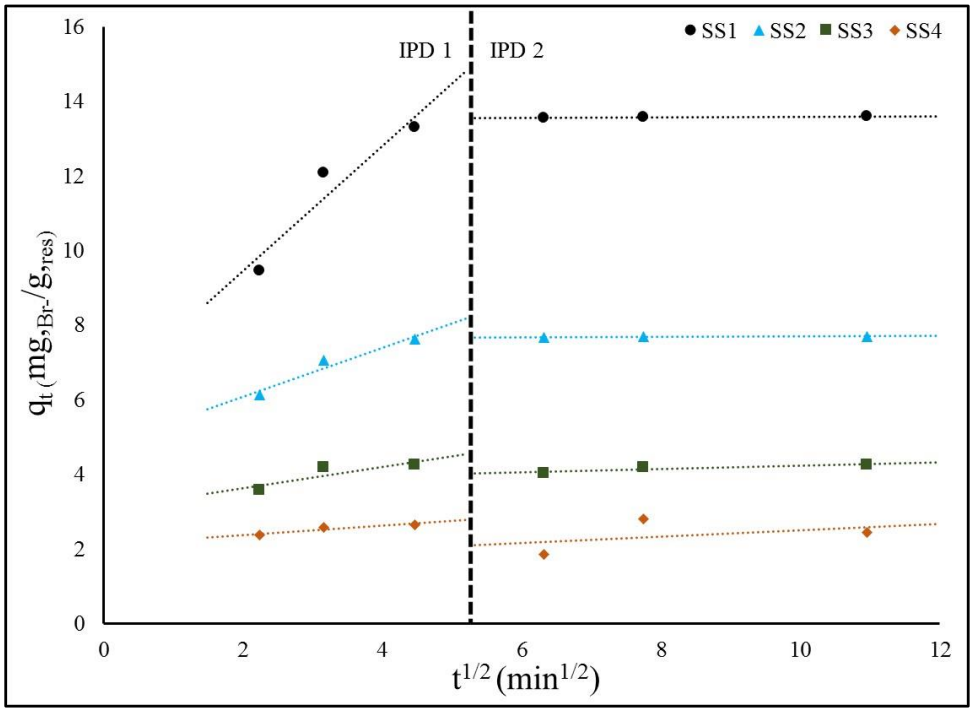

Figure 38: IPD Linear Plots

Table 29 presents the IPD model kinetic parameters of IPD 1 and IPD 2. R^2 is used to describe best-fit for the IPD model applied to each solution. Chemisorption is assumed to take place within the first 5min of the reaction. From there, both intra-particle and film diffusion mechanisms seemed to be present. Looking at SS1, intra-particle diffusion and film diffusion seemed to be taking place in the first 20min of adsorption following chemisorption. Continuing the reaction from 40min to equilibrium in SS1, intra-particle diffusion appeared to be the sole rate-controlling step. As CBMRs increased, there was a shift in the time at which this same trend occurred, happening earlier in the reaction. There was a decrease in intra-particle diffusion in IPD 2 as the CBMR of solution increased. The presence of increased chloride concentrations appeared to drive external mass transfer (film diffusion) earlier in the adsorption process, allowing intra-particle diffusion to begin occurring earlier. This is consistent with the trend of increasing PSO rate kinetics of bromide adsorption at increasing CBMRs. Though intra-particle diffusion seemed to be occurring earlier as CBMRs increased, the rate constant, k_{IPD1}, of IPD 1 decreased. Additionally, the boundary layer thickness of intra-particle diffusion, C_{IPD}, decreased with increased CBMRs.

Table 29: IPD Model Values

Synthetic Solution	**k_{IPD1} mg g^{-1} ($(min^{1/2})^{-1}$)**	**C_{IPD1} (mg/g)**	**R^2**	**k_{IPD2} mg g^{-1} ($(min^{1/2})^{-1}$)**	**C_{IPD2} (mg/g)**	**R^2**
SS1	1.67	6.13	0.910	0.010	13.5	0.993
SS2	0.655	4.78	0.944	0.006	7.64	0.953
SS3	0.286	3.06	0.737	0.042	3.81	0.789
SS4	0.124	2.13	0.853	0.084	1.67	0.173

Equilibrium

Equilibrium isotherms were developed using the linear-forms of the FIM and LIM, given in Equations (6) and (7). Experimental equilibrium adsorption capacity values of bromide were plotted against the CBMR of solution. Bromide concentrations were held constant and chloride concentrations were increased to assess the impacts of bromide equilibrium adsorption at different CBMRs. Figure 39 displays the linear plots of the FIM and Figure 40 presents the linear plots of the LIM for SS1 through SS5. Table 30 shows the isotherm model values derived from the linear regression analysis. The FIM results in an unconventional negative slope, seeing a decrease in bromide adsorption as chloride increases. Both models adequately described adsorption equilibrium of bromide in the presence of varying chloride concentrations, yielding R^2 values of 0.992 and 0.991 for the FIM and LIM linear plots respectively.

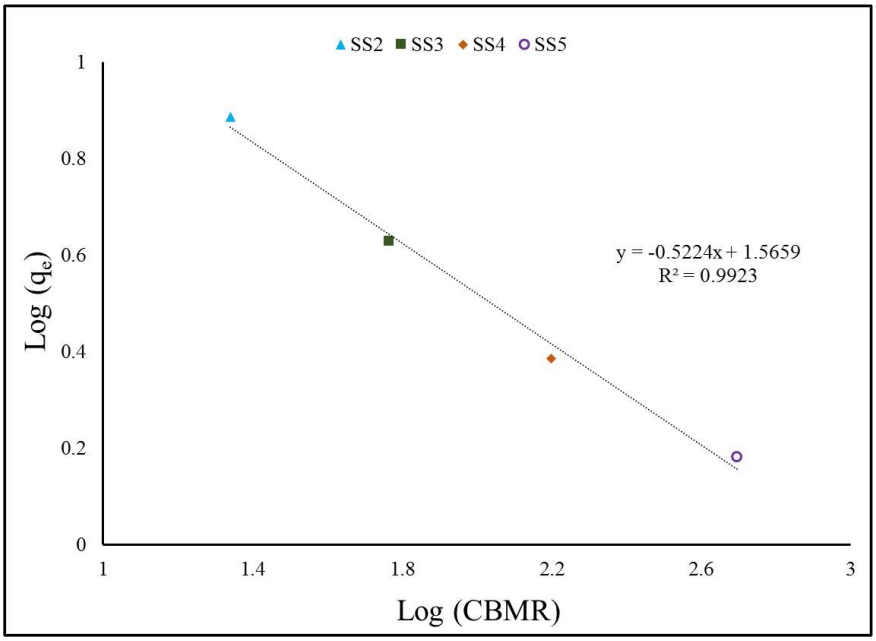

Figure 39: Linear Plot of FIM

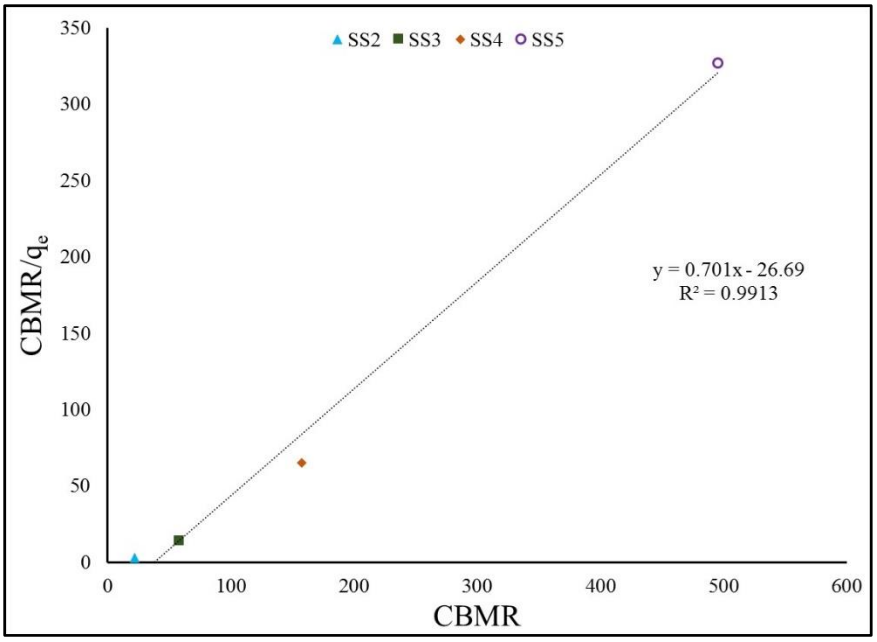

Figure 40: Linear Plot of LIM

Table 30: FIM and LIM Values

Freundlich			Langmuir		
K_f	n	R^2	b	q_{max}	R^2
0.195	-1.91	0.992	-0.026	1.43	0.991

Brominated Disinfection By-Product Impacts

Observed bromide elution from seawater-based regeneration was found to increase brominated DBPs after the addition of free chlorine. Four synthetic groundwater solutions (GS1-GS4), containing varying bromide concentrations and the CITY's Verna groundwater, were used to assess the impacts of bromide on DBP formation. The 96-hr formation of TTHMs and HAA5s are compared for their species composition against initial bromide concentrations. Shifts in DBP speciation were identified and presented.

Figure 41 illustrates the 96-hr formation of TTHMs and initial bromide concentrations of the four tested groundwater solutions. The predominant trihalomethane species formed in GS1, containing the highest amount of initial bromide, was bromoform. As initial bromide concentrations decrease, GS1 through GS4, there is a shift in formed species from bromoform toward chlorinated trihalomethanes. This shift is seen clearly from GS3 to GS4, decreasing in bromoform with appreciable increases sequentially in dibromochloromethane, bromodichloromethane, and chloroform. At initial bromide concentrations above 1 mg/L, the trend of increased TTHMs matched that of bromoform, distinctly shown from GS2 to GS1. The increase in TTHMs from GS2 to GS1 equaled approximately 34 μg/L, with an increase in bromoform of around 41 μg/L.

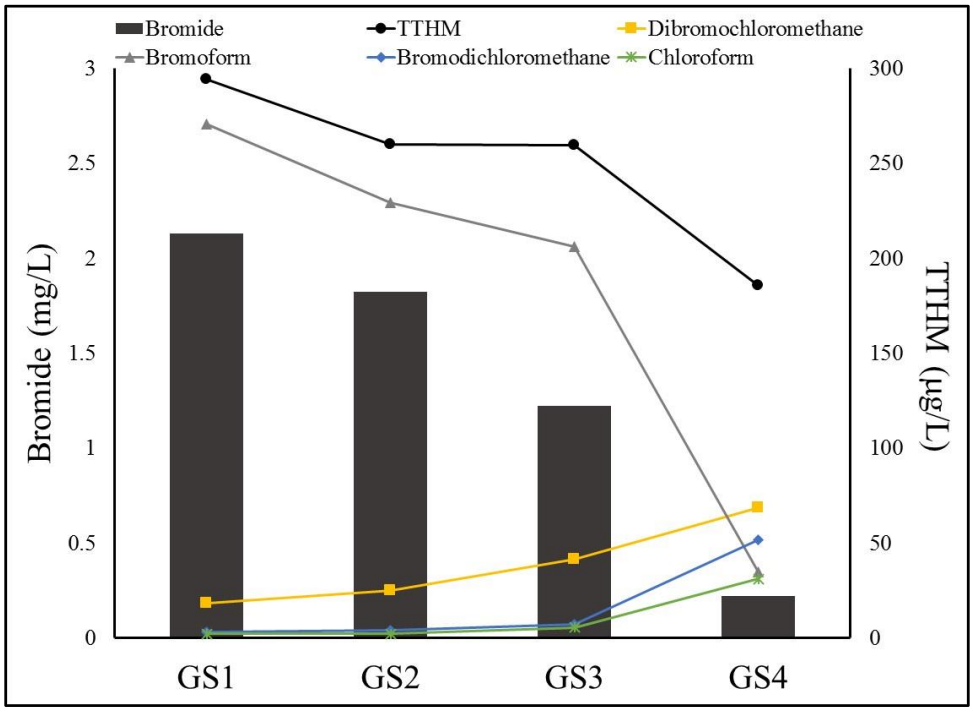

Figure 41: Comparison of 96-hr TTHM Composition and Initial Bromide Concentration

Figure 42 presents the 96-hr formation of HAA5s and initial bromide concentrations of the four tested groundwater solutions. The predominant haloacetic acid species formed in GS1, containing the highest amount of initial bromide, was dibromoacetic acid. A similar trend is observed in HAA5 formation, decreasing in brominated HAA5 species as initial bromide concentrations decrease. This shift is most apparent from GS3 to GS4, decreasing in dibromoacetic acid toward trichloro- and dichloro- acetic acid. At initial bromide concentrations above 1 mg/L, the trend of increased HAA5s matched that of dibromoacetic, distinctly shown from GS3 through GS1. The increase in HAA5s from GS3 through GS1 equaled approximately 3 μg/L, with an increase in dibromoacetic acid of 3 μg/L.

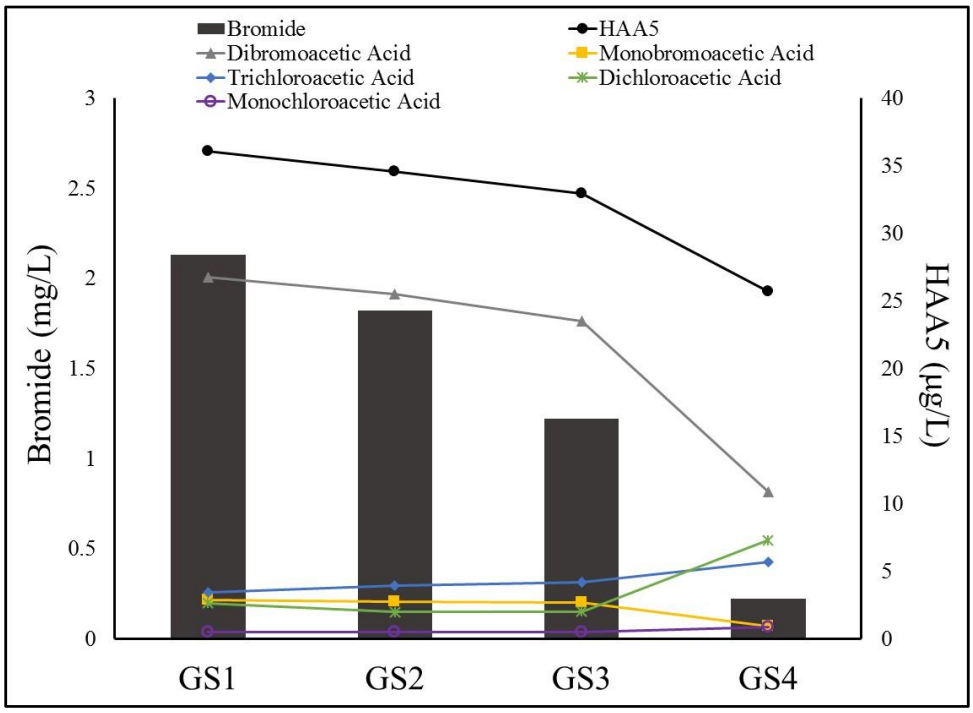

Figure 42: Comparison of 96-hr HAA5 Composition and Initial Bromide Concentration

Figure 41 and Figure 42 indicate that bromide elution concentrations from seawater-based regeneration resulted in increased brominated DBPs, particularly bromoform with respect to trihalomethanes and dibromoacetic acid concerning haloacetic acids. Decreases in initial bromide concentrations from GS1 to GS3 demonstrated a comparable decrease in bromoform and dibromoacetic acid. Initial bromide concentrations below 1 mg/L, GS4, exhibited inverse relationships between brominated DBPS and chlorinated DBPs. At initial bromide concentrations above 1 mg/L, increased TTHMs were largely related to increased bromoform and increased HAA5s were due to dibromoacetic acid.

CHAPTER 6: SUMMARY, CONCLUSIONS, AND RECOMMENDATIONS

Bench-Scale Column Testing

The operational performance and secondary impacts of Sarasota Bay seawater regeneration for AIX processes has been evaluated. This research investigated the use of seawater, and salt-supplemented seawater, as a regenerant solution for an AIX process removing sulfate and organics in terms of performance efficiency and identifying the secondary impacts of alternative methods when compared with conventional regeneration procedures. Four bench-scale columns were operated in parallel to delineate changes in operational performance and identify impacts emanating from seawater-based regeneration.

Column Performance and Identified Impacts

Results indicate that seawater regeneration decreased operational AIX performance. Additions of salt to seawater improved performance. Conventional 10% salt regeneration experienced sulfate exhaustion at 151 BV, yielding a resin exchange capacity of 1.90 eq/L. After regenerating with SBSW, sulfate exhaustion occurred at 138 BV, equating to a resin exchange capacity of 1.74 eq/L and a loss of 8.62%. With the addition of 1% and 3% (by volume) salt to SBSW, sulfate exhaustion occurred at 141 BV and 147 BV respectively; improving exchange capacity to 1.77 eq/L (6.84% loss compared with conventional salt) and 1.85 eq/L (2.63% loss compared with conventional salt) accordingly. Natural organic matter removal was consistent, between 85.8% and 89.2% average removal as measured by DOC. Similar observations were noted in UV-254 measurements, averaging a 65.2% to 73.6% reduction.

Clumping/fouling of the anion resin was observed during operational experiments under each regenerant solution condition. Clumping/fouling of the anion resin may have resulted in performance loss due to channeling or resin poisoning (resin inactivation). Analysis was not performed on the unknown material contributing to resin clumping/fouling in this work. It was hence reasoned that the cause of resin clumping/fouling was independent of the regeneration process, forming consistently under each regenerant condition. It is suspected that the complex water matrix of the Verna feed groundwater contributed to resin clumping/fouling.

Seawater regeneration resulted in the incidental uptake of bromide, competing with chloride for exchange sites on the anion resin during regeneration and eluting during subsequent operational runs. A correlation between bromide elution and regenerant chloride concentration was observed. As the CBMR increased, the anion resin's selectivity toward chloride increased, decreasing bromide elution. Bromide elution was observed at an average of 2.13 mg/L when SBSW was used for regeneration, containing a CBMR of 516. Bromide elution decreased to an average of 1.82 mg/L with the addition of 1% salt to SBSW, wielding a CBMR of 684. Further increasing the CBMR to 1021 with the addition of 3% salt to SBSW, bromide elution decreased to an average of 1.25 mg/L. Bromide elution was not detected after using conventional 10% salt conditions typically used for IX regeneration.

Conceptual Regeneration Cost Comparison

A conceptual full-scale AIX system was modeled using operating performance values obtained during bench-scale studies to quantify seawater regeneration costs as compared to salt-supplemented seawater, and conventional 10% salt. Regeneration capital costs were amortized at

an annual interest rate of 4.5% over a 10-year design life and added to annual O&M regeneration costs to produce total regeneration process costs of each option. Conventional 10% salt regeneration was found to be approximately twice as expensive when compared to seawater regeneration, producing a 10-year total regeneration process cost of $0.50/kgal compared to $0.25/kgal. Salt-supplemented seawater regeneration yielded total regeneration process costs of $0.38/kgal and $0.46/kgal for 1% and 3% salt respectively. Over a design life of 10 years, conventional regeneration using 10% salt was found to be approximately twice as expensive compared to SBSW regeneration.

Jar Testing

Understanding the kinetic and equilibrium reactions taking place during AIX regeneration is important when alternative regeneration methods are being considered. Funasaki (1979) identified changes to equilibrium and kinetic reactions under variable salt conditions, which is typical in chloride-form AIX regenerant solutions. To explicate the phenomenon of bromide exchange during seawater-based regeneration, kinetic and equilibrium studies were performed at various CBMRs under jar testing conditions. The experiments examined changes to equilibrium values, kinetic rates, and rate-controlling steps of bromide adsorption in the presence of high chloride concentrations.

Kinetics

Bromide adsorption curves were developed and fitted to PFO and PSO models. Bromide adsorption in solutions of varying CBMRs can be accurately described by PSO rate kinetics, indicating chemisorption is the primary rate-controlling step. Plots of the linearized form of the

PSO model yielded R^2 values of 0.999 in solutions containing up to 58.4 CBMRs. An R^2 value 0.976 was obtained for the linearized PSO model at a CBMR of 158. The PSO rate constant, k_2, was found to increase as CBMRs increased. Inversely correlated to k_2 values, the initial PSO adsorption rate constant, h_0, decreased as CBMRs increased.

Even though the PSO model indicated that reaction kinetics are controlled by chemisorption, there may indeed be more than one rate-controlling step. The linearized form of the IPD model was fitted to kinetic data to elucidate diffusion-based mechanisms. Multi-linear plots were skewed from the origin axis, indicating more than one rate-controlling step could be present. Chemisorption was reasoned to take place within the first 5min of the reaction. From 5min to 20min, both intra-particle and film diffusion mechanisms appeared to be the predominant mass transfer present. From 40min to equilibrium, intra-particle diffusion appeared to be the sole rate-controlling step. As CBMRs increased, there was a shift in the time at which this same trend occurred. The presence of increased chloride concentrations appeared to increase external mass transfer (film diffusion) earlier on in the adsorption process, driving the reaction in the early phases after chemisorption, allowing intra-particle diffusion to occur earlier. This is consistent with the trend of increased PSO rate kinetics of bromide adsorption with increased CBMRs. Though intra-particle diffusion appeared to be present initially, as CBMRs increased, the rate constant, k_{IPD1}, of IPD 1 decreased. Additionally, the boundary layer thickness of intra-particle diffusion, C_{IPD}, decreased with increased CBMRs.

Equilibrium

Equilibrium bromide adsorption values were experimentally determined for different CBMR solutions. Equilibrium adsorption capacity, q_e, of bromide decreased as chloride concentrations

increased. A plot of equilibrium bromide adsorption capacity values against the solution's CBMR resulted in a logarithmic decay as CBMRs increased in synthetic solutions, starting at 13.6 mg/g at a CBMR of 0 and ending at 1.96 mg/g at a CBMR of 496. An experimental function was derived to approximate bromide equilibrium adsorption capacity, q_e, in relation to a solutions CBMR, yielding an R^2 of 0.938. Using Equation (24), equilibrium adsorption capacity of bromide can be approximated for solutions containing different CBMRs, such as brackish groundwater and seawater commonly used in potable water production; however, this function does not account for the additional ions found in natural water matrices.

$$q_e = -1.09 \ln(CBMR) + 9.0001 \quad (24)$$

The q_e of SBSW was found to be 0.340 mg/g, equating to approximately 2.19% bromide exchange. This matched well with the observed bromide elution of 2.13 mg/L from seawater regeneration during bench-scale column studies, equaling around 2.62% bromide exchange. Separation factors of bromide with respect to chloride were determined, ranging from 0.623 to 4.52 in synthetic solutions of CBMRs from 0 to 496. The SBSW tested yielded a bromide separation factor of 73.7, significantly higher than values obtained with synthetic solutions and likely due to the high competing sulfate concentrations found in the SBSW regenerant.

Equilibrium isotherms were developed using the linear-forms of the FIM and LIM to identify the behavior of the adsorption process. Experimental equilibrium adsorption capacity values of bromide were plotted against the CBMR of solution. Bromide concentrations were held constant and chloride concentrations were increased to assess the impacts of bromide equilibrium adsorption at different CBMRs. A straight-line plot of the FIM revealed a negative slope,

suggesting decreased bromide adsorption as chloride increased. Both models described bromide adsorption behavior accurately, producing an R^2 of 0.992 for the FIM and 0.991 for the LIM. FIM constants, K_f and n, equaled 0.195 and -1.91 severally. LIM constants, b and q_{max}, were -0.026 and 1.43 respectively.

Disinfection By-Product Formation

Seawater can contain elevated quantities of bromide, approximately 81.3 mg/L in SBSW, leading to bromide exchange during AIX seawater-based regeneration and subsequent bromide elution into treated water streams. Bromide contributes to increased DBPs, shifting the type of DBP species that are formed with decreasing chlorinated DBP species and increased brominated DBP species, consistent with the findings of others (Dyck et al., 2015; Kolb et al., 2017; Richardson et al., 1999). The data also established that brominated DBPs carry higher health associated risks, correlating to higher cytotoxicity and genotoxicity than chlorinated DBPs (Kolb et al., 2017; Richardson et al., 1999; Sharma et al., 2014; Yang et al., 2014; Zhai & Zhang, 2011; Zhai et al., 2014). The impacts of bromide elution from seawater-based regeneration on the formation of DBPs was assessed using the CITY's aerated Verna groundwater and spiked bromide mass at concentrations that were observed during column testing. Verna groundwater contained an average DOC concentration of 1.77 mg/L and an average UV-254 measurement of 0.047 cm^{-1}. Free chlorine was used as a disinfectant.

TTHM Formation and Speciation

The 96-hr TTHM formation increased as initial bromide concentration increased. At an initial bromide concentration of 2.13 mg/L, 96-hr TTHM formation equaled 294 μg/L. Reducing the

initial bromide concentration to 0.22 mg/L, TTHM formation decreased to 186 μg/L. Bromoform was found to be the dominant trihalomethane species in solutions containing initial bromide concentrations greater than 1 mg/L, comprising 79.4% to 92.0% of TTHMs formed. As initial bromide content decreased, there was a shift from brominated species toward chlorinated trihalomethanes. Furthermore, this shift results in a decrease in bromoform with appreciable increases in dibromochloromethane, bromodichloromethane, and chloroform.

HAA5 Formation and Speciation

The 96-hr HAA5 formation followed a similar trend, increasing as initial bromide concentration increased, but the discrepancy was not as pronounced as TTHM formation. 96-hr HAA5 formation was 36.1 μg/L at an initial bromide concentration of 2.13 mg/L, decreasing to 25.7 μg/L at an initial bromide concentration of 0.22 mg/L. Dibromoacetic acid made up the majority of 96-hr HAA5 formation, approximately 71.4% to 74.1% in solutions containing initial bromide concentrations greater than 1 mg/L. Dibromoacetic acid decreased as initial bromide concentrations decreased, shifting to more chlorinated species.

Recommendations

This work has demonstrated that filtered and disinfected seawater can be used to effectively regenerate an anion exchange process removing sulfate and organics if properly managed. Additionally, this work has evaluated the impacts stemming from seawater-based regeneration, elucidating the propensity for bromide competition with chloride that can limit the efficiency of the treatment process due to the formation of brominated DBPs. Although this research

demonstrated that bromide elution and leakage are present, additional work is required to enhance the current understanding. The following recommendations are offered in this regard:

- This work evaluated sulfate and natural organic matter removal using anion exchange and identified bromide as having a residual impact. However, the removal performance of other inorganic constituents when regenerating with seawater-based regenerants could be performed: phosphate, fluoride, nitrate, chromate, and dichromate.
- Compare the performance and impacts of anion exchange regeneration employing seawater from other locations around the world with different water matrix compositions and characteristics than what was evaluated in this work.
- Investigate the possibility that microbiological activity within the anion exchange bed is complicit in observed fouling (clumping) of the resin.
- Incorporate additional ions, commonly found in seawater, into the experimentally-derived model utilizing the CBMR of solutions for the prediction of bromide elution.
- Evaluate the equilibrium and kinetic relationship between bromide and chloride at high CBMRs comprised of varying sulfate concentrations.
- Assess the impacts of brominated DBP formation stemming from bromide elution when disinfectants other than chlorine are employed.

APPENDIX A: PSEUDO 1ST AND 2ND ORDER RATE LAWS

Pseudo 1st Order Integration

$$\frac{dq_t}{dt} = k_1(q_e - q_t)$$

$$\frac{dq_t}{(q_e - q_t)} = k_1 dt$$

$$\int_0^{q_t} \frac{dq_t}{(q_e - q_t)} = k_1 \int_0^t dt$$

U Substitution
U = qe-qt
dU = -dqt

$$-\int \frac{1}{U} dU = k_1 t$$

$$lnU|k_1 t$$

$$\ln(q_e - q_t)\Big|_0^{q_t} = k_1 t$$

$$lnq_e - \ln(q_e - q_t) = k_1 t$$

$$\ln(q_e - q_t) = lnq_e - k_1 t$$

Pseudo 2nd Order Integration

$$\frac{dq_t}{dt} = k_2(q_e - q_t)^2$$

$$\frac{dq_t}{(q_e - q_t)^2} = k_2 dt$$

$$\int_0^{q_t} \frac{dq_t}{(q_e - q_t)^2} = k_2 \int_0^t dt$$

U Substitution
U = qe-qt
dU = -dqt

$$-\int \frac{1}{U^2} dU = k_2 t$$

$$\frac{1}{U} | k_2 t$$

$$\frac{1}{q_e - q_t} \Big|_0^{q_t} = k_2 t$$

$$\frac{1}{q_e - q_t} = k_2 t + \frac{1}{q_e}$$

$$q_t = \frac{k_2 t {q_e}^2}{1 + k_2 t q_e}$$

$$\frac{t}{q_t} = \frac{1}{k_2 q_e^2} + \frac{1}{q_e} t$$

APPENDIX B: ANALYTICAL WATER QUALITY METHODS

Table 31: Analytical Water Quality Methods

Test	Test Location	Method	Equipment Description	Method Detection Level
pH	WTF/UCF Laboratory	SM: 4500-H+ B. Electrometric Method	HACH HQ 40d	0.01 s.u.
DOC	UCF Laboratory	SM: 5310 C. Persulfate-Ultraviolet or Heated –Persulfate Oxidation Method	Teledyne Tekmar Total Organic Carbon Fusion UV/Persulfate Analyzer	0.10 mg/L
Conductivity	WTF/UCF Laboratory	SM: 2510 B. Laboratory Method	HACH HQ 40d	0.01µS/cm
TDS	UCF Laboratory	SM: 2540 C. Total Dissolved Solids Dried at 180°C	Mettler Toledo ML104/03 Analytical Balance Thermo-Scientific HERA Therm Oven	4 mg/L
Apparent Color	UCF Laboratory	SM: 2120 C. Spectrophotometric-Single-Wavelength Method	HACH DR 2700 Spectrophotometer	1 PCU
UV_{254}	UCF Laboratory	SM: 5910 B. Ultraviolet Absorption Method	HACH DR 5000 Spectrophotometer	0.01 cm^{-1}
Alkalinity	UCF Laboratory	SM: 2320 B. Titration Method	Sulfuric Acid Burette Titration	5 mg/L as CaCO3
Calcium	UCF Laboratory	SM: 3120 B. Inductively Coupled Plasma (ICP) Method	ICP Sectrometer - Perkin Elmer Optima 2100 DV	0.01 mg/L
Magnesium	UCF Laboratory	SM: 3120 B. ICP Method	ICP Spectrometer - Perkin Elmer Optima 2100 DV	0.03 mg/L
Sodium	UCF Laboratory	SM: 3120 B. IC Method	ICP Spectrometer - Perkin Elmer Optima 2100 DV	0.03 mg/L

Test	Test Location	Method	Equipment Description	Method Detection Level
Silica	UCF Laboratory	SM: 3120 B. Inductively Coupled Plasma (ICP) Method	Inductively Coupled Plasma Spectrometer - Perkin Elmer Optima 2100 DV	0.02 mg/L
Potassium	UCF Laboratory	SM: 3120 B. Inductively Coupled Plasma (ICP) Method	Inductively Coupled Plasma Spectrometer - Perkin Elmer Optima 2100 DV	0.1 mg/L
Strontium	UCF Laboratory	SM: 3120 B. Inductively Coupled Plasma (ICP) Method	Inductively Coupled Plasma Spectrometer - Perkin Elmer Optima 2100 DV	0.005 mg/L
Barium	UCF Laboratory	SM: 3120 B. Inductively Coupled Plasma (ICP) Method	Inductively Coupled Plasma Spectrometer - Perkin Elmer Optima 2100 DV	0.005 mg/L
Iron	UCF Laboratory	SM: 3120 B. Inductively Coupled Plasma (ICP) Method	Inductively Coupled Plasma Spectrometer - Perkin Elmer Optima 2100 DV	0.01 mg/L
Manganese	UCF Laboratory	SM: 3120 B. Inductively Coupled Plasma (ICP) Method	Inductively Coupled Plasma Spectrometer - Perkin Elmer Optima 2100 DV	0.001mg/L
Bromide	UCF Laboratory	SM: 4110 B. Ion Chromatography	Ion Chromatography - Dionex ICS-1100 with AS40 Automated Sampler	0.2 mg/L

Test	Test Location	Method	Equipment Description	Method Detection Level
Chloride	UCF Laboratory	SM: 4110 B. Ion Chromatography	Ion Chromatography - Dionex ICS-1100 with AS40 Automated Sampler	0.004 mg/L
Fluoride	UCF Laboratory	SM: 4110 B. Ion Chromatography	Ion Chromatography - Dionex ICS-1100 with AS40 Automated Sampler	0.1 mg/L
Sulfate	UCF Laboratory	SM: 4110 B. Ion Chromatography	Ion Chromatography - Dionex ICS-1100 with AS40 Automated Sampler	0.018 mg/L
Sulfide	UCF Laboratory	SM: 4500 F. Iodometric Method	Iodine Burette Titration	0.1 mg/L
Free Chlorine	UCF Laboratory	SM: 4500 G. DPD Colorimetric Method	HACH DR 2700 Spectrophotometer	0.01 mg/L
TTHMs	UCF Laboratory	SM: 5710	Gas Chromatography	4 μg/L
HAA5	Advanced Environmental Laboratories, Inc.	EPA 552.2	-	0.50 μg/L

APPENDIX C: COLUMN PERFORMANCE SUMMARY TABLE AND GRAPHS

Table 32: Average Column Performance Data

Parameter	Column			
	1	2	3	4
Breakthrough (BV) (10% of feed)	67.5	74.4	72.4	76.6
Exhaustion (BV) (90% of feed)	138	141	147	151
Exchange Capacity ($eq/L_{res,wet}$)	1.74	1.77	1.85	1.90
Specific Throughput ($L/g_{res,dry}$)	0.371	0.378	0.395	0.405
Sulfate Leakage (mg/L)	10.2	9.90	10.6	13.5

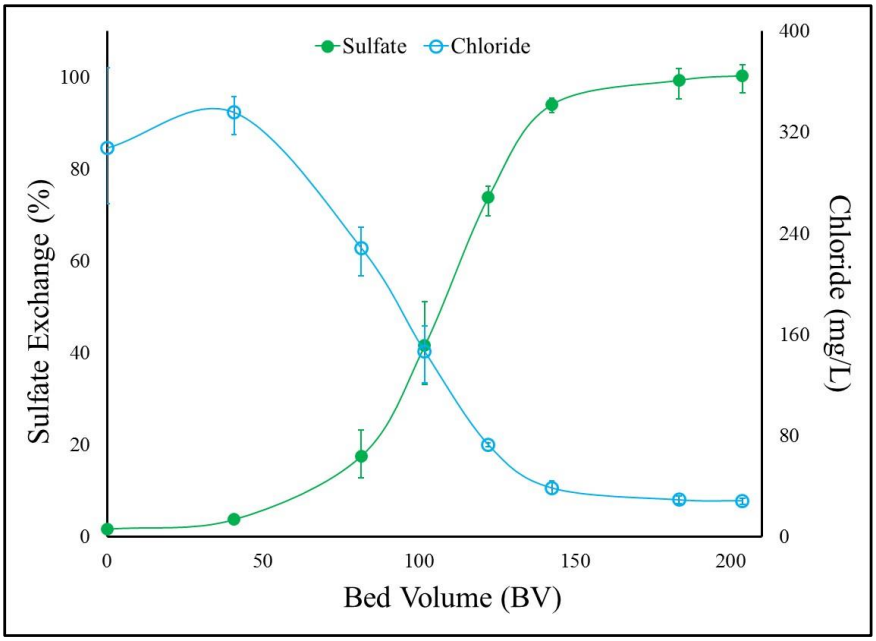

Figure 43: Column 1 Sulfate and Chloride Curves

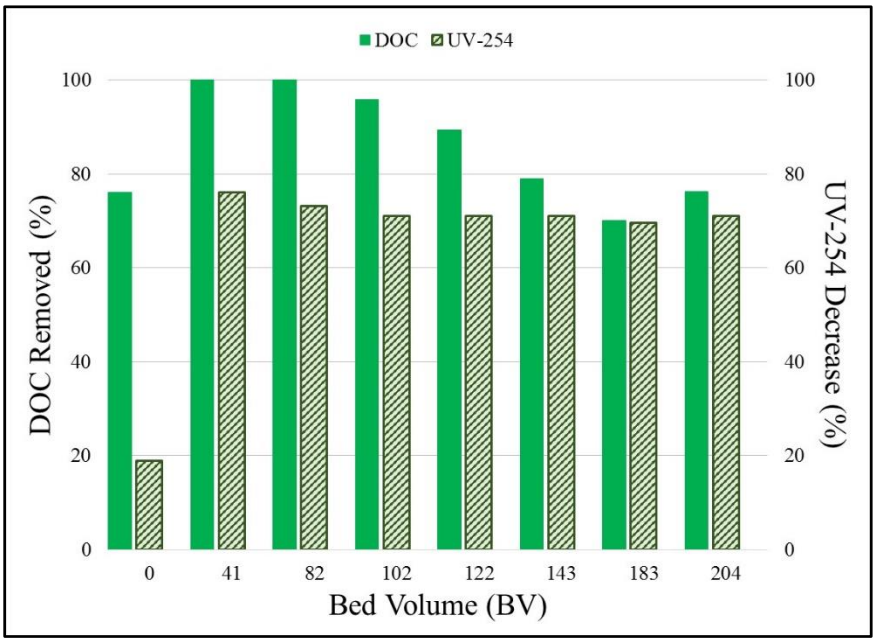

Figure 44: Column 1 DOC and UV-254 Values

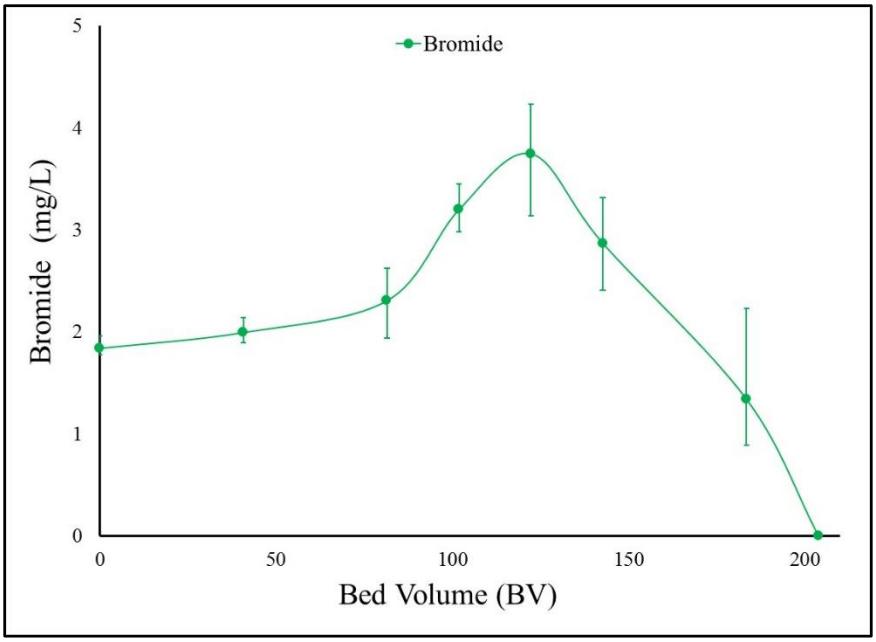

Figure 45: Column 1 Bromide Elution Curve

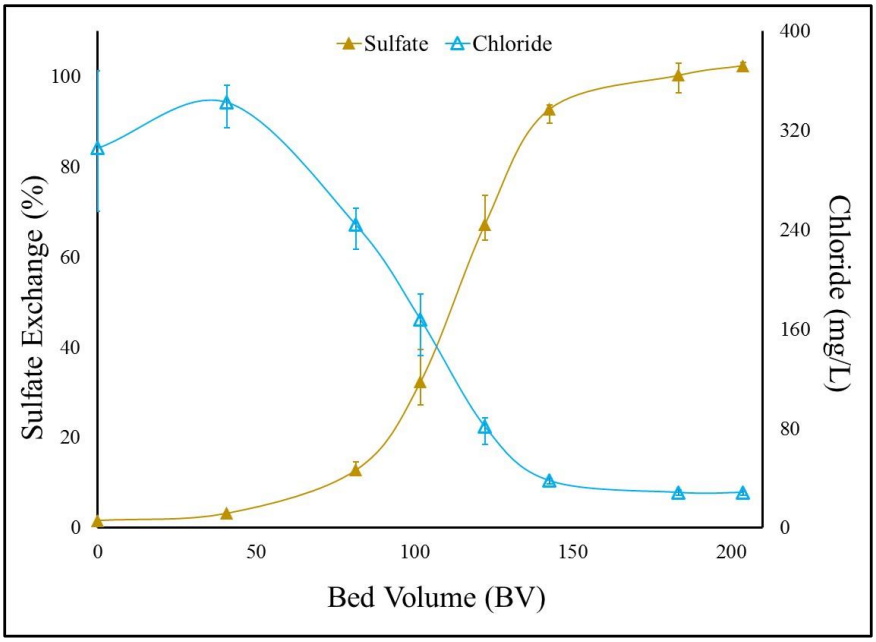

Figure 46: Column 2 Sulfate and Chloride Curves

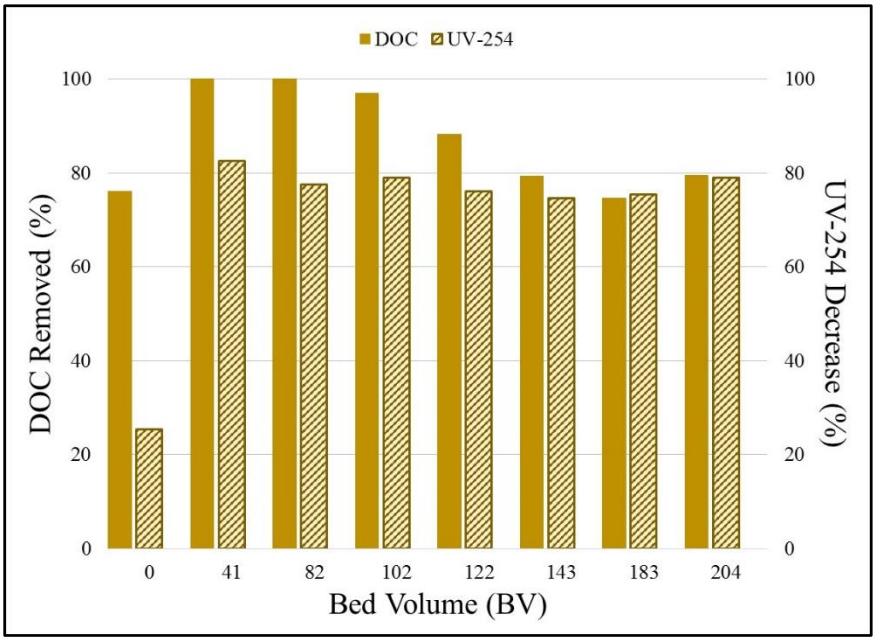

Figure 47: Column 2 DOC and UV-254 Values

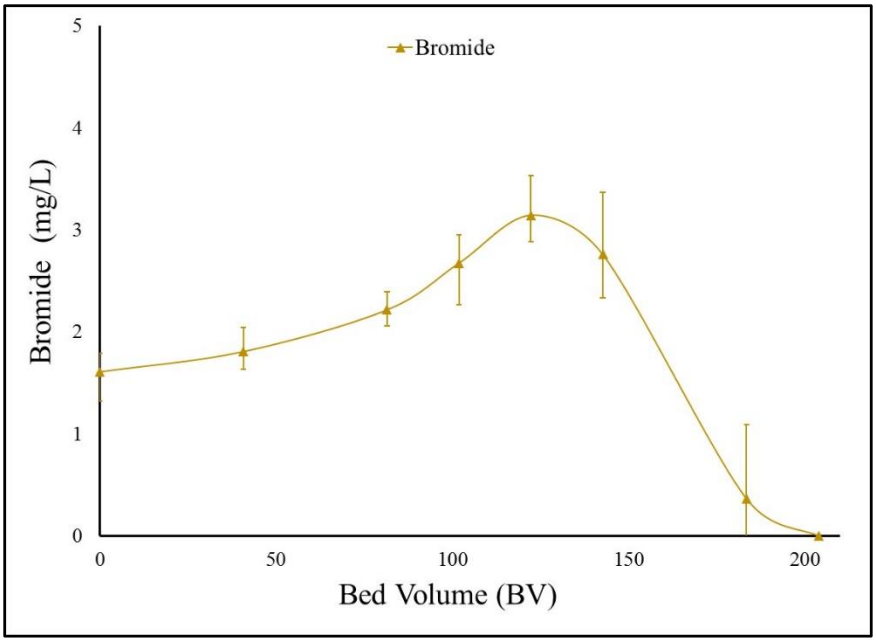

Figure 48: Column 2 Bromide Elution Curve

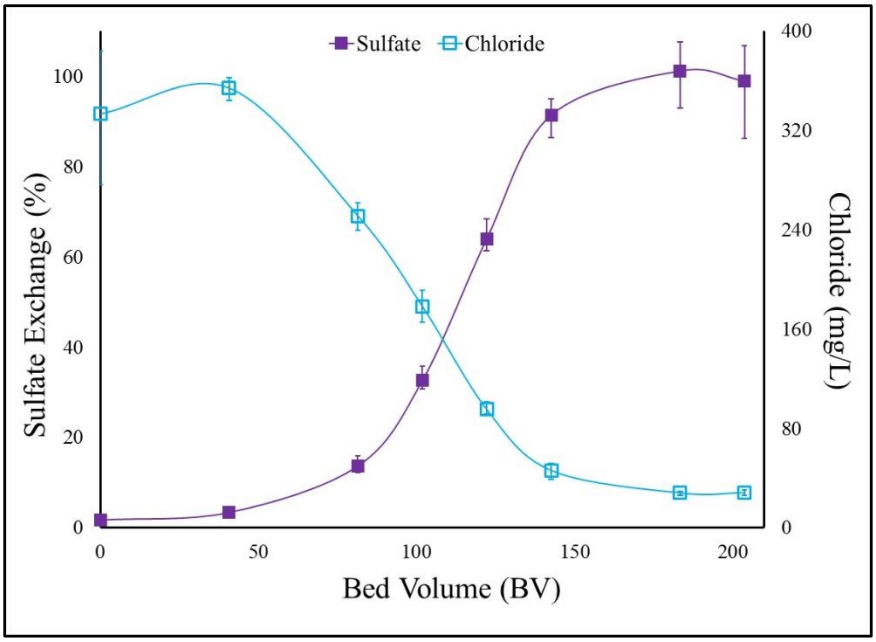

Figure 49: Column 3 Sulfate and Chloride Curves

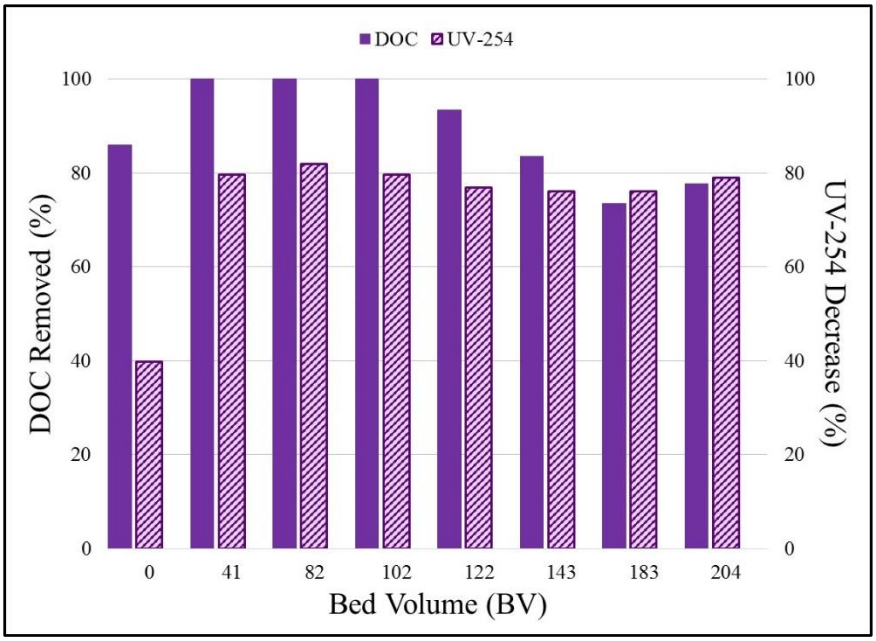

Figure 50: Column 3 DOC and UV-254 Values

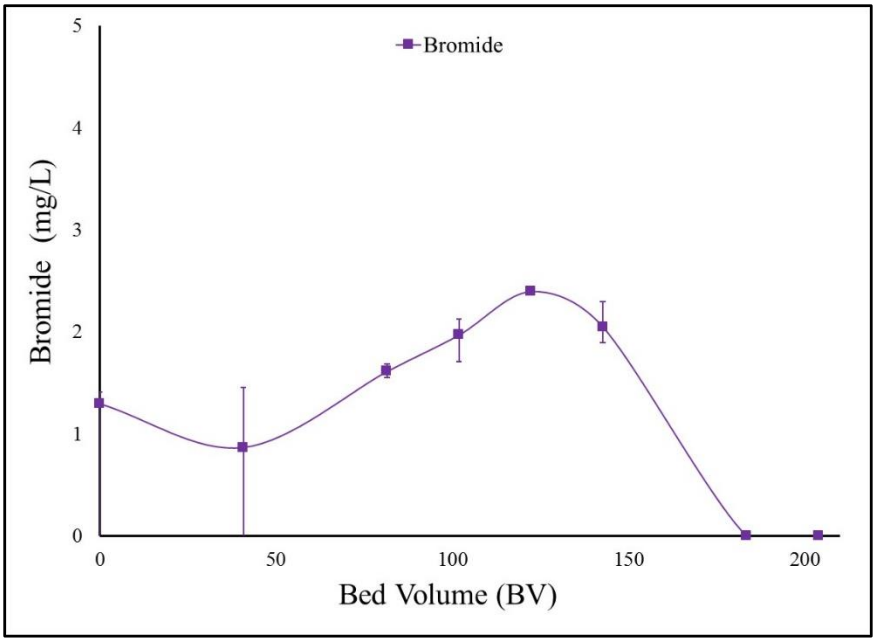

Figure 51: Column 3 Bromide Elution Curve

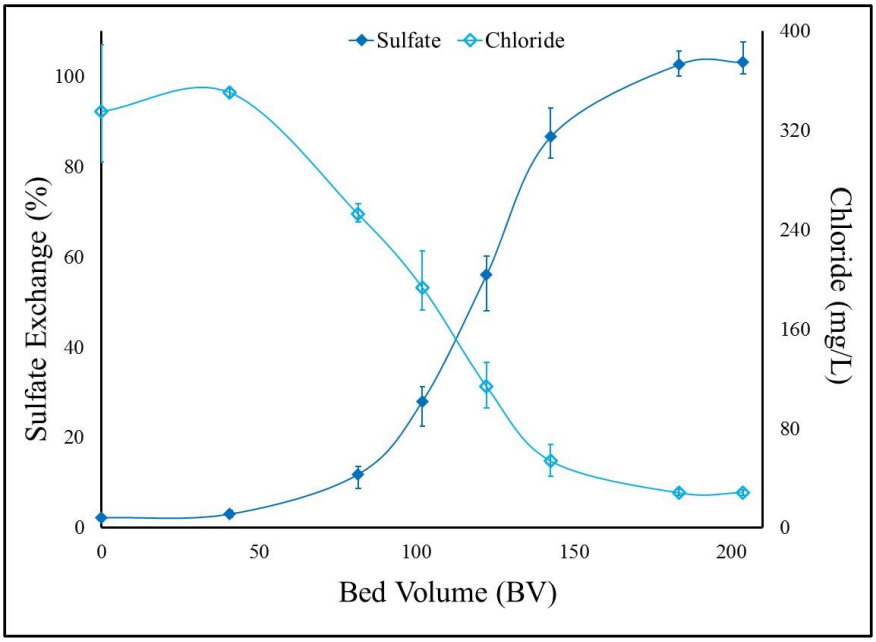

Figure 52: Column 4 Sulfate and Chloride Curves

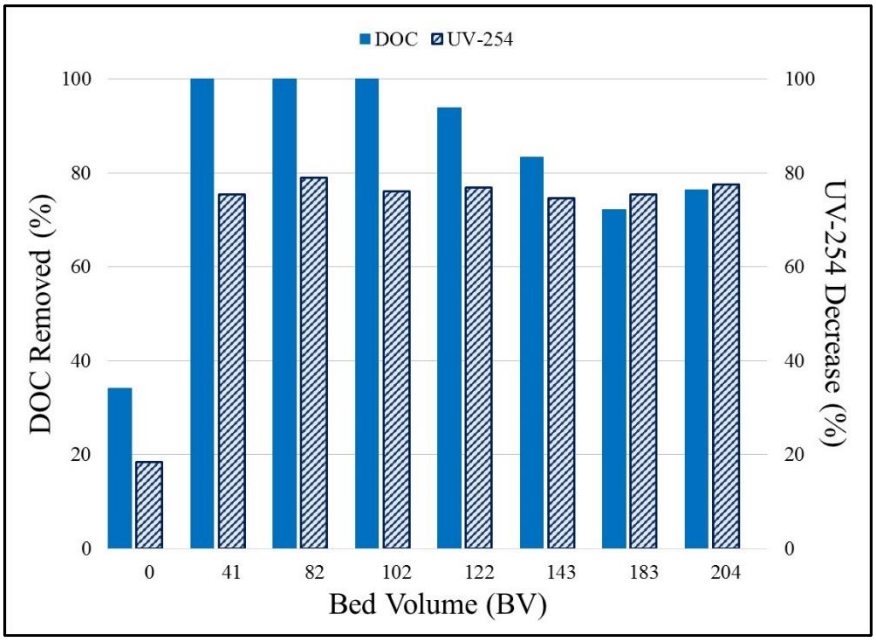

Figure 53: Column 4 DOC and UV-254 Values

APPENDIX D: DISINFECTION BY-PRODUCT FORMATION GRAPHS

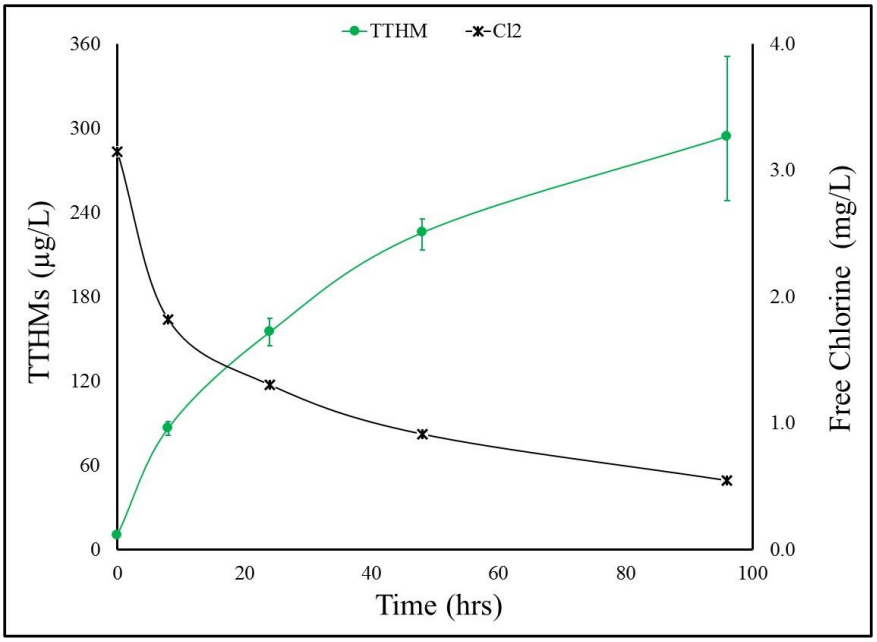

Figure 54: GS1 TTHM Formation Potential and Free Chlorine Curves

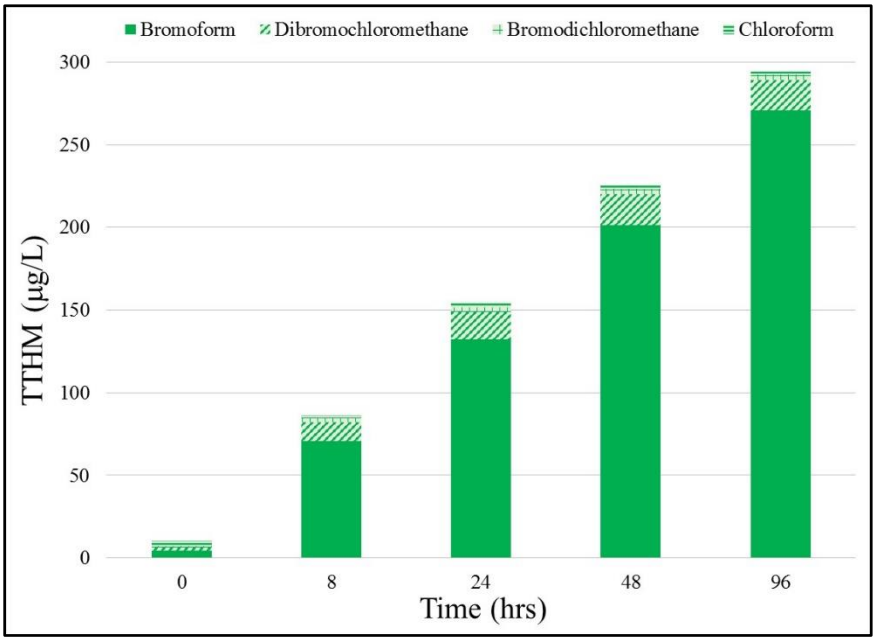

Figure 55: GS1 TTHM Composition Graph

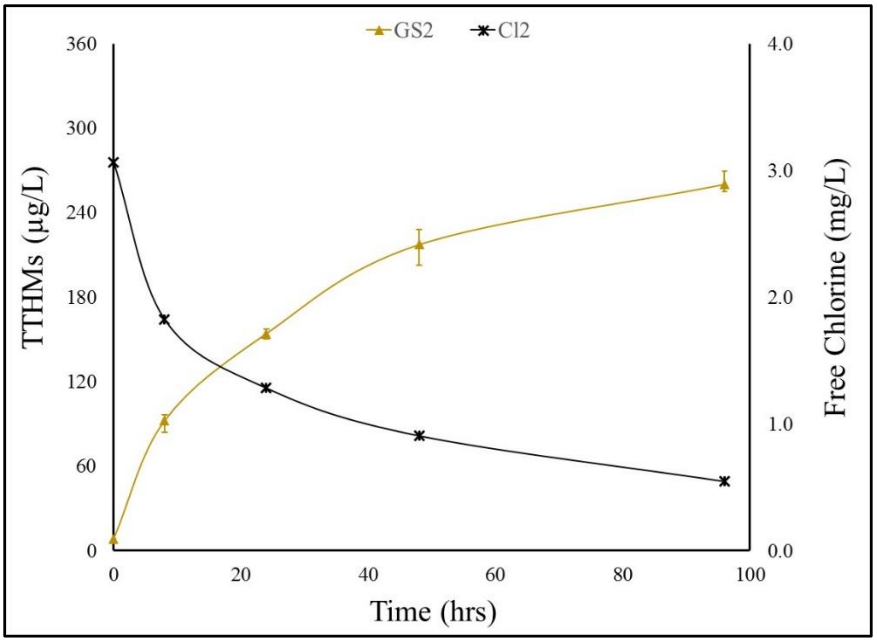

Figure 56: GS2 TTHM Formation Potential and Free Chlorine Curves

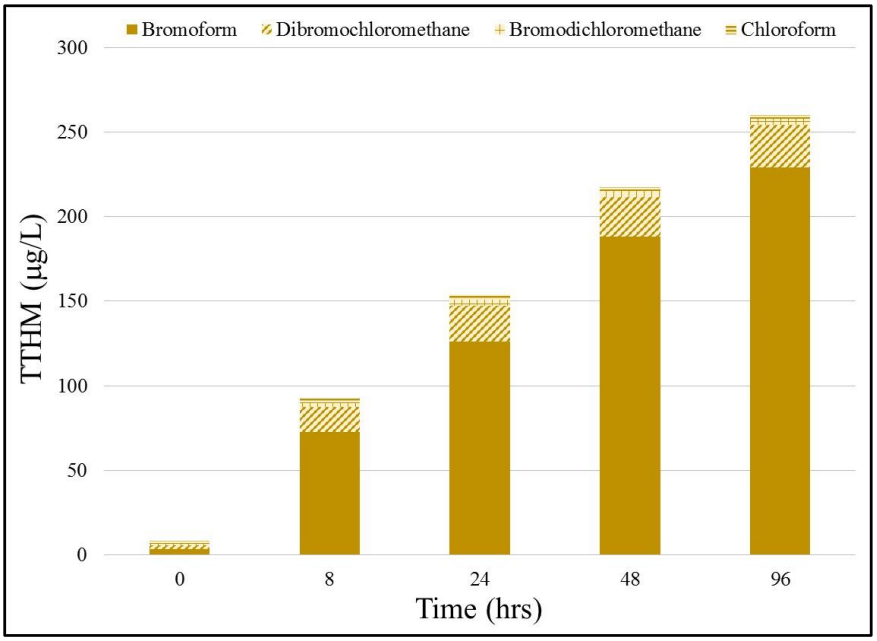

Figure 57: GS2 TTHM Composition Graph

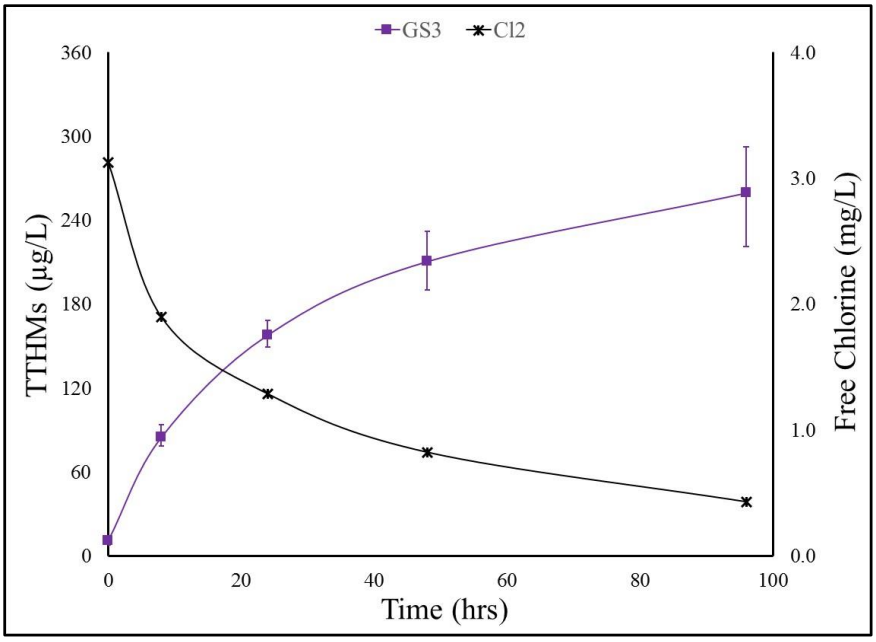

Figure 58: GS3 TTHM Formation Potential and Free Chlorine Curves

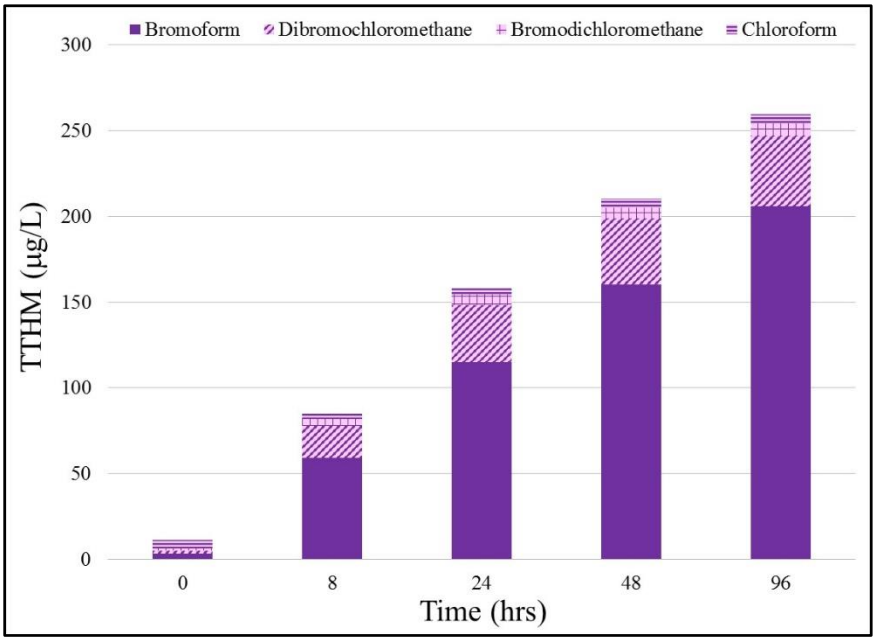

Figure 59: GS3 TTHM Composition Graph

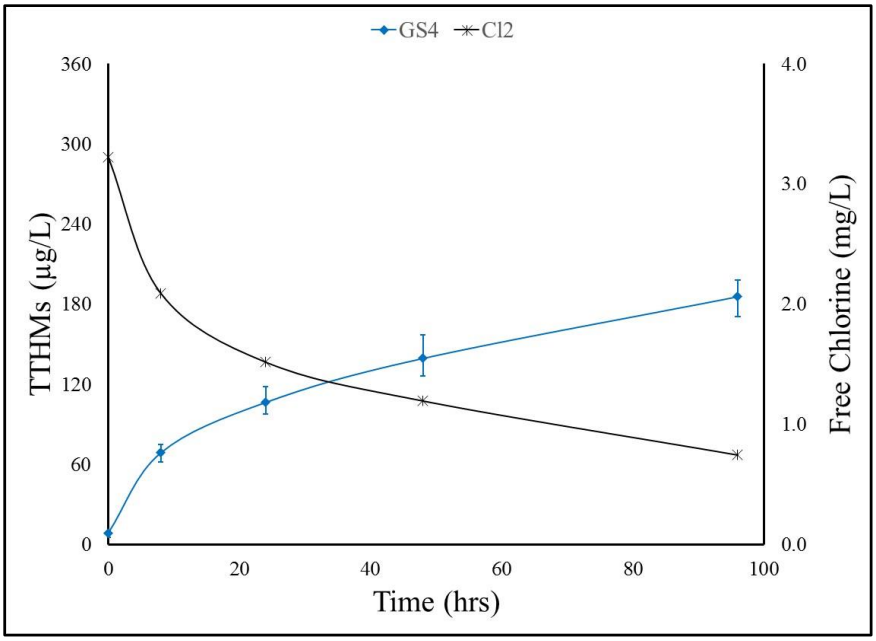

Figure 60: GS4 TTHM Formation Potential and Free Chlorine Curves

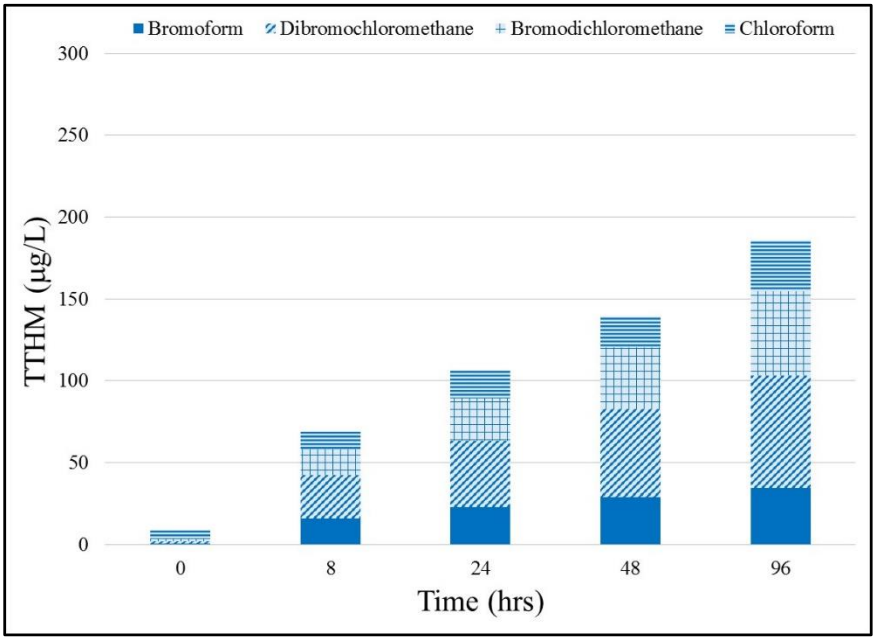

Figure 61: GS4 TTHM Composition Graph

APPENDIX E: PSEUDO 2ND ORDER AND INTRA-PARTICLE DIFFUSION GRAPHS

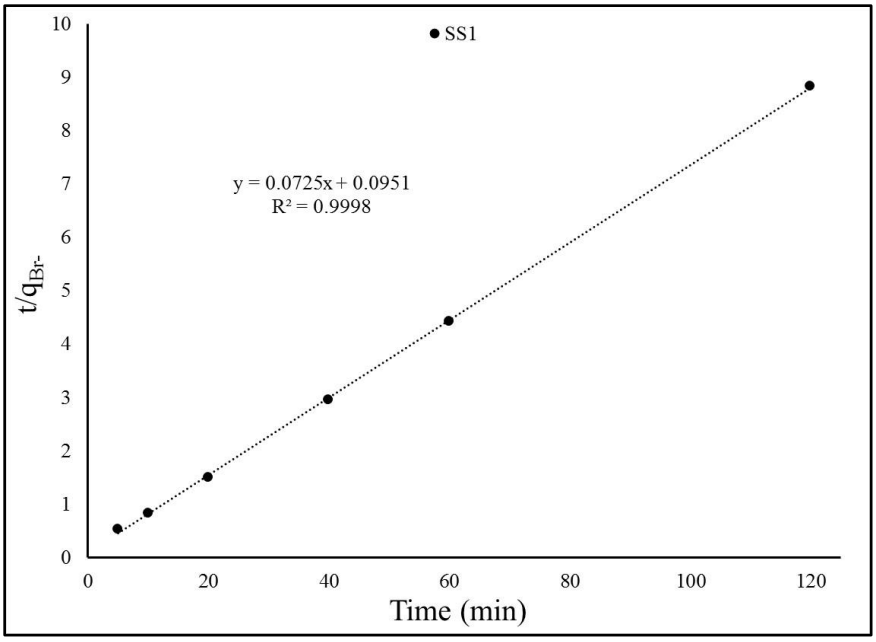

Figure 62: SS1 PSO Linear Plot

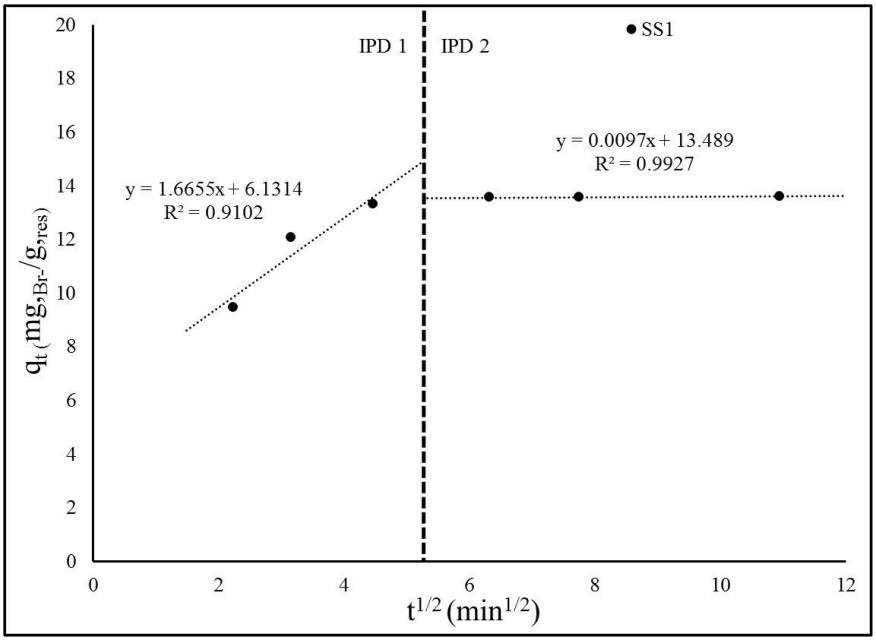

Figure 63: SS1 IPD Linear Plots

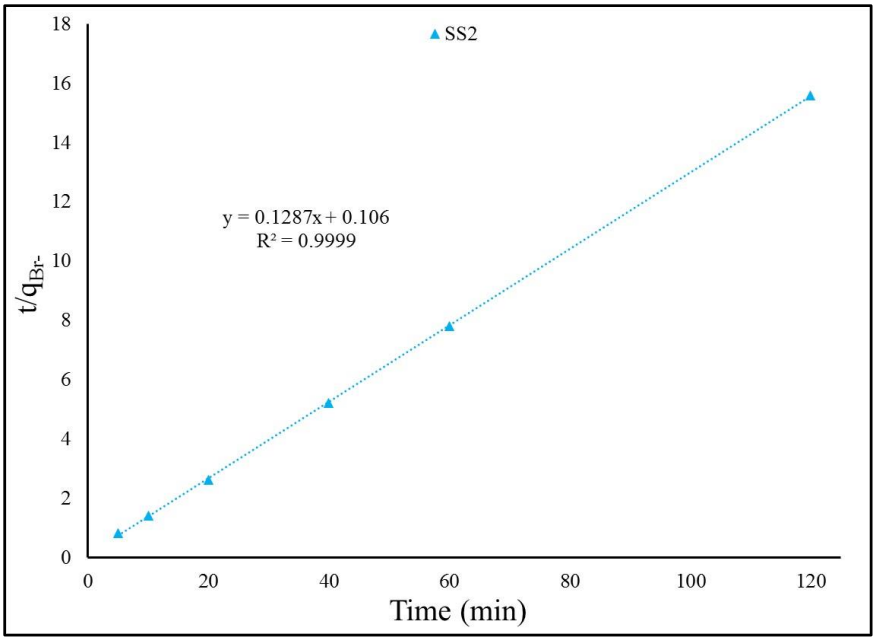

Figure 64: SS2 PSO Linear Plot

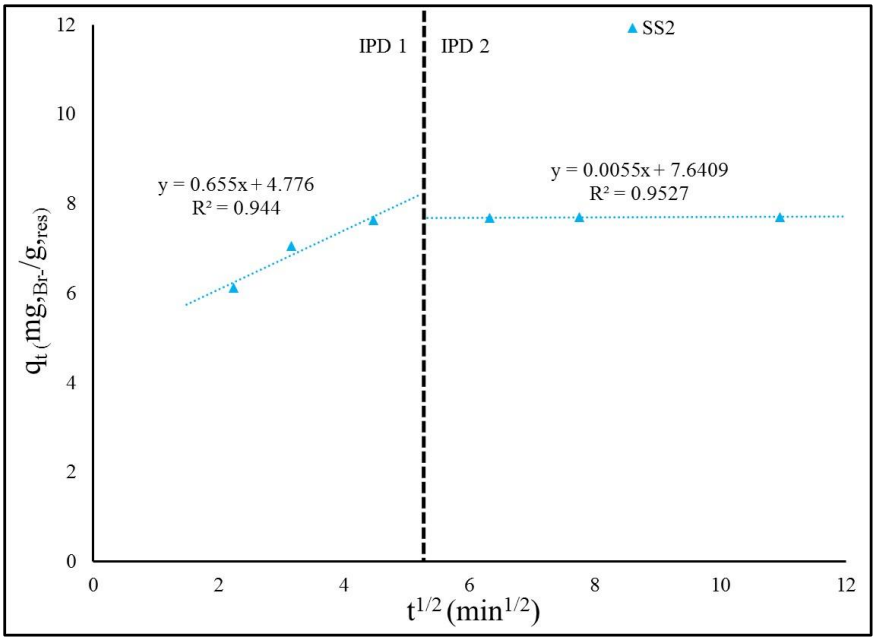

Figure 65: SS2 IPD Linear Plots

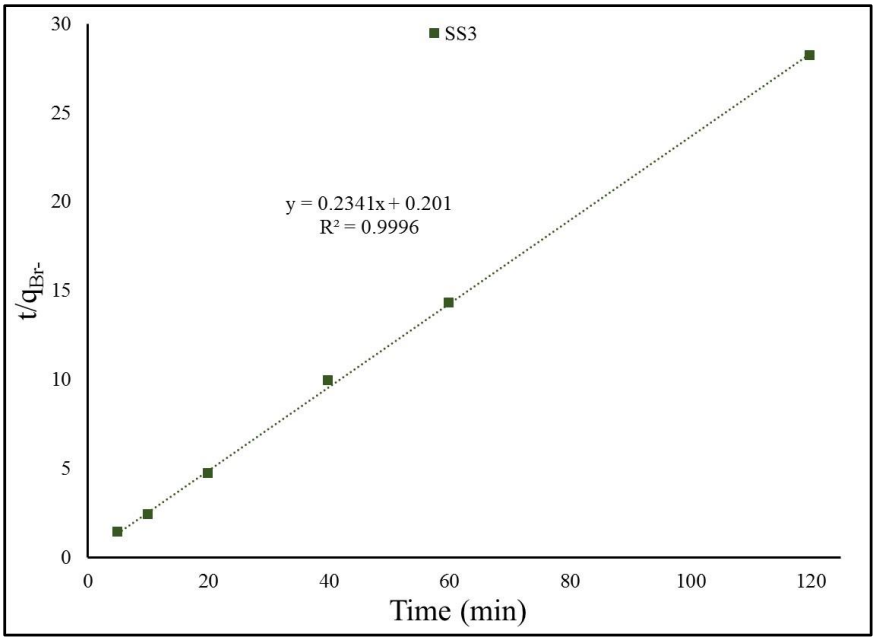

Figure 66: SS3 PSO Linear Plot

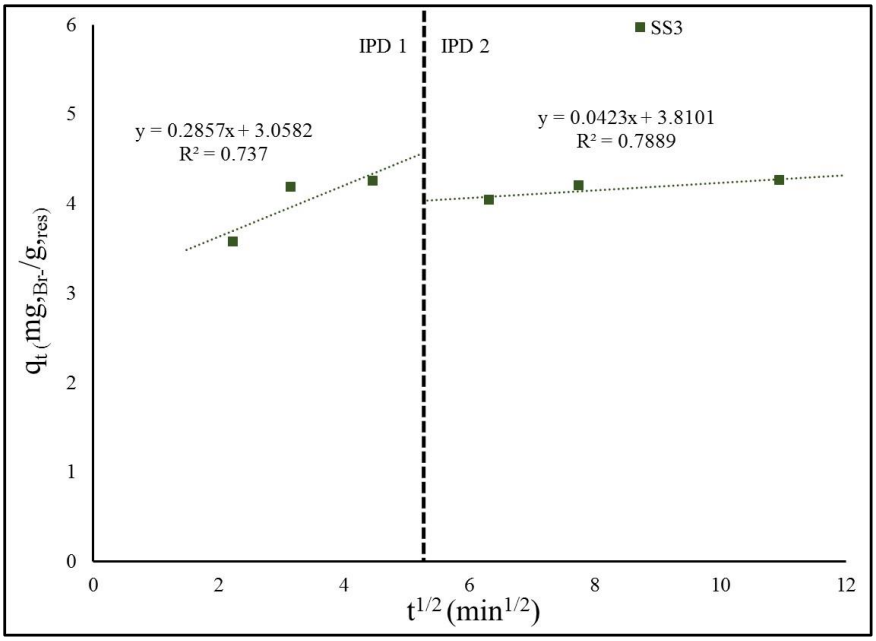

Figure 67: SS3 IPD Linear Plots

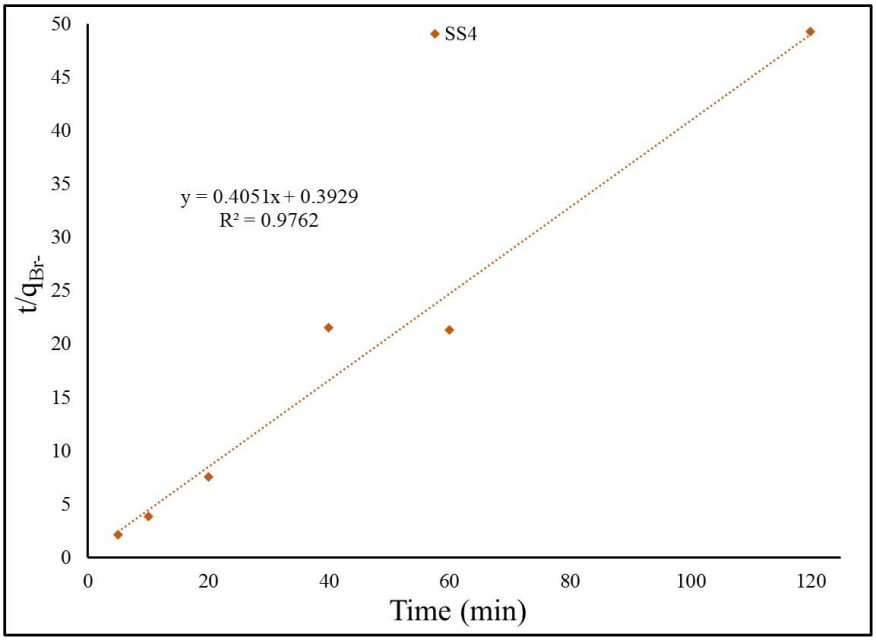

Figure 68: SS4 PSO Linear Plot

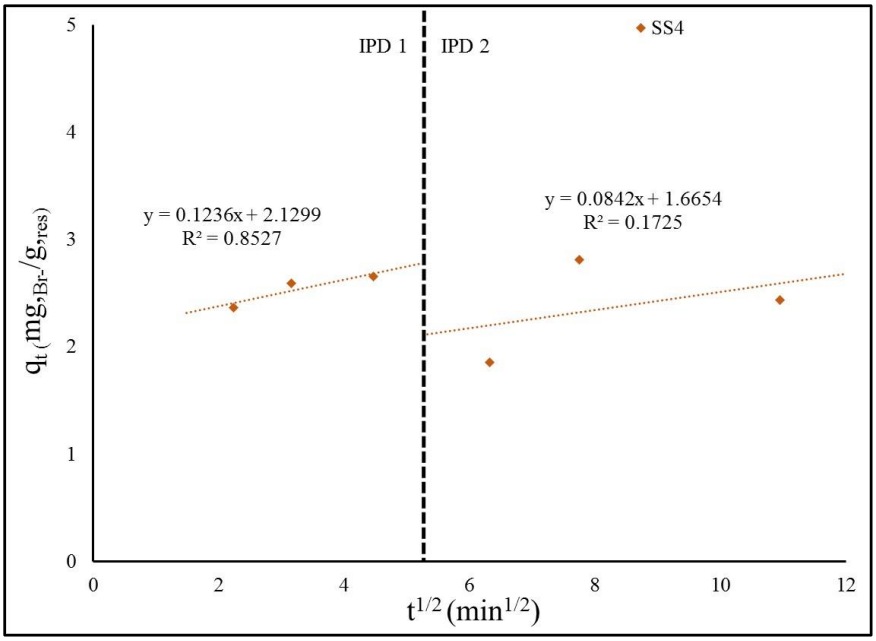

Figure 69: SS4 IPD Linear Plots

APPENDIX F: QUALITY ASSURANCE AND QUALITY CONTROL

In efforts to ensure the quality of appurtenant data, certain control measures were taken during sampling, transportation, storage, and analysis. Samples bottles used in collection procedures were washed/prepped in accordance with Table 33. Storage of samples took place in a fridge kept at 4°C on shelving designated for drinking water samples, reducing the potential for cross contamination. Data collection procedures conform to the recommendations in *Standard Methods for the Examination of Water and Wastewater* (Baird et al., 2017)

Table 33: Sample Container/Glassware Cleaning Procedures

Container Type	Required Cleaning Steps
Glass amber bottles	Steps 1-5, 7, 9-10
Plastic bottles	1-6
Large plastic drums/containers (≥15 gallons)	Step 3
Analytical glassware (beakers, flasks, graduated cylinders)	Steps 1-5, 11
Glass vials	Steps 1-5, 7, 9-10

Cleaning Steps	
1.	Remove outside labels (if any).
2.	Wash inside with tap water and lab-ware detergent solution.
3.	Wash/Rinse with tap water.
4.	Rinse with 1:1 hydrochloric acid solution.
5.	Rinse with distilled water.
6.	Air dry and cap prior to storage.
7.	Cover lid with aluminum foil, perforate for moisture passage.
8.	Air dry and cover contents with aluminum foil prior to storage.
9.	Bake for a minimum of 2 hours at 400°C, then cooling to room temperature prior to storage.
10.	Cover lid with aluminum foil.
11.	Air dry

To maintain quality control, precision was evaluated through the collection of laboratory replicates and sample duplicates and triplicates; approximately one replicate was prepared for every five samples. Precision was calculated using the industrial statistic (I-Statistic) displayed in Equation (25). Control charts were created to monitor data set variation during analysis. These charts were created for the analysis of anions, and other pertinent constituents of interest throughout the work. Control limits, displayed in Equations (26) and (27) were utilized on precision charts.

$$I = \frac{|Sample\ Value - Duplicate\ Sample\ Value|}{(Sample\ Value + Duplicate\ Sample\ Value)} \tag{25}$$

$$\text{UCL} = \mu + 3s \tag{26}$$

Where,

μ = mean value
s = standard deviation of mean value's data set

$$\text{UWL} = \mu + 2s \tag{27}$$

Analytical methods used throughout this work can be found in Table 31 of Appendix B for constituents of interest. The equipment used and the detection limits for each constituent can also be found in Table 31 of Appendix B. Constituent values were considered undetected below the specified detection limits provided.

Lab Replicate Precision Charts

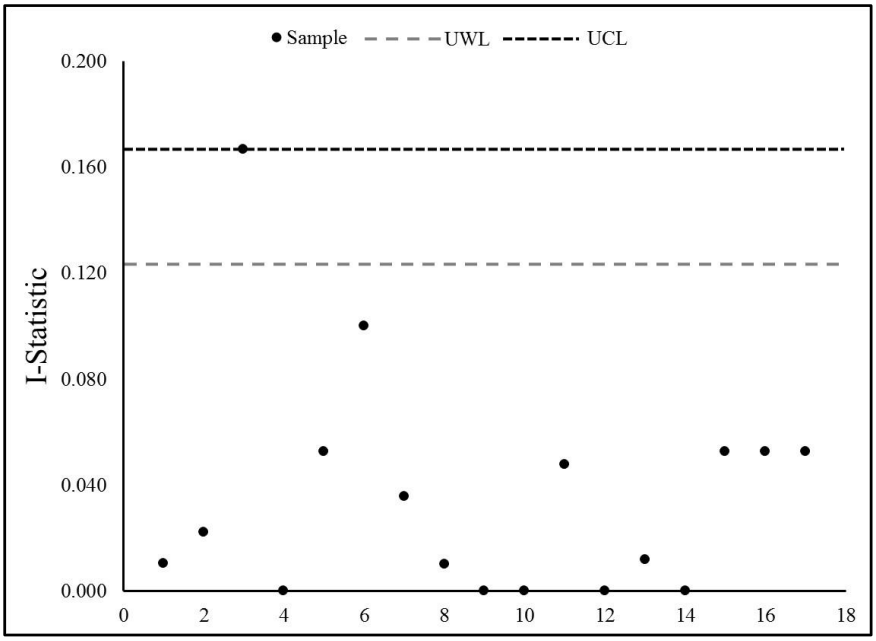

Figure 70: UV-254 Lab Replicate Precision Chart

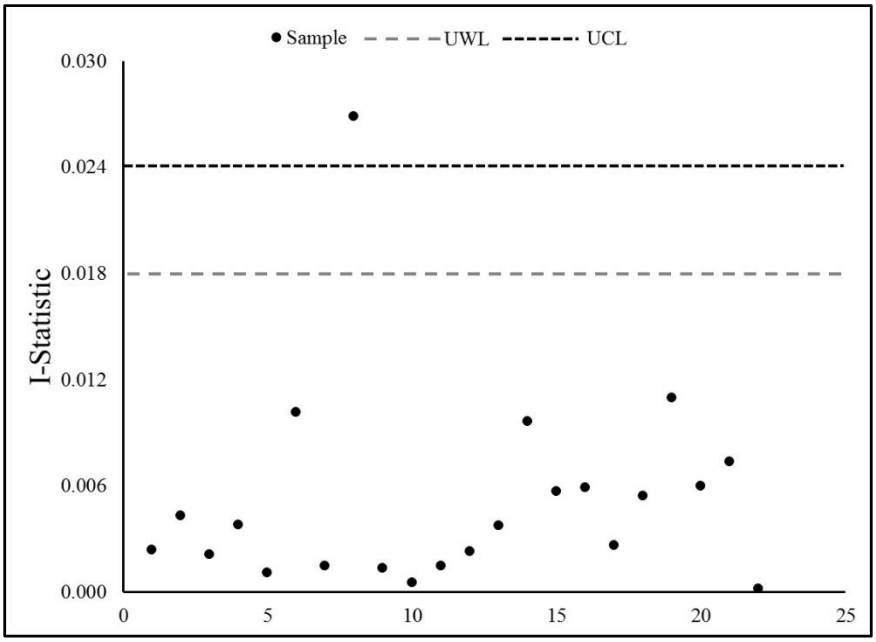

Figure 71: Sulfate Lab Replicate Precision Chart

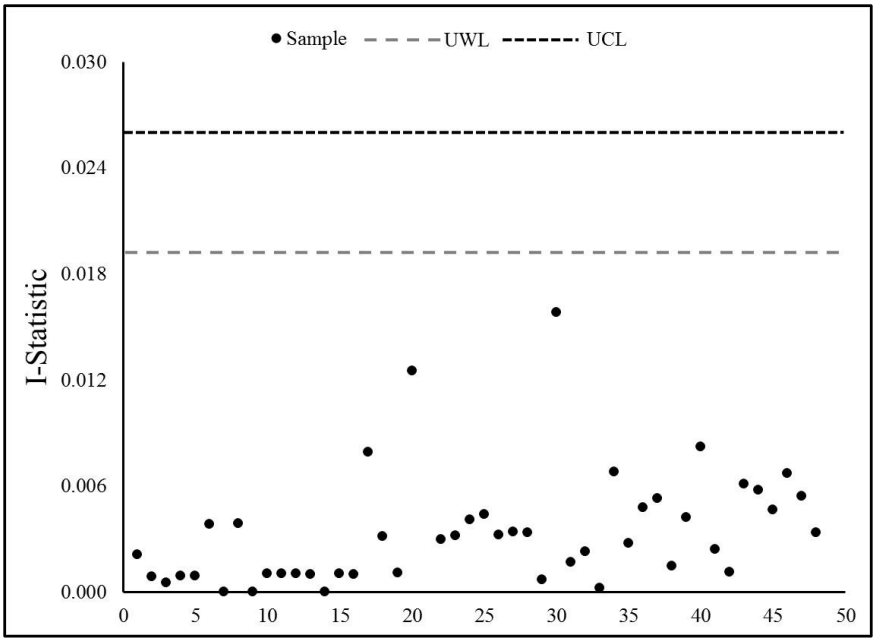

Figure 72: Chloride Lab Replicate Precision Chart

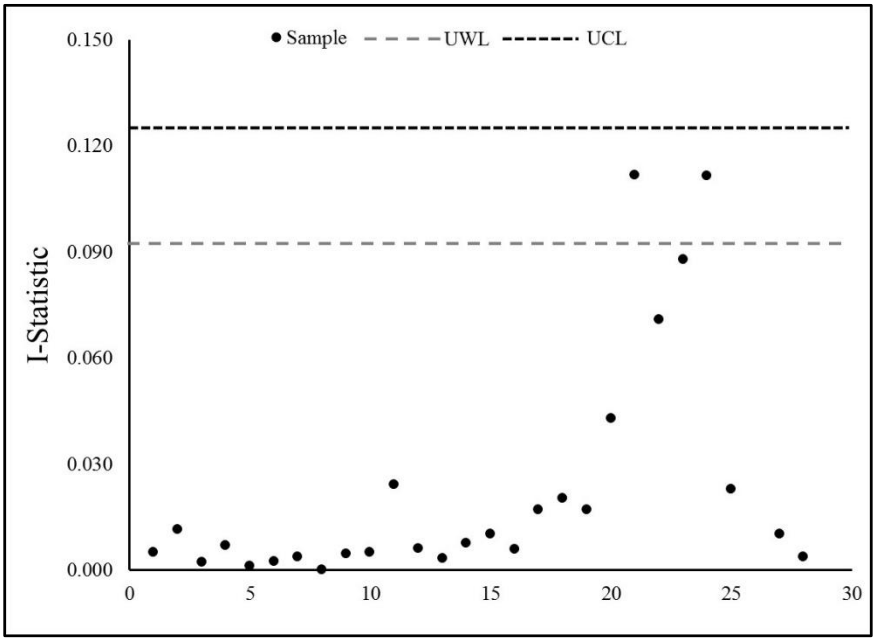

Figure 73: Bromide Lab Replicate Precision Chart

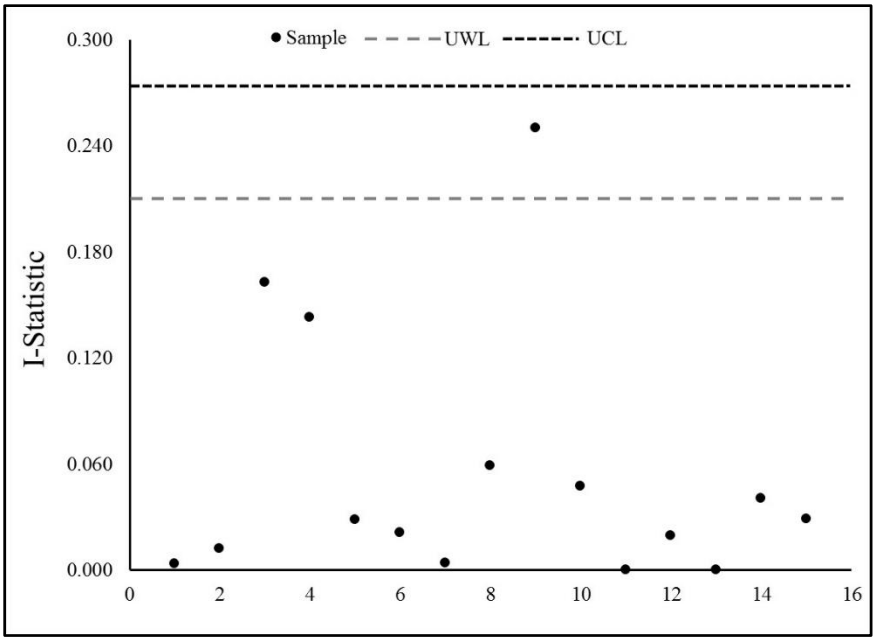

Figure 74: TOC Lab Replicate Precision Chart

Sample Duplicate and Triplicate Precision Charts

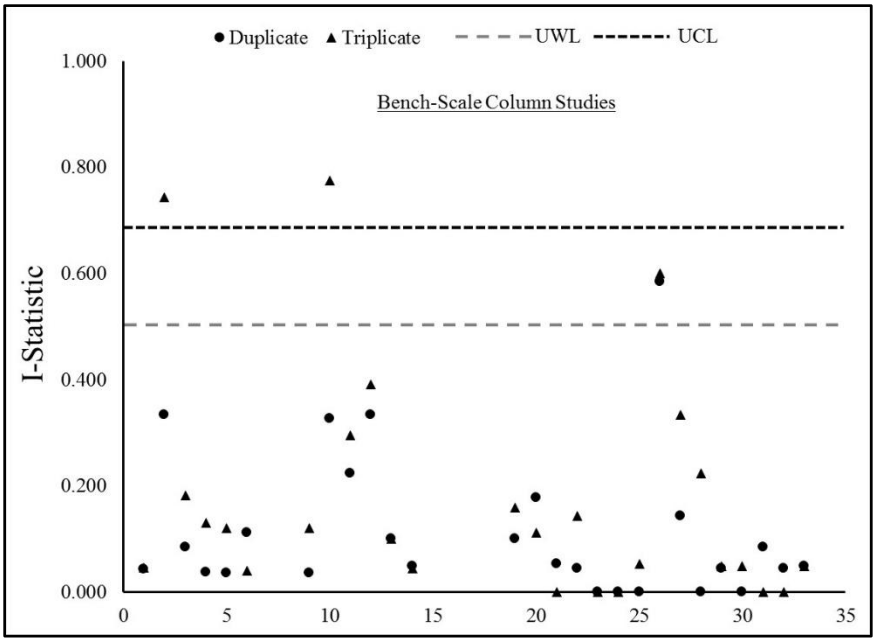

Figure 75: UV-254 Experimental Duplicate and Triplicate Precision Chart

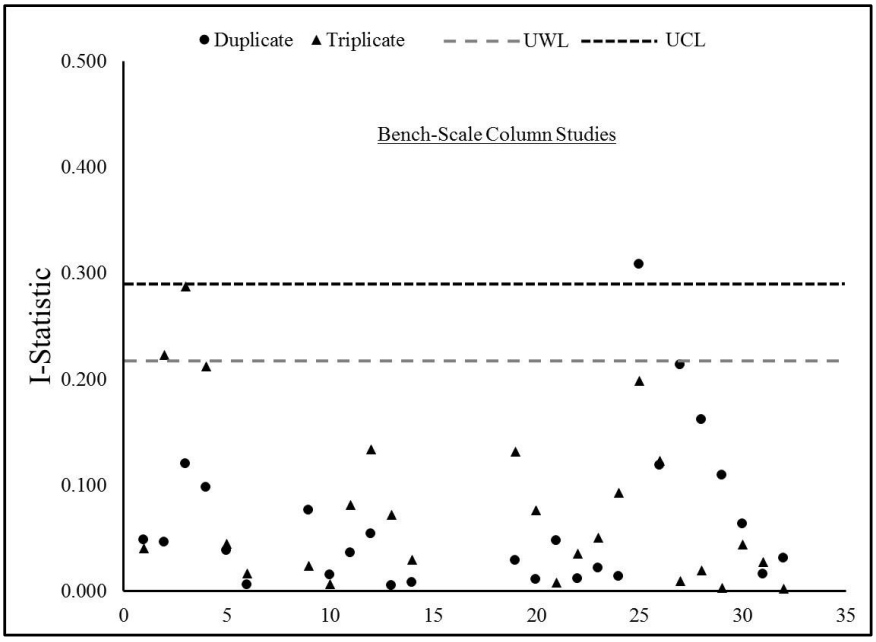

Figure 76: Sulfate Experimental Duplicate and Triplicate Precision Chart

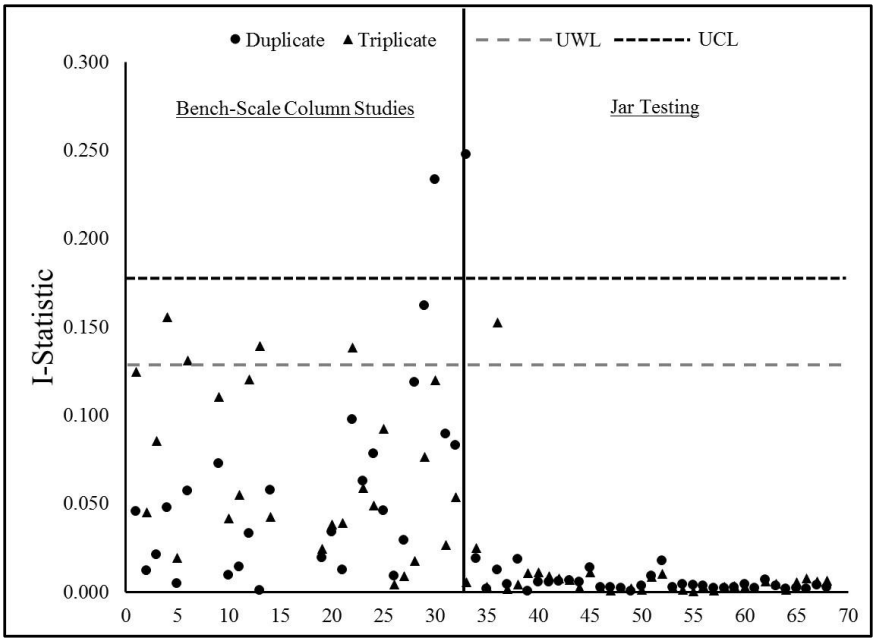

Figure 77: Chloride Experimental Duplicate and Triplicate Precision Chart

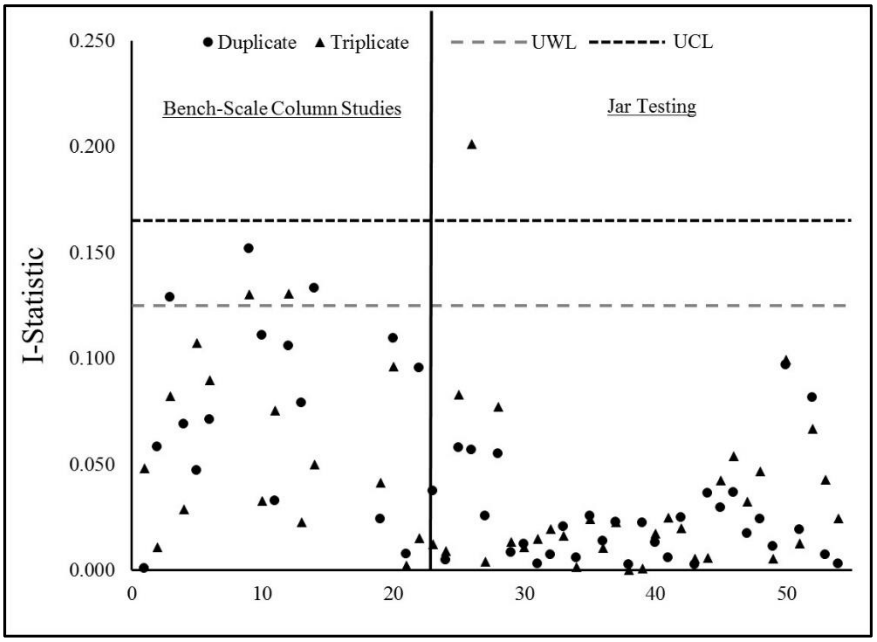

Figure 78: Bromide Experimental Duplicate and Triplicate Precision Chart

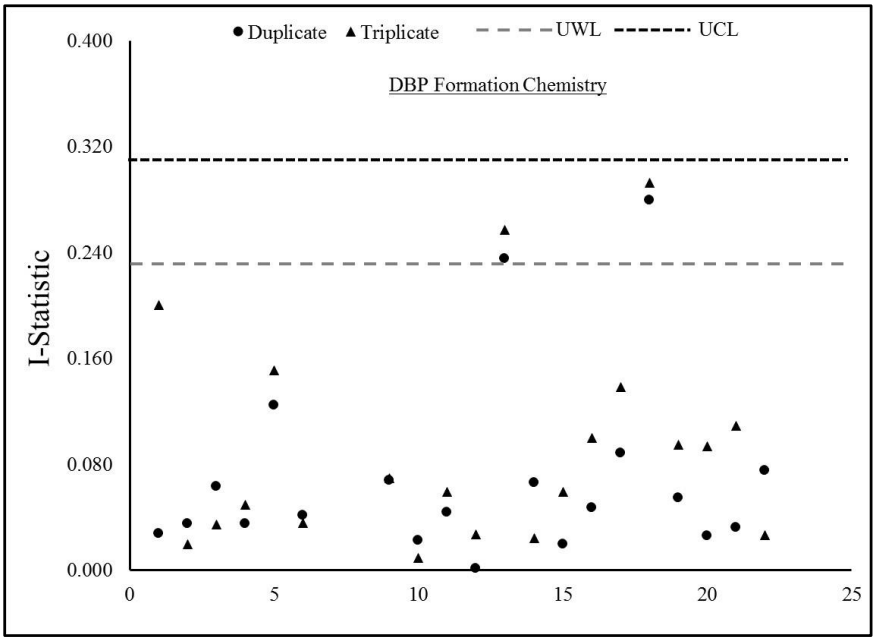

Figure 79: TTHM Experimental Duplicate and Triplicate Precision Chart

REFERENCES

Acelas, N. Y., Martin, B. D., López, D., & Jefferson, B. (2015). Selective removal of phosphate from wastewater using hydrated metal oxides dispersed within anionic exchange media. *Chemosphere, 119*, 1353-1360.

Ackerson, N. O. B., Liberatore, H. K., Plewa, M. J., Richardson, S. D., Ternes, T. A., & Duirk, S. E. (2020). Disinfection byproducts and halogen-specific total organic halogen speciation in chlorinated source waters–The impact of iopamidol and bromide. *Journal of Environmental Sciences, 89*, 90-101.

Adusei-Gyamfi, J., Ouddane, B., Rietveld, L., Cornard, J., & Criquet, J. (2019). Natural organic matter-cations complexation and its impact on water treatment: A critical review. *Water Research, 160*, 130.

Alcalá, F., & Custodio, E. (2005). Use of the Cl/Br ratio as a tracer to identify the origin of salinity in some coastal aquifers of spain. Paper presented at the *18th Salt Water Intrusion Meeting, IGME y IAH, Cartagena*, 481-497.

Alharati, A., Swesi, Y., Fiaty, K., & Charcosset, C. (2017). Boron removal in water using a hybrid membrane process of ion exchange resin and microfiltration without continuous resin addition. *Journal of Water Process Engineering, 17*, 32-39.

Alyüz, B., & Veli, S. (2009). Kinetics and equilibrium studies for the removal of nickel and zinc from aqueous solutions by ion exchange resins. *Journal of Hazardous Materials, 167*(1-3), 482-488.

Arroyo, F., Morillo, J., Usero, J., Rosado, D., & El Bakouri, H. (2019). Lithium recovery from desalination brines using specific ion-exchange resins. *Desalination, 468*, 114073.

Ates, N., & Incetan, F. B. (2013). Competition impact of sulfate on NOM removal by anion-exchange resins in high-sulfate and low-SUVA waters. *Industrial & Engineering Chemistry Research, 52*(39), 14261-14269.

Baird, B. R., Eaton, D. A., Rice, W. E., & Bridgewater, L. L. (Eds.). (2017). *Standard methods for the examination of water and wastewater* (23rd ed.). 800 Street, NW, Washington, DC 20001-3710: American Public Health Association; American Water Works Association; Water Environment Federation.

BCC Research, M. F. (2016). *Comparison of water main ppeline installation lengths and costs in ohio.* (Special Research Study No. Pipeline Comparison). 49 Walnut Park, Wellesley, Massachusetts, USA: BCC Research.

Bolto, B., Dixon, D., & Eldridge, R. (2004). Ion exchange for the removal of natural organic matter. *Reactive and Functional Polymers, 60*, 171-182.

Boyer, T. H., & Singer, P. C. (2006). A pilot-scale evaluation of magnetic ion exchange treatment for removal of natural organic material and inorganic anions. *Water Research, 40*(15), 2865-2876.

Chen, C., Chen, P., Wei, C., Huang, H., Jou, C., Wei, Y., & Wang, H. P. (2017). Lithium recovery with LiTi2O4 ion-sieves. *Marine Pollution Bulletin, 124*(2), 1106-1110.

Chen, J. P., Chua, M., & Zhang, B. (2002). Effects of competitive ions, humic acid, and pH on removal of ammonium and phosphorous from the synthetic industrial effluent by ion exchange resins. *Waste Management, 22*(7), 711-719.

Chubar, N. (2011). New inorganic (an) ion exchangers with a higher affinity for arsenate and a competitive removal capacity towards fluoride, bromate, bromide, selenate, selenite, arsenite and borate. *Water Science and Technology: Water Supply, 11*(5), 505-515.

Chubar, N., Kanibolotskyy, V., Strelko, V., Gallios, G., Samanidou, V., Shaposhnikova, T., . . . Zhuravlev, I. (2005). Adsorption of phosphate ions on novel inorganic ion exchangers. *Colloids and Surfaces A: Physicochemical and Engineering Aspects, 255*(1-3), 55-63.

Chubar, N., Samanidou, V., Kouts, V., Gallios, G., Kanibolotsky, V., Strelko, V., & Zhuravlev, I. (2005). Adsorption of fluoride, chloride, bromide, and bromate ions on a novel ion exchanger. *Journal of Colloid and Interface Science, 291*(1), 67-74.

Comstock, S. E., & Boyer, T. H. (2014). Combined magnetic ion exchange and cation exchange for removal of DOC and hardness. *Chemical Engineering Journal, 241*, 366-375.

Cooper, W. J., Zika, R. G., & Steinhauer, M. S. (1985). Bromide-Oxidant interactions and THM formation: A literature review. *Journal-American Water Works Association, 77*(4), 116-121.

Crittenden, C. J., Trussell, R. R., Hand, W. D., Howe, J. K., & Tchobanoglous, G. (Eds.). (2005). *Water treatment: Principles and design* (2nd Edition ed.). Hoboken, New Jersy: John Wiley & Sons, Inc.

D'alelio, G. F. (1942). *Experimental plastics and synthetic resins*. Synthetic Chemistry. John Wiley & Sons, CR 1942.

Darwish, N. B., Kochkodan, V., & Hilal, N. (2015). Boron removal from water with fractionized amberlite IRA743 resin. *Desalination, 370*, 1-6.

Davis, S. N., Whittemore, D. O., & Fabrykaâ€• Martin, J. (1998). Uses of chloride/bromide ratios in studies of potable water. *Groundwater, 36*(2), 338-350.

Digesti, R.D. and Weeth, H.J. (1976). A defensible maximum for inorganic sulfate in drinking water of cattle. *J. Animal Sci*. 42(6), 1498-1502.

Ding, L., Deng, H., Wu, C., & Han, X. (2012). Affecting factors, equilibrium, kinetics and thermodynamics of bromide removal from aqueous solutions by MIEX resin. *Chemical Engineering Journal, 181*, 360-370.

Dixit, F., Barbeau, B., & Mohseni, M. (2018). Simultaneous uptake of NOM and microcystin-LR by anion exchange resins: Effect of inorganic ions and resin regeneration. *Chemosphere, 192*, 113-121.

Domaine, J. D., Swain, R., & Hougen, O. (1943). Cation-exchange water softening rates. *Industrial & Engineering Chemistry, 35*(5), 546-553.

Dyck, R., Cool, G., Rodriguez, M., & Sadiq, R. (2015). Treatment, residual chlorine and season as factors affecting variability of trihalomethanes in small drinking water systems. *Frontiers of Environmental Science & Engineering, 9*(1), 171-179.

Edwards, M., & Triantafyllidou, S. (2007). Chloride-to-sulfate mass ratio and lead leaching to water. *Journal-American Water Works Association, 99*(7), 96-109.

Emaraa, M. M., Salmana, A. A., Mahmoudd, N. M., & Fattaha, S. A. (2017). Removal of fluoride from aqueous solution using amberlite-IRA-aluminum sorbent nanoexchanger. *Desalination and Water Treatment, 81*, 152-161.

Fierro, V., Torné-Fernández, V., Montané, D., & Celzard, A. (2008). Adsorption of phenol onto activated carbons having different textural and surface properties. *Microporous and Mesoporous Materials, 111*(1-3), 276-284.

Florida Administrative Code. (2011a). Department of Environmental Protection Chapter 62-550.430 Public Notification - Secondary Standards. Tallahassee, FL.

Foo, K. Y., & Hameed, B. H. (2010). Insights into the modeling of adsorption isotherm systems. *Chemical Engineering Journal, 156*(1), 2-10.

Freundlich, H. (1906). Over the adsorption in solution. *J.Phys.Chem, 57*(385471), 1100-1107.

Funasaki, N. (1979). Micellar effects on the kinetics and equilibrium of chemical reactions in salt solutions. *Journal of Physical Chemistry, 83*(15), 1998-2003.

Gando-Ferreira, L. M., Romão, I. S., & Quina, M. J. (2011). Equilibrium and kinetic studies on removal of Cu2 and Cr3 from aqueous solutions using a chelating resin. *Chemical Engineering Journal, 172*(1), 277-286.

Gans, R. (1905). Zeolites and similar compounds, their constitution and meaning for technology and agriculture. *Jahrbuch Der Königlich Preussischen Geologischen Landesanstalt, 26*, 179.

Gregor, H. P., Belle, J., & Marcus, R. (1954). Studies on ion exchange resins. IX. capacity and specific volumes of quaternary base anion exchange Resins1. *Journal of the American Chemical Society, 76*(7), 1984-1987.

Heeb, M. B., Criquet, J., Zimmermann-Steffens, S. G., & Von Gunten, U. (2014). Oxidative treatment of bromide-containing waters: Formation of bromine and its reactions with inorganic and organic compounds—A critical review. *Water Research, 48*, 15-42.

Ho, Y., & McKay, G. (1998). Sorption of dye from aqueous solution by peat. *Chemical Engineering Journal, 70*(2), 115-124.

Hongve, D., Baann, J., Becher, G., & Beckmann, O. (1999). Experiences from operation and regeneration of an anionic exchanger for natural organic matter (NOM) removal. *Water Science and Technology, 40*(9), 215-221.

Hsu, S., & Singer, P. C. (2010). Removal of bromide and natural organic matter by anion exchange. *Water Research, 44*(7), 2133-2140.

Hu, H., Du, Y., Wu, Q., Zhao, X., Tang, X., & Chen, Z. (2016). Differences in dissolved organic matter between reclaimed water source and drinking water source. *Science of the Total Environment, 551*, 133-142.

Hu, Y., & Boyer, T. H. (2017). Integrated bicarbonate-form ion exchange treatment and regeneration for DOC removal: Model development and pilot plant study. *Water Research, 115*, 40-49.

Hu, Y., Foster, J., & Boyer, T. H. (2016). Selectivity of bicarbonate-form anion exchange for drinking water contaminants: Influence of resin properties. *Separation and Purification Technology, 163*, 128-139.

Hrudey, S.E. (2009). Chlorination disinfection by-products, public health risk tradeoffs and me. *Water Research*. 43(8), 2057-2092.

Indarawis, K., & Boyer, T. H. (2012). Alkaline earth metal cation exchange: Effect of mobile counterion and dissolved organic matter. *Environmental Science & Technology, 46*(8), 4591-4598.

Ishii, S. K., & Boyer, T. H. (2011). Evaluating the secondary effects of magnetic ion exchange: Focus on corrosion potential in the distribution system. *Desalination, 274*(1-3), 31-38.

Jung, S., & Kim, M. (2016). Optimal conditions for recovering boron from seawater using boron selective resins. *Korean Journal of Chemical Engineering, 33*(8), 2411-2417.

Kearney, M., & Rearick, D. (2003). Weak cation exchange softening: Long term experience and recent developments. Paper presented at the *Proceedings from the 32nd Biennial ASSBT Meeting, TX, USA,*

Kinniburgh, D. G. (1986). General purpose adsorption isotherms. *Environmental Science & Technology, 20*(9), 895-904.

Kolb, C., Francis, R. A., & VanBriesen, J. M. (2017). Disinfection byproduct regulatory compliance surrogates and bromide-associated risk. *Journal of Environmental Sciences, 58*, 191-207.

Korak, J. A., Huggins, R., & Arias-Paic, M. (2017). Regeneration of pilot-scale ion exchange columns for hexavalent chromium removal. *Water Research, 118*, 141-151.

Koshy, N., & Pathak, P. (2020). Removal of strontium by physicochemical adsorptions and ion exchange methods. *Strontium contamination in the environment* (pp. 185-202) Springer.

Kumar, S., & Jain, S. (2013). History, introduction, and kinetics of ion exchange materials. *Journal of Chemistry, 2013*

Lagergren, S., Lagergren, S., Lagergren, S., & Sven, K. (1898). The theory of so-called adsorption of gel substances. *Handlingar, 24(4)*, 1-39.

Lange, A. L., & Kawczynski, E. (1978). Controlling organics: The contra costa county water district experience. *Journal-American Water Works Association, 70*(11), 653-660.

Langmuir, I. (1918). The adsorption of gases on plane surfaces of glass, mica and platinum. *Journal of the American Chemical Society, 40*(9), 1361-1403.

Largitte, L., & Pasquier, R. (2016). A review of the kinetics adsorption models and their application to the adsorption of lead by an activated carbon. *Chemical Engineering Research and Design, 109*, 495-504.

Lehman, S. G., Badruzzaman, M., Adham, S., Roberts, D. J., & Clifford, D. A. (2008). Perchlorate and nitrate treatment by ion exchange integrated with biological brine treatment. *Water Research, 42*(4-5), 969-976.

Levchuk, I., Màrquez, J. J. R., & Sillanpää, M. (2018). Removal of natural organic matter (NOM) from water by ion exchange–A review. *Chemosphere, 192*, 90-104.

Liberti, L., & Helfferich, F. G. (1983). *Mass transfer and kinetics of ion exchange*. The Hague: Martinus Nijhoff Publishers.

Liu, S., Zhu, Z., Qiu, Y., & Zhao, J. (2011). Effect of ferric and bromide ions on the formation and speciation of disinfection byproducts during chlorination. *Journal of Environmental Sciences, 23*(5), 765-772.

Liu, Z., Shah, A. D., Salhi, E., Bolotin, J., & von Gunten, U. (2018). Formation of brominated trihalomethanes during chlorination or ozonation of natural organic matter extracts and model compounds in saline water. *Water Research, 143*, 492-502.

Lokhande, R., & Singare, P. (1998). Comparative study of forward and reverse ion exchange reaction in amberlite IRA-400 by application of tracer isotope-131 I. *Asian Journal of Chemistry, 10*(4), 890-893.

Maul, G. A., Kim, Y., Amini, A., Zhang, Q., & Boyer, T. H. (2014). Efficiency and life cycle environmental impacts of ion-exchange regeneration using sodium, potassium, chloride, and bicarbonate salts. *Chemical Engineering Journal, 254*, 198-209.

McBurney, C. H. (1952). In Rohm & Haas Company (Ed.), *Resinous insoluble reaction products of tertiary amines with haloalkylated vinyl aromatic hydrocarbon coploymers* (2,591,573 ed.). Philadelphia, United States:

Medina, B. B., Boyer, T., & Indarawis, K. (2018). Evaluating options for regenerant brine reuse in magnetic ion exchange systems. *Journal-American Water Works Association, 110*(5), E2-E10.

Michener, W. J., & Lundberg, E. H. (1956). Equipment and process design. *Ion exchange technology* (pp. 28-51). 111 Fifth Avenue, New York 10003: ACADEMIC PRESS INC.

Millar, G. J., Papworth, S., & Couperthwaite, S. J. (2014). Exploration of the fundamental equilibrium behaviour of calcium exchange with weak acid cation resins. *Desalination, 351*, 27-36.

Moody, G. J., & Thomas, J. (1968). Inorganic ion exchange in organic and aqueous-organic solvents. A review. *Analyst, 93*(1110), 557-588.

Moussout, H., Ahlafi, H., Aazza, M., & Maghat, H. (2018). Critical of linear and nonlinear equations of pseudo-first order and pseudo-second order kinetic models. *Karbala International Journal of Modern Science, 4*(2), 244-254.

Muhammad, A., Soares, A., & Jefferson, B. (2019). The impact of background wastewater constituents on the selectivity and capacity of a hybrid ion exchange resin for phosphorus removal from wastewater. *Chemosphere, 224*, 494-501.

Nawaz, T., & Sengupta, S. (2017). Silver recovery from greywater: Role of competing cations and regeneration. *Separation and Purification Technology, 176*, 145-158.

Phetrak, A., Lohwacharin, J., Watanabe, N., Murakami, M., Sakai, H., Oguma, K., & Takizawa, S. (2012). Competitive removal of dissolved organic matter (DOM) and inorganic anions by anion exchange resins (AERs). *Water Science and Technology: Water Supply, 12*(5), 630-636.

Piazzoli, A., & Antonelli, M. (2018). Feasibility assessment of chromium removal from groundwater for drinking purposes by sorption on granular activated carbon and strong base anion exchange. *Water, Air, & Soil Pollution, 229*(6), 193.

Piazzoli, A., & Antonelli, M. (2018). Feasibility assessment of chromium removal from groundwater for drinking purposes by sorption on granular activated carbon and strong base anion exchange. *Water, Air, & Soil Pollution, 229*(6), 193.

Rengaraj, S., Joo, C. K., Kim, Y., & Yi, J. (2003). Kinetics of removal of chromium from water and electronic process wastewater by ion exchange resins: 1200H, 1500H and IRN97H. *Journal of Hazardous Materials, 102*(2-3), 257-275.

Richardson, S. D., Thruston, A. D., Caughran, T. V., Chen, P. H., Collette, T. W., Floyd, T. L., . . . Majetich, G. (1999). Identification of new ozone disinfection byproducts in drinking water. *Environmental Science & Technology, 33*(19), 3368-3377.

Rook, J. J., & JJ, R. (1974). Formation of haloforms during chlorination of natural waters. *Journal Water Treatment Examination, 23*, 234-243.

Ross, W.D. (1927). *The Works of Aristotle*. Volume VII, Problemata by E.S. Forster. Book XXIII Salt Water and the Sea. Translated into English under the Editorship of W.D. Ross, M.A. London: Oxford University Press (Clarendon Press).

Runtti, H., Tolonen, E.T., Tuomikoski, S., Luukkonen, T, and Lassi, U. (2018). How to tackle the stringent sulfate removal requirements in mine water treatment – A review of potential methods. *Environmental Research*. 167, 207-222.

Samatya, S., Yüksel, Ü., Arda, M., Kabay, N., & Yüksel, M. (2006). Investigation of selectivity and kinetic behavior of strong-base ion exchange resin purolite A 520E for nitrate removal from aqueous solution. *Separation Science and Technology, 41*(13), 2973-2988.

Schubert, J., & Nachod, C. F. (1956). Introduction. In J. Schubert, & C. F. Nachod (Eds.), *Ion exchage technology* (pp. 1-6). 111 Fifth Avenue, New York 10003: Academic Press Inc.

Sharma, V. K., Zboril, R., & McDonald, T. J. (2014). Formation and toxicity of brominated disinfection byproducts during chlorination and chloramination of water: A review. *Journal of Environmental Science and Health, Part B, 49*(3), 212-228.

Singare, P., Lokhande, R., & Nadar, M. (2009). Ion exchange equilibrium study using strongly basic anion exchange resin indion-102. *Oriental Journal of Chemistry, 25*(3), 587.

Soldatov, V., Sokolova, V., Medyak, G., Shunkevich, A., & Akulich, Z. (2007). Binary ion exchange equilibria in systems containing NO3-, cl− and SO42-on fibrous anion exchangers with tetraalkylammomium groups. *Reactive and Functional Polymers, 67*(12), 1530-1539.

Soyluoglu, M., Ersan, M. S., Ateia, M., & Karanfil, T. (2020). Removal of bromide from natural waters: Bromide-selective vs. conventional ion exchange resins. *Chemosphere, 238*, 124583.

Sparks, D. L. (2003). *Environmental soil chemistry*. Academic Press Inc.

Szczuka, A., Parker, K. M., Harvey, C., Hayes, E., Vengosh, A., & Mitch, W. A. (2017). Regulated and unregulated halogenated disinfection byproduct formation from chlorination of saline groundwater. *Water Research, 122*, 633-644.

Tan, L. C., Calix, E. M., Rene, E. R., Nancharaiah, Y. V., van Hullebusch, E. D., & Lens, P. N. (2018). Amberlite IRA-900 ion exchange resin for the sorption of selenate and sulfate: Equilibrium, kinetic, and regeneration studies. *Journal of Environmental Engineering, 144*(11), 04018110.

Tan, Y., & Kilduff, J. E. (2007). Factors affecting selectivity during dissolved organic matter removal by anion-exchange resins. *Water Research, 41*(18), 4211-4221.

Tang, S. C., Birnhack, L., Cohen, Y., & Lahav, O. (2018). Selective separation of divalent ions from seawater using an integrated ion-exchange/nanofiltration approach. *Chemical Engineering and Processing-Process Intensification, 126*, 8-15.

Tharamapalan, J., Boyd, C.C. and Duranceau, S.J. (2013). 3 - Step Approach Towards Evaluation and Elimination of Acid Use in Pre-Treatment for a Brackish Water RO Process. *J. of Environmental Management*. 124: 115-120.

Thompson, H.S. (1850). On the absorbent power of soils. *Journal of the Royal Agricultural Society of England*, 11, 68.

U.S. Department of the Interior, & U.S. Geological Survey. (2016). The USGS water science school, water hardness. Retrieved from https://water.usgs.gov/edu/hardness.html

Vaaramaa, K., & Lehto, J. (2003). Removal of metals and anions from drinking water by ion exchange. *Desalination, 155*(2), 157-170.

Venkatesan, A., & Wankat, P. C. (2011). Simulation of ion exchange water softening pretreatment for reverse osmosis desalination of brackish water. *Desalination, 271*(1-3), 122-131.

Wachinski, M. A. (2006). *Ion exchange treatment for water*. 6666 West Quincy Avenue, Denver, CO: American Water Works Association.

Walker, K. M., & Boyer, T. H. (2011). Long-term performance of bicarbonate-form anion exchange: Removal of dissolved organic matter and bromide from the st. johns river, FL, USA. *Water Research, 45*(9), 2875-2886.

Wang, Q., Li, A., Wang, J., & Shuang, C. (2012). Selection of magnetic anion exchange resins for the removal of dissolved organic and inorganic matters. *Journal of Environmental Sciences, 24*(11), 1891-1899.

Way, I.T. (1850). On the power of soils to absorb manure. *Journal of the Royal Agricultural Society of England*, 11, 313- 379.

Weber, W. J., & Morris, J. C. (1963). Kinetics of adsorption on carbon from solution. *Journal of the Sanitary Engineering Division, 89*(2), 31-60.

Wilf, M., Konstantin, M., & Chencinsky, A. (1980). Evaluation of an ion exchange system regenerated with seawater for the increase of product recovery of reverse osmosis brackish water plant. *Desalination, 34*(3), 189-197.

Willauer, H. D., Hardy, D. R., Lewis, M. K., Ndubizu, E. C., & Williams, F. W. (2010). Extraction of CO2 from seawater and aqueous bicarbonate systems by ion-exchange resin processes. *Energy & Fuels, 24*(12), 6682-6688.

Willison, H., & Boyer, T. H. (2012). Secondary effects of anion exchange on chloride, sulfate, and lead release: Systems approach to corrosion control. *Water Research, 46*(7), 2385-2394.

Wu, F., Tseng, R., & Juang, R. (2009). Initial behavior of intraparticle diffusion model used in the description of adsorption kinetics. *Chemical Engineering Journal, 153*(1-3), 1-8.

Yang, Y., Komaki, Y., Kimura, S. Y., Hu, H., Wagner, E. D., Mariñas, B. J., & Plewa, M. J. (2014). Toxic impact of bromide and iodide on drinking water disinfected with chlorine or chloramines. *Environmental Science & Technology, 48*(20), 12362-12369.

Ye, L., You, H., Yao, J., & Su, H. (2012). Water treatment technologies for perchlorate: A review. *Desalination, 298*, 1-12.

Yonge, D. (2016). *Modeling mass transfer and assessing cost and performance of a hollow fiber nanofiltration membrane process.* (Unpublished Doctor of Philosophy). University of Central Florida,

Zhai, H., & Zhang, X. (2011). Formation and decomposition of new and unknown polar brominated disinfection byproducts during chlorination. *Environmental Science & Technology, 45*(6), 2194-2201.

Zhai, H., Zhang, X., Zhu, X., Liu, J., & Ji, M. (2014). Formation of brominated disinfection byproducts during chloramination of drinking water: New polar species and overall kinetics. *Environmental Science & Technology, 48*(5), 2579-2588.

Zhang, H., & Yang, M. (2018). Characterization of brominated disinfection byproducts formed during chloramination of fulvic acid in the presence of bromide. *Science of the Total Environment, 627*, 118-124.

Zhu, L., Granda, C. B., & Holtzapple, M. T. (2011). Prevention of calcium sulfate formation in seawater desalination by ion exchange. *Desalination and Water Treatment, 36*(1-3), 57-64.